

Structural and Functional Analysis of the Mitochondrial Presequence Translocase

PhD Thesis

In partial fulfillment of the requirements
for the degree “Doctor of Philosophy (PhD)”
in the Molecular Biology Program
at the Georg August University Göttingen,
Faculty of Biology

submitted by

Oleksandr Lytovchenko

born in

Kharkiv, Ukraine

Göttingen, 2012

Member of the Thesis Committee (First Reviewer):

Prof. Dr. Peter Rehling

Department of Biochemistry II

Center for Biochemistry and Molecular Cell Biology

Georg-August University, Göttingen, Germany

Member of the Thesis Committee (Second Reviewer):

Prof. Dr. Holger Stark

3D-Cryo Electron Microscopy group

Max Planck Institute for Biophysical Chemistry, Göttingen, Germany

Member of the Thesis Committee:

Prof. Dr. Dirk Fasshauer

Department of Cell Biology and Morphology

Faculty of Biology and Medicine

University of Lausanne, Switzerland

Affidavit:

I herewith declare that this thesis has been written independently and with no other sources and aids than explicitly quoted.

Oleksandr Lytovchenko

Göttingen, 28.06.2012

List of publications

Parts of this thesis have been published previously:

Alkhaja, A. K., Jans, D. C., Nikolov, M., Vukotic, M., Lytovchenko, O., Ludewig, F., Schliebs, W., et al. (2012). MINOS1 is a conserved component of mitofilin complexes and required for mitochondrial function and cristae organization. *Molecular biology of the cell*, 23(2), 247-57.

Schulz, C., Lytovchenko, O., Melin, J., Chacinska, A., Guiard, B., Neumann, P., Ficner, R., et al. (2011). Tim50's presequence receptor domain is essential for signal driven transport across the TIM23 complex. *The Journal of cell biology*, 195(4), 643-56.

Other results of the project will be communicated in the following publication:

Lytovchenko, O., Melin, J., Schulz, C., Hutu, D. P., Kilisch, M., Rehling, P. Mitochondrial matrix targeting signals dissociate their receptor Tim50 from Tim21 during protein import. *In preparation*.

Acknowledgements

First of all, I would like to thank my supervisor Prof. Dr. Peter Rehling for giving me the opportunity to work on both interesting and challenging projects, for his outstanding patience, encouragement, guidance and support in word and deed.

Special thanks go to Prof. Dr. Holger Stark for giving us access to the electron microscopy facility in his department, as well as for his wise advice and helpful suggestions during our meetings.

I am also grateful to Prof. Dr. Dirk Fasshauer for being supportive in every situation and for remaining a member of my PhD committee in the toughest of times.

This study would not have been possible without Dr. Florian Hauer, who patiently analyzed all our electron microscopy samples and always remained optimistic and positive.

Jonathan Melin and I shared many ups and downs, working together on several projects, and a significant part of this work would not have been possible without his help. Besides that, I would like to acknowledge his critical reading of all our manuscripts and documents (including this one).

Christian Schulz was always supportive in sharing his constructs, strains, primers, peptides and proteins. I am also grateful to him for interesting discussions and co-working on the Tim50 project.

I learned a lot about FPLC from Klaus Neifer, who also helped a lot with protein purifications. Markus Kilisch taught me, how to operate SPR and actively participated in all our SPR measurements.

Alwaleed, Bartek, Bettina, Christine, Dana, David, Fabian, Isotta, Jan, Maria, Markus, Martina, Milena, Mirjam, Moritz, Robert, Sara and Sven are responsible for the best possible working atmosphere. I am very grateful to them for always being helpful and supportive.

I would also like to thank the IMPRS Molecular Biology program and especially Dr. Steffen Burkhardt for many interesting and purposeful years in Göttingen.

And, of course, nothing would be possible without the support and care of my wife and my parents. Many thanks to them!

Table of Contents

List of publications.....	iii
Acknowledgements	iv
Table of Contents.....	v
List of Figures	viii
List of Tables.....	ix
Abbreviations.....	x
Abstract.....	1
1. Introduction.....	2
1.1. The significance of mitochondria	2
1.2. Endosymbiotic origin of mitochondria.....	3
1.3. Mitochondrial respiratory chain	4
1.4. Mitochondrial import pathways	6
1.4.1. Mitochondrial targeting signals	6
1.4.2. The variety of import pathways.....	7
1.4.3. Presequence pathway and the TIM23 complex	10
1.5. The aims of the work.....	14
2. Materials and methods	17
2.1. Materials	17
2.1.1. Chemicals, oligonucleotides and peptides.....	17
2.1.2. Buffers and solutions.....	19
2.1.3. Antibodies	19
2.1.4. Plasmids.....	19
2.1.5. Yeast strains	19
2.1.1. <i>E. coli</i> strains	20
2.1.2. Kits and disposals	22
2.1.3. Equipment.....	22
2.1.4. Software.....	24
2.2. Cultivation of <i>E. coli</i>	24
2.2.1. Media and growth conditions for <i>E. coli</i>	24
2.2.2. Preparation of transformation competent <i>E. coli</i> cells.....	25
2.2.3. Transformation of <i>E. coli</i>	25
2.3. Molecular biology techniques	25
2.3.1. DNA isolation from <i>E. coli</i>	25
2.3.2. Polymerase chain reaction (PCR).....	26
2.3.3. Agarose gel electrophoresis	26
2.3.4. Molecular cloning.....	27
2.3.5. Site-directed mutagenesis.....	28
2.3.6. Sequencing of DNA	28
2.4. Cultivation of <i>S. cerevisiae</i> and preparation of mitochondria	29
2.4.1. Yeast media and growth conditions.....	29
2.4.2. Yeast transformation	29

2.4.3.	Preparation of mitochondria.....	30
2.5.	Purification of proteins and protein complexes	31
2.5.1.	Expression of recombinant proteins in <i>E. coli</i>	31
2.5.2.	Immobilized metal affinity chromatography	31
2.5.3.	Ion exchange chromatography.....	32
2.5.4.	Size exclusion chromatography	33
2.5.5.	IgG affinity chromatography	33
2.5.6.	Coimmunoprecipitation	34
2.5.7.	Protein precipitation by trichloroacetic acid (TCA)	35
2.6.	Biochemical analysis of proteins and protein complexes	35
2.6.1.	Determination of protein concentration	35
2.6.2.	Chemical cross-linking <i>in vitro</i>	36
2.6.3.	SDS-PAGE	36
2.6.4.	BN-PAGE	37
2.6.5.	Coomassie Brilliant Blue staining	37
2.6.6.	Colloidal Coomassie staining.....	38
2.6.7.	Western blotting and immunodecoration	38
2.6.8.	Digital autoradiography	39
2.6.9.	Glycerol density gradient centrifugation	39
2.6.10.	Surface plasmon resonance (SPR) measurements.....	39
2.6.11.	Mass-spectrometry.....	40
2.7.	Assays in isolated mitochondria	40
2.7.1.	<i>In vitro</i> translation of ³⁵ S radiolabeled proteins.....	40
2.7.2.	Protein import into isolated mitochondria	40
2.7.3.	Mitochondrial membrane solubilization.....	41
2.7.4.	Precursor arrest and formation of TOM-TIM23 supercomplex	41
2.7.5.	Preparation of mitoplasts by osmotic swelling of mitochondria	42
2.7.6.	Chemical cross-linking in mitochondria.....	42
2.8.	Electron microscopy.....	43
2.8.1.	Gradient fixation (GraFix) of purified protein complexes	43
2.8.2.	Preparation of negatively stained electron microscopy samples	43
2.8.3.	Transmission electron microscopy	44
2.8.4.	Image processing and analysis	45
3.	Results	46
3.1.	Analysis of protein-protein interactions in the TIM23 translocase.....	46
3.1.1.	Identification of Tim50 cross-linking adducts.....	46
3.1.2.	The IMS domains of Tim21 and Tim50 interact <i>in vitro</i>	49
3.1.3.	Presequence binding to Tim50 is independent of Tim21	53
3.1.4.	Dynamics of Tim50 interactions in response to presequence	56
3.1.5.	Dynamics of the TIM23 complex.....	58
3.2.	Electron microscopy.....	61
3.2.1.	Initial electron microscopy analysis of the TIM23 complex	61
3.2.2.	Reduction of contaminations and background in EM samples.....	64
3.2.3.	Preparation of TIM22 and respiratory chain complexes for EM.....	65
3.2.4.	Optimization of conditions for TIM23 complex purification	68
3.2.5.	EM structure of the TOM-TIM supercomplex.....	72
4.	Discussion.....	75
4.1.	Dynamic interactions within the TIM23 complex	75
4.1.1.	Interactions of Tim50 <i>in organello</i> and <i>in vitro</i>	75

4.1.2. Presequence-induced changes in Tim50 interactions.....	77
4.1.3. Dynamics and mobility of TIM23 components.....	78
4.1.4. A model of preprotein import.....	79
4.2. Structural analysis of the TIM23 translocase.....	82
4.2.1. The background problem	82
4.2.2. Biochemical approaches to improve sample quality	84
4.2.3. Low-resolution structure of the TOM-TIM supercomplex.....	86
4.2.4. Perspectives and outlook.....	86
5. Summary and Conclusions.....	88
6. References	90
Curriculum Vitae	100

List of Figures

Figure 1.1.	Overview of the mitochondrial import pathways	9
Figure 1.2.	Two models of the TIM23 organization	14
Figure 3.1	Structures of the Tim21, Tim23 and Tim50 fragments	47
Figure 3.2	Identification of Tim50 cross-linking partners in mitochondria	48
Figure 3.3	Protein purification from <i>E. coli</i>	50
Figure 3.4	IMS domains of Tim21 and Tim50 interact <i>in vitro</i>	51
Figure 3.5	PBD of Tim50 is not required for interaction with Tim21	52
Figure 3.6	SPR analysis of Tim21 ^{IMS} -Tim50 ^{IMS} interaction	53
Figure 3.7	SPR analysis of presequence interaction with Tim50 fragments	54
Figure 3.8	Presequences do not affect Tim21-Tim50 interaction <i>in vitro</i>	55
Figure 3.9	Presequence peptides affect interactions between Tim21, Tim23 and Tim50 <i>in organello</i>	56
Figure 3.10	IMS domain of Tim23 affects Tim21 ^{IMS} -Tim50 interaction in mitoplasts	57
Figure 3.11	Co-immunoprecipitation experiments after presequence treatment	59
Figure 3.12	Non-denaturing analysis of the TIM23 complex	60
Figure 3.13	Purification and electron microscopy of the TIM23 complex	62
Figure 3.14	Gradient fixation of the purified TIM23 complex	63
Figure 3.15	Typical contaminations found in buffers and solutions	64
Figure 3.16	Removal of EM contaminations	65
Figure 3.17	Purification and EM of respiratory chain supercomplexes	67
Figure 3.18	Purification and negative stain EM of the TIM22 complex	68
Figure 3.19	Detergent exchange in GraFix	70
Figure 3.20	Optimizing detergent conditions	71
Figure 3.21	Import arrest of the b ₂ (167) _Δ -DHFR precursor and formation of the TOM-TIM supercomplex	72
Figure 3.22	Single particle EM analysis of the isolated TOM-TIM supercomplex	73
Figure 4.1	A model of matrix-targeted preprotein import	81

List of Tables

Table 2.1	List of chemicals	17
Table 2.2	Antibodies used in this study	20
Table 2.3	Plasmids used in this study	21
Table 2.4	Yeast strains used in this study	21
Table 2.5	Commercial kits and disposals	22
Table 2.6	Laboratory equipment	22
Table 2.7	Software used in this study	24
Table 2.8	Specific conditions for purification of His-tagged proteins	32
Table 3.1	Parameters of protein-protein interactions measured by SPR	52

Abbreviations

aa	amino acids
ATP	adenosine triphosphate
BN-PAGE	blue native polyacrylamide gel electrophoresis
BSA	bovine serum albumin
Cryo-EM	cryo electron microscopy
CD	cyclodextrin
DNA	deoxyribonucleic acid
DDM	dodecylmaltoside
dNTP	2'-deoxynucleoside-5'-triphosphate
DTT	dithiothreitol
<i>E. coli</i>	<i>Escherichia coli</i>
ECL	enhanced chemical luminescence
EDTA	ethylenediaminetetraacetic acid
EM	electron microscopy
ER	endoplasmic reticulum
FeS	iron-sulfur
HEPES	4-(2-hydroxyethyl)-1-piperazineethanesulfonic acid
IgG	immunoglobulin G
IMP	inner membrane peptidase
IMM	inner mitochondrial membrane
IMS	intermembrane space
IP	immunoprecipitation
IPTG	isopropyl- β -D-thiogalactopyranoside
kDa	kilodalton
MPP	mitochondrial processing peptidase
MNG	maltose-neopentyl glycol
mRNA	messenger RNA
NAD ⁺	nicotinamide adenine dinucleotide (oxidized)
OD	optical density

OMM	outer mitochondrial membrane
PAGE	polyacrylamide gel electrophoresis
PAM	presequence translocase associated motor
PBD	presequence-binding domain
PBS	phosphate buffered saline
PCR	polymerase chain reaction
PMSF	phenylmethanesulphonyl fluoride
PVDF	polyvinylidene fluoride
RNA	ribonucleic acid
RC	respiratory chain
rpm	rotations per minute
<i>S. cerevisiae</i>	<i>Saccharomyces cerevisiae</i>
SAM	sorting and assembly machinery of outer membrane
SEM	standard error of the mean
SEM buffer	sucrose-EDTA-MOPS buffer
SDS	sodium dodecyl sulfate
SDS-PAGE	sodium dodecyl sulfate-polyacrylamide gel electrophoresis
SPR	surface plasmon resonance
TAE	Tris / Acetate / EDTA buffer
TIM22	carrier translocase of the inner mitochondrial membrane
TIM23	presequence translocase of the inner mitochondrial membrane
TM	transmembrane span
TOM	translocase of the outer mitochondrial membrane
UV	ultraviolet
v/v	volume per volume
w/v	weight per volume
WB	western blot
wt	wild type
$\Delta\Psi$	membrane potential

Abstract

The yeast, *Saccharomyces cerevisiae*, mitochondrial proteome consists of approximately 1000 proteins, most of which are synthesized on cytosolic ribosomes and therefore require specialized transport systems to reach their final destinations. The TIM23 complex is a protein translocase localized to the inner mitochondrial membrane and responsible for transporting proteins containing N-terminal targeting signals, referred to as presequences. Presequence recognition by components of the translocase triggers a sequence of events, which cause significant rearrangements within the complex, leading to protein release into the mitochondrial matrix or its insertion into the inner mitochondrial membrane. Protein interactions involved in this pathway, especially at its early stages, are not studied thoroughly enough to create a non-controversial TIM23 mechanistic model. In this study, the dynamics of the translocase in response to presequences was investigated, focusing primarily on interaction partners of Tim50, an essential TIM23 component. Using a cross-linking approach, we identified a previously unknown interaction between Tim50 and Tim21, which was lost after presequence addition. Co-immunoprecipitation experiments connect the loss of this newly identified interaction to translocase isoform switching and concomitantly suggest Tim21 and Tim50 to be highly dynamic components of the TIM23 translocase.

A comprehensive understanding of protein transport via the presequence translocase is not possible without its structural characterization. One of the goals of this study was to obtain the structure of the TIM23 complex by means of single particle electron microscopy. The achievement of this goal was not possible, due to strong background signal caused by the detergent digitonin, required to maintain TIM23 stability. However, here we present a low-resolution structure of a negatively stained TOM-TIM supercomplex and its 3D reconstruction, providing novel insights into structural organization of the mitochondrial translocation machinery.

Together, our data contribute to the understanding of the mitochondrial presequence import pathway and provide a basis for further structural investigation of the TIM23 translocase.

1. Introduction

1.1. The significance of mitochondria

Evolution of all modern eukaryotic forms of life during the last 1.5-2 billion years would not be possible without mitochondria (Lane & Martin, 2010; Martin, 2011). Mitochondria are often referred to as the "powerhouses of the cell" for their ability to pump protons across the inner mitochondrial membrane, generating membrane potential, which is used to drive ATP synthesis.

However, their role in the cell is not restricted to the generation of energy. Mitochondria fulfill essential metabolic functions: biosynthesis of heme and iron-sulfur (FeS) clusters; participation in amino acid, nucleotide and lipid metabolism; generation of metabolic intermediates in the tricarboxylic acid cycle; regulation of metabolite levels in the cell (Lill & Mühlenhoff, 2005, 2008; Nunnari & Suomalainen, 2012). Besides that, mitochondria participate in cellular calcium homeostasis; they are critical players in apoptosis; in homeothermic organisms they participate in the thermogenesis by controlled uncoupling of substrate oxidation and ADP phosphorylation (Glancy & Balaban, 2012; Lenaz et al., 2010; Mailloux & Harper, 2011; Muñoz-Pinedo, 2012; Nunnari & Suomalainen, 2012).

It is important to mention that the energetic function of mitochondria may be not essential under certain conditions in many fermenting organisms, including baker's yeast *Saccharomyces cerevisiae* (*S. cerevisiae*), used as a model organism in this study. Moreover, in mitochondrion-related organelles of some microbial eukaryotes (such as mitosomes of *Trichomonas vaginalis* and *Giardia intestinalis*) this function is absent. The only common function for mitochondria and their derivatives in all species seems to be the biogenesis of FeS clusters, used by all organisms in enzymatic catalysis and electron transport (Shiflett & Johnson, 2010; van der Giezen & Tovar, 2005).

Considering the variety of mitochondrial functions, it is not surprising that mitochondrial dysfunction is related to a variety of diseases including cancer, neurodegenerative diseases, psychiatric disorders, ageing and diabetes (Brandon et al.,

2006; Correia et al., 2012; Lee & Wei, 2012; Ma et al., 2012; Newsholme et al., 2012; Nunnari & Suomalainen, 2012).

1.2. Endosymbiotic origin of mitochondria

According to the most widely accepted endosymbiotic theory, modern mitochondria evolved from an α -proteobacterial ancestor, which was acquired by an archaeobacterial-type cell, giving rise to all modern eukaryotic forms of life (Davidov & Jurkevitch, 2009; Martin, 2011). Many features of this gram-negative bacterium have been inherited by mitochondria (Dolezal et al., 2006; Kutik et al., 2009; Lithgow & Schneider, 2010; Schmidt et al., 2010). Similar to Gram-negative bacteria, mitochondria possess two membranes, the outer (OMM) and the inner mitochondrial membrane (IMM), enclosing two aqueous compartments, the matrix and the intermembrane space (IMS). The entire genetic system of the proteobacterial ancestor, including circular DNA and its transcription and translation machineries, has been maintained (Gray, 1999; Lang & Gray, 1999). Many components of the electron transport chain, metabolite carriers and protein import systems are also highly conserved, and striking similarities can be found between these systems in modern bacteria and in mitochondria (Becker, Böttinger, & Pfanner, 2011a; Dolezal et al., 2006; Kutik et al., 2009; Lithgow & Schneider, 2010).

However, in the course of evolution, ancestral mitochondria underwent significant changes. Most of the mitochondrial genes have been transferred to the host cell genome, and only few out of 1000-1500 mitochondrial proteins are now synthesized on mitochondrial ribosomes. The remaining 99% have to be imported via one of the specialized protein transport machineries (Forner et al., 2006; Kutik et al., 2009; Lithgow & Schneider, 2010; Sickmann et al., 2003). This work has been devoted to investigating such protein transport mechanisms, focusing primarily on one of them, the translocase of the inner mitochondrial membrane (TIM23), also called presequence translocase (section 1.4.3).

1.3. Mitochondrial respiratory chain

Production of energy by oxidative phosphorylation is the major function of the modern mitochondria. In this process, oxidation of substrates is utilized to generate membrane potential on the inner mitochondrial membrane, which is subsequently used by F_1F_0 ATP synthase as an energy source for ADP phosphorylation. Generation of the membrane potential is performed by respiratory chain, which consists of several membrane-spanning proton-pumping complexes. Organization of these complexes in different species can vary, but general features are highly conserved (Lenaz & Genova, 2010).

Complex I, the NADH-coenzyme Q oxidoreductase (or NADH dehydrogenase), is the first proton-translocating complex of the respiratory chain. It oxidases NADH and transfers two electrons to ubiquinone, using the released energy to translocate 4 protons from mitochondrial matrix to the IMS. This complex is absent in *S. cerevisiae*, where oxidation of cytosolic NADH is performed by such enzymes as Ndi1, Nde1 and Nde2; in this case, no proton translocation takes place (Carroll et al., 2006; Efremov & Sazanov, 2011; Friedrich & Böttcher, 2004; Lenaz & Genova, 2010). Complex I is the only respiratory chain complex, for which crystal structure is not available; however, significant structural information about its organization has been obtained by single particle electron microscopy. In all investigated species, it has a characteristic L-like shape, with two arms, a membrane one and a peripheral one (Dudkina et al., 2010a, 2010b).

Complex II, the succinate:quinone oxidoreductase (or succinate dehydrogenase), catalyzes oxidation of succinate to fumarate. Besides its metabolic role in the Krebs cycle, this reaction supplies two electrons to the respiratory chain, which are directly used for reducing ubiquinone. Complex II is the smallest respiratory chain complex, consisting only of four nuclear-encoded subunits; it does not participate in proton pumping (Lenaz & Genova, 2010; Oyedotun & Lemire, 2004).

Ubiquinone is a small hydrophobic molecule, which serves as a mobile electron carrier between complexes I and II, from the one side, and complex III, from the other (Genova & Lenaz, 2011). The reduced ubiquinone is oxidized by complex III, the

ubiquinol-cytochrome *c* oxidoreductase (also called the cytochrome *bc₁* complex). Yeast complex III consists of three catalytic (cytochrome *b*, Rieske iron-sulfur protein and cytochrome *c₁*) and seven auxiliary subunits (Cor1, Qcr2, Qcr6, Qcr7, Qcr8, Qcr9, and Qcr10) (Hunte, 2003). At least one of these subunits, Qcr6, is involved in interactions with the TIM23 complex via Tim21 (see below).

Complex IV, the cytochrome *c* oxidase, is the terminal complex of the electron transport chain. It is a heme-copper oxygen reductase, catalyzing reduction of oxygen to water; together with complex III, it contributes to generation of the proton gradient. In yeast complex IV consists of 11 subunits, 3 of which are encoded in the mitochondrial genome.

The respiratory chain complexes, both in yeast and higher eukaryotes, tend to form higher-order structures, termed respiratory chain supercomplexes, or respirasomes. This organization provides kinetic advantages in electron transfer and reduces formation of reactive oxygen species (Lenaz et al., 2010). In *S. cerevisiae*, such supercomplexes can include two units of complex III and one or two units of complex IV. The supercomplexes can be observed after purification in mild detergent, such as digitonin, using native electrophoresis techniques, such as Blue native PAGE (BN-PAGE). Their structures from different species, including *S. cerevisiae*, have been recently obtained using single particle electron microscopy (Dudkina et al., 2010; Heinemeyer et al., 2007; Mileykovskaya et al., 2012).

Mitochondrial F₁F₀ ATP synthase (complex V) utilizes proton gradient produced by the respiratory chain complexes III and IV (in higher eukaryotes, also complex I) to catalyze ATP synthesis from ADP and inorganic phosphate. The structure of the F₁F₀ ATP synthase, both from yeast and higher eukaryotes, has been extensively studied by electron microscopy, with different studies focusing on particular features or fragments of the complex (Bueler & Rubinstein, 2008; Couoh-Cardel et al., 2010; Lau et al., 2008; Lau & Rubinstein, 2010; Rubinstein et al., 2005; 2003). These studies contributed significantly to our understanding of the overall architecture and organization of this complex (Muench et al., 2011). The mitochondrial ATP synthase forms dimers and higher

oligomers in the membrane. This oligomerization is considered to be a prerequisite for membrane bending and cristae formation (Wagner et al., 2009).

1.4. Mitochondrial import pathways

1.4.1. Mitochondrial targeting signals

Mitochondrial proteome consists of about 1000 proteins in *S. cerevisiae* and 1500 proteins in higher eukaryotes. At the same time, yeast mitochondrial genome encodes only 8 of them; in human mitochondria, 13 proteins are synthesized on mitochondrial ribosomes (Forner et al., 2006; Mick et al., 2011; Prokisch et al., 2004; Reinders et al., 2006; Sickmann et al., 2003). Mitochondrial-encoded proteins are mostly represented by highly hydrophobic components of the respiratory chain and utilize the OXA1 export machinery for their translocation (Bonney et al., 2009). This pathway utilizes co-translational insertion mechanism, as the OXA1 complex directly recruits ribosomes to the membrane. To the contrary, all the nuclear-encoded proteins have to be transported post-translationally. There are four possible destinations in mitochondria: the outer and the inner mitochondrial membranes, matrix and intermembrane space. Specific signals within the protein sequence ensure proper targeting to each of these locations (Bolender et al., 2008; Chacinska et al., 2009). There are several types of such targeting signals; the most common ones are described below.

Presequences, the N-terminal cleavable amphipathic sequences, 15-100 amino acid residues in length, represent the most abundant and well-defined type of the signal (Vögtle et al., 2009). Transport of these proteins across the outer mitochondrial membrane is mediated by the TOM complex, followed by the inner membrane translocase TIM23 (see below). In most cases, presequence-containing proteins (also called precursors or preproteins) are targeted into the mitochondrial matrix. In this case, presequence is removed by a mitochondrial processing peptidase (MPP) (Taylor et al., 2001). However, in some proteins the presequence is followed by a non-cleavable hydrophobic sorting signal. This signal causes translocation arrest in the TIM23 complex and subsequent lateral release of the preprotein into the inner mitochondrial membrane. For a few IMS-targeted proteins, additional cleavage event by an inner membrane peptidase releases the protein from the membrane into the IMS (Chacinska et al., 2009).

Although presequences are the most common targeting signals, at least 30% of mitochondrial proteins contain non-cleavable signals. These signals are not completely characterized poorly defined; however, they can be divided into several classes (Bolender et al., 2007; Chacinska et al., 2009).

Outer membrane proteins never contain presequences. Instead they use signals of two types: (1) a C-terminal β -signal, utilized by β -barrel outer membrane proteins and recognized by TOM and SAM (see below), and (2) α -helical-type signals, utilized by the α -helical outer membrane proteins, which are inserted via Mim1 pathway (Chacinska et al., 2009; Kutik et al., 2008).

Finally, multispanning inner membrane proteins, such as the members of the metabolite carrier family, have multiple internal signals distributed over the entire protein sequence. These proteins are transported by the TIM22 complex (Rehling et al., 2003; Chacinska et al., 2009).

1.4.2. The variety of import pathways

The translocase of the outer mitochondrial membrane, TOM, is the general entry gate for mitochondrial proteins. It consists of the channel-forming subunit Tom40, presequence receptors Tom20, Tom22 and Tom70, and three small Tom proteins (Tom5, Tom6 and Tom7). Tom40 is a beta-barrel protein, together with the small Tom's forming the protein-conducting channel of the complex, also referred to as the general import pore (Model et al., 2008). Tom20 and Tom70 act as primary receptors for the incoming proteins, the former being responsible predominantly for presequence recognition, and the latter recognizing hydrophobic internal targeting signals. Tom22 plays important structural role in the complex and is also responsible for binding preproteins on the both sides of the outer mitochondrial membrane (Abe et al., 2000; Dudek et al., 2012). 3D electron microscopic structure of the TOM complex was obtained, revealing its 3-fold symmetry and presence of two or three transmembrane channels (Model et al., 2008).

However, not all mitochondrial proteins are transported via Tom40. Mim1 pathway, the most recently identified protein insertion machinery of the outer mitochondrial membrane, does not depend on the protein translocation via the Tom40 channel. This

pathway is used for α -helical outer membrane proteins, such as most of the components of the TOM machinery itself (Becker et al., 2011; Dudek et al., 2012).

β -barrel proteins of the outer membrane are first imported by TOM into the IMS. In the IMS they are chaperoned by so-called small Tim's, which form two hexameric complexes: the essential Tim9-Tim10 and Tim8-13, involved mainly in the biogenesis of Tim23 (Becker et al., 2011). Further insertion of these proteins into the membrane is done by the sorting and assembly machinery of the outer mitochondrial membrane, the SAM complex (also known as the translocase of outer membrane beta-barrel proteins, TOB). The complex contains Sam50, the pore-forming subunit, and two peripheral components, Sam35 and Sam37 (Wiedemann et al., 2003; Dudek et al., 2012; Kutik et al., 2008).

The majority of IMS proteins is imported by the MIA pathway. The intermembrane space of mitochondria is considered to be homologous to the periplasm of the ancestral α -proteobacterium. Similar to the bacterial periplasm and in contrast to the predominantly reducing cytosol, IMS provides oxidative environment to the imported proteins (Herrmann et al., 2009; Kutik et al., 2009). The MIA pathway utilizes cysteine residues for protein import into the IMS. The proteins are transferred through the Tom40 channel in a reduced state; Mia40 binds to them in the IMS and forms transient disulfide bonds with characteristic cysteine motifs Cx₃C or Cx₉C. Erv1, a sulfhydryl oxidase of the intermembrane space, catalyzes oxidation of sulfhydryl bonds in Mia40; the resulting electrons are moved to respiratory chain via cytochrome *c* (Herrmann & Riemer, 2012; Becker et al., 2011).

Non-cleavable multispanning inner membrane proteins are inserted into the membrane by the TIM22 complex. Chaperoning of these proteins through the IMS requires action of the small Tim proteins, which are also needed for the SAM-mediated insertion of outer membrane proteins. The TIM22 complex itself consists of the following components: Tim54, Tim22, Tim18, and Sdh3, and associates with the small Tim's (Tim9, Tim10 and Tim12). 2D electron microscopic structure revealed the presence of a twin pore, which is formed by the central subunit of the complex, Tom22 (Rehling et al., 2003).

The described import pathways are presented in Fig. 1.1.

The presequence pathway, mediated by the presequence translocase of the inner mitochondrial membrane, executes matrix import and inner membrane insertion of presequence-carrying precursors. For protein translocation into the matrix it interacts with a presequence translocase associated motor, PAM. This pathway will be discussed in more details the next section.

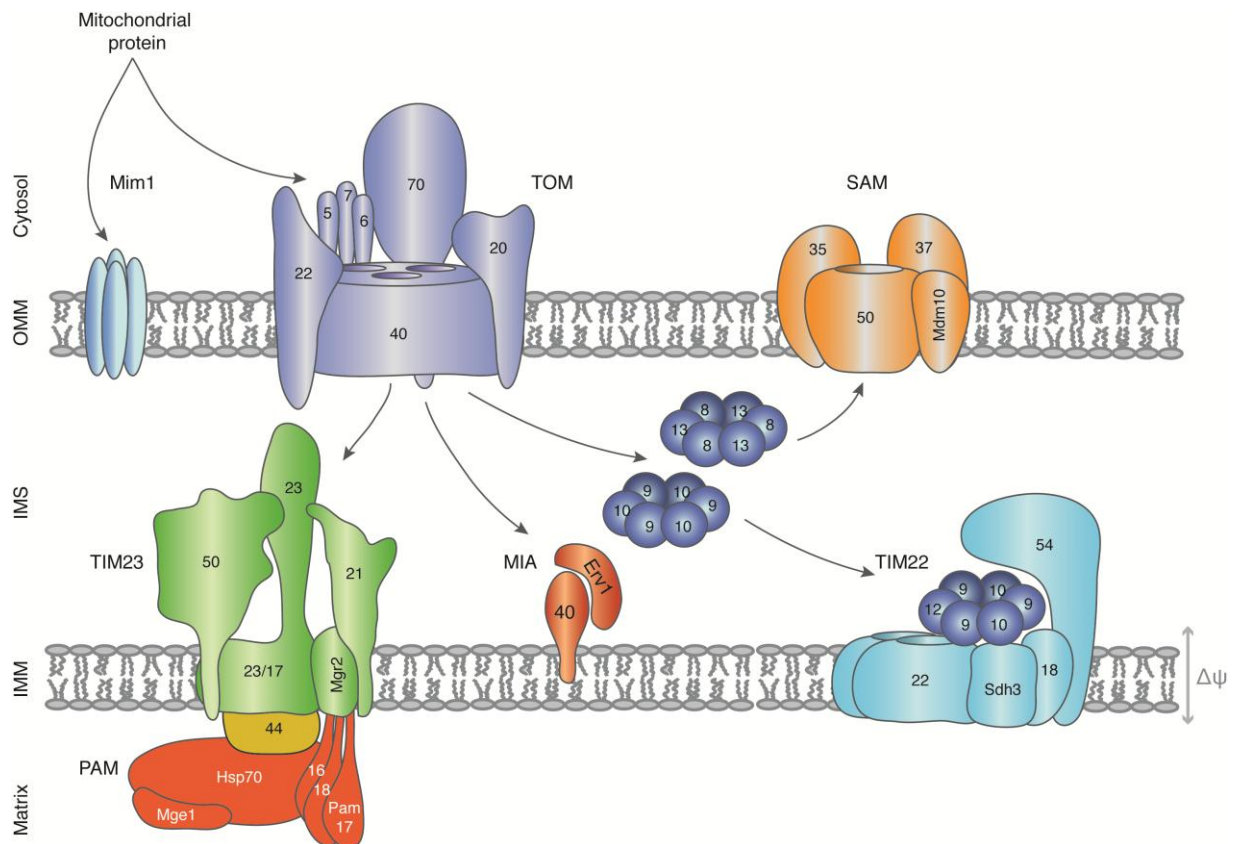


Figure 1.1. Overview of the mitochondrial import pathways

General import mechanisms of the mitochondrial proteins are shown. Outer membrane insertion via TOM and SAM complexes, as well as Mim1-dependent insertion are shown. Small Tim chaperones in the IMS (essential Tim9-Tim10 complex and non-essential Tim8-Tim13) deliver proteins to TIM22 and SAM. Mia40 and its sulfhydryl oxidase Erv1 are the key players in the disulfide relay system. TIM23 is shown in a single-entity form, with all components present (this instance not existent in the cell). $\Delta\psi$, membrane potential; IMM, inner mitochondrial membrane; OMM, outer mitochondrial membrane; IMS, intermembrane space. Arrows indicate divergence of pathways.

1.4.3. Presequence pathway and the TIM23 complex

Most of the mitochondrial proteins utilize cleavable N-terminal signaling sequences, referred to as presequences (Vögtle et al., 2009). Import of these proteins across the inner mitochondrial membrane or their insertion into it is mediated by a translocase of the inner mitochondrial membrane, the TIM23 complex (or the presequence translocase). For matrix transport, its association with its subcomplex, presequence translocase-associated motor (PAM) is required.

The first essential component of the complex, known for almost 20 years, is Tim23 (Dekker et al., 1993). Tim23 is the central channel-forming translocase subunit (Alder et al., 2008a; Truscott et al., 2001; van der Laan et al., 2007). Although Tim17 also contributes to the channel formation, purified Tim23 alone is able to form a voltage-gated, presequence-activated, cation-specific channel in a lipid bilayer (Truscott et al., 2001).

Tim23 is a multispanning membrane protein, with its C-terminus forming four transmembrane helices and an N-terminal domain, Tim23^{IMS}, exposed to the intermembrane space. This domain participates in the presequence recognition and was shown to dimerize in an inactive state of the translocase in a Tim50-dependent manner (Bauer et al., 1996; Meinecke et al., 2006; de la Cruz et al., 2010). Presequences dissociate the Tim23 dimer and thus contribute to the opening of the channel (Bauer et al., 1996; Meinecke et al., 2006).

It was suggested that the first twenty N-terminal residues of the Tim23^{IMS} penetrate the outer mitochondrial membrane and are exposed to the cytosol in an active translocase during preprotein import (Donzeau et al., 2000; Popov-Čeleketić et al., 2008). However, in other studies this observation has been questioned (Chacinska et al., 2003) and will not be addressed in the current work.

Another essential protein that contributes to formation of the channel is Tim17. Despite significant homology to Tim23 and Tim22 and its evolutionary conservation (Bömer et al., 1996), Tim17 itself does not form a protein-conducting channel. Instead, it stabilizes the Tim23-formed channel and is responsible for its voltage sensitivity. Patch-clamp studies revealed that normally the TIM23 channel contains two cooperatively

gated equal pores, whereas in the absence of Tim17 only one pore is formed (Martinez-Caballero et al., 2006). In addition, Tim17 may regulate differential sorting of matrix-targeted and laterally released proteins by the TIM23 complex; also its role for tethering PAM to TIM23 has been suggested (Chacinska et al., 2005, 2010). Tim17 may also play an unrelated role in the maintenance of the mitochondrial genome, at least in higher eukaryotes, as can be judged from its ability to suppress mitochondrial DNA instability in human cell culture model (Iacovino et al., 2009).

The third essential TIM23 component is Tim50, discovered in 2002. It is one of the central components of the TIM23 translocase; a significant part of this study has been devoted to investigating its physical interactions with other proteins. To date, known interaction partners of Tim50 include Tim23, Tom22 and presequences. Tim50 contains a transmembrane span and a large C-terminal domain exposed to the IMS (Fig. 3.1). (Geissler et al., 2002; Mokranjac et al., 2003; Yamamoto et al., 2002).

Tim50 is the first protein in the IMS that binds emerging presequences; this interaction is essential for the subsequent presequence transfer to the TIM23 channel (Geissler et al., 2002; Mokranjac et al., 2003; Yamamoto et al., 2002). Interaction of Tim50 with Tim23 has been actively studied in the recent years and was shown to be also essential for preprotein transport (Alder et al., 2008b; Gevorgyan-Airapetov et al., 2009; Tamura et al., 2009).

There has been some controversy concerning presequence binding to Tim50. Initial experiments suggested that Tim50–presequence interaction is dependent on the presence of Tim23 (Mokranjac et al., 2003; Mokranjac & Sichtung, 2009; Yamamoto et al., 2002). Several possible explanations have been suggested, including Tim23-induced conformational changes in Tim50, necessary for presequence binding, or formation of presequence-binding site by both proteins (Marom et al., 2011). However, more focused studies revealed that Tim50 can act as a primary presequence receptor and presequence binding does not depend on the Tim23-Tim50 interaction. Moreover, an essential role of presequence recognition by a C-terminal fragment of Tim50, named presequence-binding domain (PBD), was shown (Schulz et al., 2011). At the same time, another potential presequence-binding region has been suggested, based on a crystal structure of

a core Tim50 fragment (amino acids 164-361), lacking the PBD (Qian et al., 2011). In the current work, this discrepancy has been addressed, resulting in a suggestion that both sites might contribute to presequence binding (section 3.1.3).

Another essential function of the Tim50 IMS domain is maintaining the Tim23 channel closed when no precursor protein is present, in order to prevent ion leakage and membrane potential dissipation. This effect is presequence-dependent and was suggested to be mediated by regulated oligomerization of the Tim23^{IMS} (Meinecke et al., 2006).

Tim21 is a non-essential, although conserved, component of the translocase. Tim21 deletion has no effect on respiratory and fermentative growth of yeast under normal conditions. Similar to Tim50, Tim21 has a single transmembrane span and an IMS domain, Tim21^{IMS}. Tim21^{IMS} interacts with the IMS domain of Tom22 and with respiratory chain complexes III and IV. Tim21 also participates in switching between different forms of the TIM23 complex: TIM23^{SORT}, which is responsible for lateral release of the proteins into the inner mitochondrial membrane, was shown to contain Tim21, whereas TIM23^{CORE}, responsible for matrix targeting, lacks Tim21 (Albrecht et al., 2006; Chacinska et al., 2005; Mokranjac et al., 2005; Gebert et al., 2012; Wiedemann et al., 2007; van der Laan et al., 2006).

Mgr2 is the most recently identified subunit of the TIM23 complex. This small non-essential protein promotes interaction between TIM23 with TOM and respiratory chain complexes. Moreover, it is involved in formation of the TIM23^{SORT} complex, being required for Tim21 binding to the core of the translocase (Gebert et al., 2012).

Matrix import of the presequence-containing proteins requires association of TIM23 with its subcomplex, the presequence translocase-associated motor, PAM. The motor consists of several subunits, which associate with the presequence translocase in a dynamic manner. Ssc1, or mitochondrial Hsp70, is the ATP-consuming motor subunit. Mge1 is its nucleotide exchange factor; Pam18 is an essential J-protein, stimulating ATPase activity of Ssc1; Pam16 binds to Pam18 and regulates its activity; Pam17 is a non-essential subunit involved in the early PAM assembly and mediating association between Pam16 and Pam18; Tim44 is essential for motor binding to TIM23 (Bolender et

al., 2008; Chacinska et al., 2009; Popov-Čeleketić et al., 2008; Schiller, 2009; Hutu et al., 2008).

TIM23 physically interacts with the respiratory chain supercomplexes formed by complexes III and IV (Gebert et al., 2012; Wiedemann et al., 2007; van der Laan et al., 2006). This interaction depends, at least to some extent, on physical binding of Tim21^{IMS} to Qcr6, a subunit of the complex III (Nils Wiedemann et al., 2007). Mgr2 is required for binding of Tim21 to the rest of the TIM23 complex (Gebert et al., 2012). Besides that, a Tim21-independent interaction between Pam16/Pam18 and respiratory chain supercomplexes has been shown (Nils Wiedemann et al., 2007).

The TIM23 complex is highly dynamic and undergoes significant rearrangements during its reaction cycle (Bohnert et al., 2007; Chacinska et al., 2009; van der Laan, Rissler, & Rehling, 2006). These rearrangements have been reflected in two polar views on its organization (Fig. 1.2). A “single-entity” translocase model (Fig.1.2A) states that all essential components of TIM23 and PAM are present in one complex at all times, and only Tim21 and Pam17, the two non-essential components of the translocation machinery, are associated with the translocase in a dynamic and mutually exclusive manner (Popov-Celeketić et al., 2008).

The other model (Fig. 1.2B) suggests modular organization of the TIM23 complex, with at least two forms existing. According to this model, the Tim21-containing complex, TIM23^{SORT}, is responsible for lateral sorting of proteins into the inner mitochondrial membrane. This complex lacks motor subunits, whereas its interaction with respiratory chain is facilitated by the presence of Tim21. Another form of the complex (TIM23^{CORE}) is associated with PAM, lacks Tim21 and is required for the matrix-targeted transport of preproteins (Chacinska et al., 2005; Wiedemann et al., 2007; van der Laan et al., 2006). According to both models, Tim21 and Pam17 modulate functions of the translocase in an antagonistic manner and are never present in it at the same time.

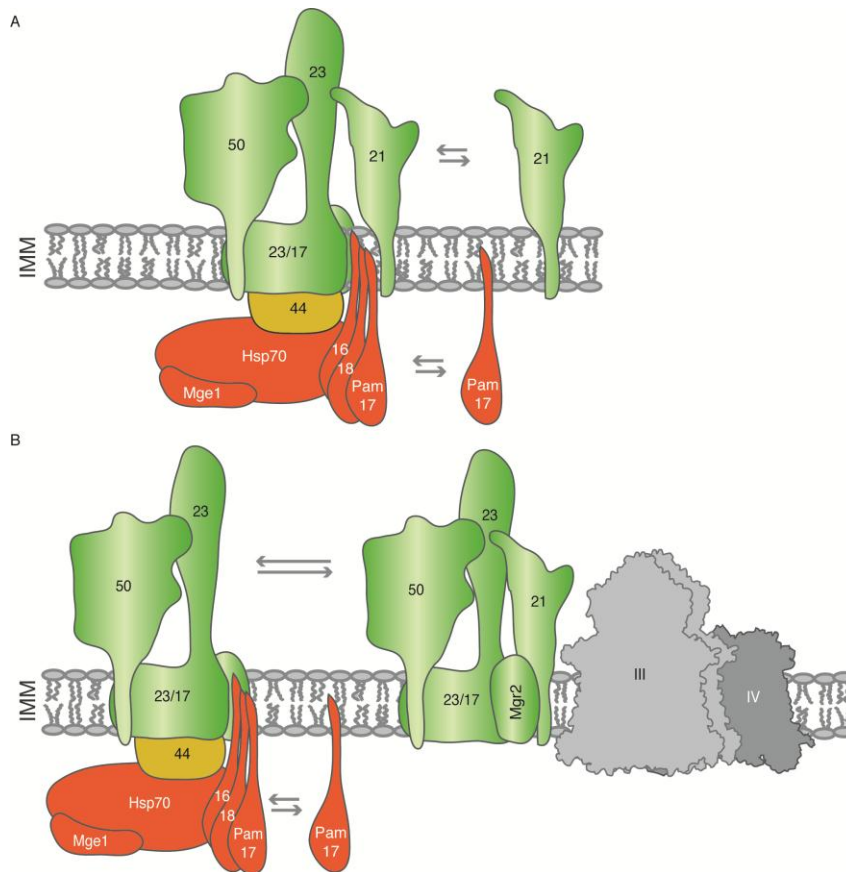


Figure 1.2. Two models of the TIM23 organization

(A) The single-entity translocase model. Arrows indicate dynamically associated components, Tim21 and Pam17, associating with the translocase in a mutually exclusive manner. (B) The modular translocase model. Pam17 participates in the early stages of precursor translocation and motor assembly and is absent from the fully assembled motor. Binding of respiratory chain and PAM are not mutually exclusive, and PAM can interact with the respiratory chain complexes independent of Tim21 (not shown). IMM, inner mitochondrial membrane; III, respiratory chain complex III; IV, respiratory chain complex IV. Further details are in the text.

It should be mentioned that most of the discrepancies between the two models are rather quantitative than qualitative. They can be explained by high dynamics of the translocase, where different forms represent particular “snap-shots” of the TIM23 working cycle (Chacinska et al., 2009). This view is reflected in the model proposed in the current work (section 4.1.4).

1.5. The aims of the work

The presequence pathway is one of the most complicated, controversial and intriguing mechanisms of mitochondrial protein import. Significant amount of data has been accumulated concerning individual components of this pathway; however, our understanding of underlying processes and mechanisms is far from being complete.

There is still a long way to go before separate pieces of data will be combined into a comprehensive non-controversial model. Contributing to this goal was the primary purpose of this study.

Investigating protein-protein interactions in the TIM23 complex was the first approach used to get functional insights into the presequence pathway. We aimed to study dynamics of these interactions, focusing on early stages of preprotein import. Several recent studies emphasized the importance of Tim50 in the early presequence pathway as one of the central translocase components and the first TIM23 protein interacting with preproteins emerging from TOM (Gevorkyan-Airapetov et al., 2009; Mokranjac et al., 2009; Qian et al., 2011; Schulz et al., 2011; Tamura et al., 2009; Zhang et al., 2012). Based on this, studying interactions of Tim50 with presequences and other proteins of the TIM23 complex was the starting point and the first aim of the project.

The import cycle of TIM23 is a multistep process based on many transient protein-protein interactions within the complex and with its partner complexes. During preprotein import, TIM23 undergoes significant rearrangements, involving association and dissociation of individual subunits and other changes (Becker, Böttinger, & Pfanner, 2011b; Chacinska et al., 2009). Different models were proposed to explain the observed effects, but, to date, the consensus has not been achieved. The next goal of the project was closely related to the first part and was to investigate mobility of the TIM23 components in response to presequences.

The last part of the study was devoted to structural investigations of the TIM23 complex by electron microscopy. Recent technical advances in single particle microscopy and cryo-electron tomography made this method increasingly important in the mitochondrial field (Althoff et al., 2011; Davies et al., 2011; Dudkina et al., 2010a, 2010b). Obtaining subnanometer resolution of a membrane-bound complex, the H⁺-driven ATP synthase from *Thermus thermophilus*, confirmed that electron microscopy can be applied to study membrane complexes with the efficiency comparable to x-ray crystallography (Rubinstein, 2007; Schmidt-Krey & Rubinstein, 2011; Lau & Rubinstein, 2012). Development of a sample preparation method, called GraFix (for gradient fixation), which combines glycerol gradient centrifugation with gradual sample fixation

(for example, in a glutaraldehyde gradient) was another important prerequisite for this study (Kastner et al., 2008; Stark, 2010). Preparation of the TIM23 complex in a form suitable for electron microscopy and obtaining its structure by single particle analysis was the final goal of this part of the project.

2. Materials and methods

2.1. Materials

2.1.1. Chemicals, oligonucleotides and peptides

Standard reagents were purchased from AppliChem (Darmstadt, Germany), Bio-Rad (Richmond, USA), Merck (including Calbiochem and Novagen) (Darmstadt, Germany), MP Biomedicals (Eschwege, Germany), Promega (Mannheim, Germany), Roche (Mannheim, Germany), Roth (Karlsruhe, Germany), Serva (Heidelberg, Germany), and Sigma-Aldrich (Taufkirchen, Germany). Some specific components for yeast and *E. coli* media were purchased from BD (Heidelberg, Germany) and MP Biomedicals (Eschwege, Germany). Enzymes and buffers for molecular biology were from Fermentas (St. Leon-Rot, Germany), New England Biolabs (Ipswich, USA), Novagen (Darmstadt, Germany), and Roche (Mannheim, Germany). Oligonucleotides were ordered at Metabion (Martinsried, Germany). Synthetic peptides pCox4 (MLSLRQSIRFFKPATRTLSSSRYL), SynB2 (MLSRQQSQRQSRQQSQRQSRYL) and pALDH-s (MLRGKQPTKSLLPQRSPKLSAAA) (Abe et al., 2000; Allison & Schatz, 1986; Schulz et al., 2011; de la Cruz et al., 2010) were purchased from JPT Peptide Technologies (Berlin, Germany). pALDH (MLRAALSTARRGPRLSRLLSAA) (Abe et al., 2000) was provided by the Proteomics Group, Max-Planck Institute for Experimental Medicine (Göttingen, Germany).

The complete list of individual products and suppliers is given in Table 2.1.

Table 2.1. List of chemicals

Chemical	Supplier
Acetic acid	Roth
Acetone	AppliChem or Merck
Acrylamide-bisacrylamide (37.5 : 1) solution	AppliChem or Roth
Acrylamide, 4x crystallized	Roth
Agarose NEEO ultra-quality	Roth
Alkaline phosphatase, shrimp	Roche
6-aminocaproic acid	Sigma-Aldrich
Ammonium acetate	Merck
Ammonium peroxodisulfate	Merck
Ampicillin	AppliChem
ATP (adenosine-5'-triphosphate)	Roche
Bacto™ Agar	BD
Bacto™ Peptone	BD
Bacto™ Tryptone	BD

2. Materials and Methods

Chemical	Supplier
Bacto™ Yeast Extract	BD
Bio-Rad Protein Assay	Bio-Rad
Bis-Tris Buffer grade	AppliChem
Bovine serum albumin	Sigma-Aldrich
Bromophenol blue	Merck
Complete amino acid supplement mixture without tryptophane (CSM-Trp)	MP Biomedicals
Complete EDTA-free protease inhibitor mix	Roche
Coomassie Brilliant Blue G250	Serva
Coomassie Brilliant Blue R250	Serva
Copper (II) sulfate, pentahydrate	Merck
Creatine kinase	Roche
Creatine phosphate	Roche
Deoxynucleotide triphosphate mix (dNTPs)	New England Biolabs
DFDNB (1,5-Difluoro-2,4-dinitrobenzene)	Thermo Scientific
Digitonin	Calbiochem
Dipotassium hydrogen phosphate	Roth
DMSO (dimethylsulfoxide)	Applichem
DNA ladder mix "Gene ruler"	Fermentas
DTT (1,4-dithiothreitol)	Roth
Ethanol	Roth
Ethidium bromide 0.07%	AppliChem
Ethylenediaminetetraacetic acid (EDTA)	Roth
Glucose, D(+)	Roth
Glutaraldehyde, EM grade	Polysciences
Glycerol	Sigma-Aldrich
Glycine	Roth
HEPES (4-(2-hydroxyethyl)-1-piperazineethanesulfonic acid)	Roth
Herring sperm DNA	Promega
High molecular weight calibration kit for native electrophoresis	GE Healthcare
Hydrochloric acid 37 %	Roth
Immunoglobulin G (IgG), bovine	BioRad
Imidazole	Merck
IPTG (isopropyl-β-D-1-thiogalactopyranoside)	AppliChem
KOD Hot Start DNA polymerase	Novagen
Lithium acetate	AppliChem
β-mercaptoethanol	Sigma-Aldrich
Methanol	Roth
[35S]- L-methionine	Hartmann Analytic
MOPS (morpholinopropanesulfonic acid)	Sigma-Aldrich
Ni2+-NTA Agarose	Qiagen
NADH (nicotinamide adenine dinucleotide, reduced disodium salt)	Roche
Novex Sharp Protein Standard	Invitrogen
Oligonucleotides for PCR (various)	Metabion
PEG-4000 (polyethylene glycol 4000)	Merck
Peptides (various)	JPT
PMSF (phenylmethanesulfonylfluoride)	Roth
Potassium chloride	Roth
Potassium dihydrogen phosphate	Merck
Proteinase K	Roche
Restriction endonucleases	New England Biolabs
Roti-Quant	Roth
Saccharose	Roth
SDS (sodium dodecyl sulfate), in pellets	Serva
SDS-PAGE molecular weight standards, broad range	Bio-Rad

2. Materials and Methods

Chemical	Supplier
Sodium azide	Sigma
Sodium borate	Sigma
Sodium chloride	Roth
Sodium deoxycholate	Sigma-Aldrich
Sorbitol	Roth
β -Mercapthoethanol	Roth
TCA (trichloroacetic acid)	Merck
TEMED (tetramethylethylenediamine)	Roth
TEV protease	Invitrogen
Tricine	Roth
Tris (tris(hydroxymethyl)aminomethane)	Roth
Triton X-100	Sigma-Aldrich
Tween-20	Roth
Yeast nitrogen base without amino acids	BD
Zymolyase 20 T	Seikagaku Biobusiness

2.1.2. Buffers and solutions

Recipes of standard buffers and solutions used in different assays are given at the end of each section. All buffers were prepared from analytical grade chemicals using distilled or Milli-Q deionized water (Millipore) and, if necessary, autoclaved or filter-sterilized. All buffer compositions, unless otherwise stated, are given at working (1x) dilution.

2.1.3. Antibodies

Rabbit polyclonal antisera produced at Gramsch Laboratories (Schwabhausen, Germany) were used as primary antibodies for immunodetection of *Saccharomyces cerevisiae* proteins. Mouse monoclonal anti-HA antibodies were from Roche (Mannheim, Germany). Horseradish peroxidase (HRP)-conjugated or fluorescent dye-conjugated polyclonal goat anti-rabbit antibodies (from Dianova and LI-COR, respectively) were used as secondary antibodies. All used antibodies are listed in Table 2.2.

2.1.4. Plasmids

Plasmids used in this study are listed in Table 2.3. All plasmids were isolated from XL1-Blue *E. coli* cells as described in section 2.3.1. For long-term storage, glycerol stocks of *E. coli* were prepared (see section 2.2.1). Isolated plasmid DNA was stored at -20°C.

2.1.5. Yeast strains

Yeast strains used in this study and their genotypes are listed in Table 2.4.

Table 2.2. Antibodies used in this study

Primary antibodies		
Antigen	Antibody type	Source
Aco1	Rabbit polyclonal	Gramsch Laboratories
Cor1	Rabbit polyclonal	Gramsch Laboratories
Cox2	Rabbit polyclonal	Gramsch Laboratories
HA tag	Mouse monoclonal	Roche
Hsp70	Rabbit polyclonal	Gramsch Laboratories
Pam16	Rabbit polyclonal	Gramsch Laboratories
Pam17	Rabbit polyclonal	Gramsch Laboratories
Pam18	Rabbit polyclonal	Gramsch Laboratories
Rip1	Rabbit polyclonal	Gramsch Laboratories
Tim12	Rabbit polyclonal	Gramsch Laboratories
Tim13	Rabbit polyclonal	Gramsch Laboratories
Tim17	Rabbit polyclonal	Gramsch Laboratories
Tim18	Rabbit polyclonal	Gramsch Laboratories
Tim21	Rabbit polyclonal	Gramsch Laboratories
Tim22	Rabbit polyclonal	Gramsch Laboratories
Tim23	Rabbit polyclonal	Gramsch Laboratories
Tim44	Rabbit polyclonal	Gramsch Laboratories
Tim50	Rabbit polyclonal	Gramsch Laboratories
Tim54	Rabbit polyclonal	Gramsch Laboratories
Tom22	Rabbit polyclonal	Gramsch Laboratories
Tom40	Rabbit polyclonal	Gramsch Laboratories
Tom70	Rabbit polyclonal	Gramsch Laboratories

Secondary antibodies		
Description	Antibody type	Vendor
Goat anti-mouse, HRP-conjugated	Goat polyclonal	Dianova
Goat anti-rabbit, HRP-conjugated	Goat polyclonal	Dianova
IRDye® 680 Conjugated Goat Anti-Rabbit	Goat polyclonal	LI-COR

2.1.1. *E. coli* strains

For molecular cloning purposes, *E. coli* strain XL1-Blue (Stratagene) was used. Expression of recombinant proteins was done in BL21 strain (Stratagene). Genotypes of both strains are given below.

XL1-Blue	recA1 endA1 gyrA96 thi-1 hsdR17 supE44 relA1 lac [F' proAB lacI ^q ZΔM15 Tn10 (Tet ^r)]
BL21	F ⁻ dcm ompT hsdS(r _B ⁻ m _B ⁻) gal

2. Materials and Methods

Table 2.3. Plasmids used in this study

Plasmid	Backbone	Insert	Purpose	Source
pFL39	-	-	Backbone for expression of proteins in <i>S. cerevisiae</i>	Bonneaud et al., 1991
pGB9607	pFL39	Tim21	Expression of wild type Tim21 in <i>S. cerevisiae</i>	AG Rehling
pProEX HTa	-	-	Backbone vector for protein expression in <i>E. coli</i>	Invitrogen
pProEX HTc	-	-	Backbone vector for protein expression in <i>E. coli</i>	Invitrogen
pR12	pProEX HTa	Tim21 ^{IMS}	Expression of 6xHis-tagged Tim21 ^{IMS} (aa 103-225) in <i>E. coli</i>	Albrecht et al., 2006
pR95	pProEX HTa	Tim21 ^{IMS-C128S}	Expression of Tim21 ^{IMS} with C128S substitution in <i>E. coli</i>	This study
pRK793	pMal-C2	TEV ^{S219V}	Expression of tobacco etch virus (TEV) protease in <i>E. coli</i>	Addgene
pR157	pProEX HTa	Tim50 ^{APBD}	Expression of 6xHis-tagged Tim50 fragment (amino acids 164-361) in <i>E. coli</i>	Qian et al., 2011
pProEX-Tim50 ^{IMS}	pProEX HTc	Tim50 ^{IMS}	Expression of 6xHis-tagged Tim50 ^{IMS} (amino acids 133-476) in <i>E. coli</i>	Schulz et al., 2011
pProEX-Tim50 ^{PBD}	pProEX HTc	Tim50 ^{PBD}	Expression of Tim50 ^{PBD} (amino acids 395-476) in <i>E. coli</i>	Schulz et al., 2011
B07	pUHE24	b ₂ (167) _Δ -DHFR	Expression of b ₂ (167) _Δ -DHFR in <i>E. coli</i>	Koll et al., 1992

Table 2.4. Yeast strains used in this study

Strain	Genotype	Reference
YPH499	MATa <i>ade2-101 his3-Δ200 leu2-Δ1 ura3-52 trp1-Δ63 lys2-801</i>	Sikorski & Hieter, 1989
MB29	MATa <i>ade2 his3 leu2 lys2 ura3 trp1 tim23::LYS2 + YCplac33-TIM23(URA3)</i>	Bömer et al., 1997
<i>tim21Δ</i>	MATa <i>ade2-101 his3-Δ200 leu2-Δ1 ura3-52 trp1-Δ63 lys2-801 tim21::HIS3MX6</i>	Chacinska et al., 2005
Tim21 ^{ProtA}	MATa <i>ade2-101 his3-Δ200 leu2-Δ1 ura3-52 trp1-Δ63 lys2-801 tim21::TIM21^{ProtA}-HIS3MX6</i>	Chacinska et al., 2005
Tim23 ^{ProtA}	MATa <i>ade2 his3 leu2 ura3 trp1 lys2 tim23::LYS2 [pRS414-TIM23^{ProtA}]</i>	Geissler et al., 2002
Tim18 ^{ProtA}	MATa <i>ade2-101 his3-Δ200 leu2-Δ1 ura3-52 trp1-Δ63 lys2-801 tim18::TIM18^{ProtA}</i>	Rehling et al., 2003
Cor1 ^{TAP}	MATa <i>his3-Δ1 leu2Δ0 met15Δ0 ura3Δ0; cor1::cor1-TAP</i>	Wiedemann et al., 2007; van der Laan et al., 2006
Tim23↓	MATa <i>ade2-101 his3-Δ200 leu2-Δ1 ura3-52 trp1-Δ63 lys2-801 tim23::Lys2 [pCS28-HIS]</i>	Schulz et al., 2011
Tim50 ^{HA}	MATa <i>ade2 his3 leu2 lys2 ura3 trp1 pTIM50:pGAL1-HIS3MX6 [pME2782-TIM50^{HA}] (LEU2)</i>	Schulz et al., 2011
Tim50 ^{APBD-HA}	MATa <i>ade2 his3 leu2 lys2 ura3 trp1 pTIM50:pGAL1-HIS3MX6 [pME2782-TIM50(1-365)^{HA}] (LEU2)</i>	Schulz et al., 2011

2. Materials and Methods

2.1.2. Kits and disposals

Commercial kits and disposals listed in Table 2.5 were purchased from different suppliers and used in accordance with the manufacturers' instructions.

Table 2.5. Commercial kits and disposals

Product	Supplier
Kits	
BigDye® Terminator v1.1 Cycle Sequencing Kit	Applied Biosystems
ECL Plus Western Blotting Detection Reagents	GE Healthcare
KOD Hot Start DNA Polymerase	Novagen
PureYield™ Plasmid Miniprep System	Promega
QuikChange™ Site-Directed Mutagenesis Kit	Stratagene (Agilent Technologies)
Rapid DNA Ligation Kit	Fermentas
TNT® Quick Coupled Transcription/Translation System	Promega
Wizard® Plus SV Minipreps DNA Purification System	Promega
Wizard® SV Gel and PCR Clean-Up System	Promega
Disposables	
Immobilon-P Transfer Membrane	Millipore
Hyperfilm™ ECL films	GE Healthcare
MEDIX XBU radiographic films	XSPEC Technology
Amicon Ultra centrifugal filter units	Millipore
Minisart® syringe filters (0.20-0.45 µm)	Sartorius AG
Mobicol spin columns, with bottom plugs and filters	MoBiTec
Micro tube 1.5 ml and 2.0 ml	Sarstedt
CELLSTAR® Centrifuge Tubes 15 ml and 50 ml	Greiner Bio-One
Pipette tips 10 µl, 200 µl and 1000 µl	Sarstedt

2.1.3. Equipment

Laboratory equipment used in this study is described in Table 2.6.

Table 2.6. Laboratory equipment

Product	Supplier
FPLC equipment	
ÄKTA Purifier 10	GE Healthcare
HiLoad 16/60 Superdex 200 pg	GE Healthcare
HiLoad 16/60 Superdex 75 pg	GE Healthcare
HisTrap HP, 1 ml and 5 ml	GE Healthcare
HiTrap Q FF 1 ml	GE Healthcare
Resource™ S 1 ml	GE Healthcare
Superose™ 6 10/300 GL	GE Healthcare
Centrifuges and rotors	
Centrifuge 5417R	Eppendorf
Centrifuge 5424	Eppendorf
Centrifuge 5804R	Eppendorf
Rotor F45-30-11	Eppendorf
Rotor F45-24-11	Eppendorf
Rotor A-4-44	Eppendorf
L-80 ultracentrifuge	Beckman Coulter

2. Materials and Methods

Product	Supplier
Centrifuges and rotors (continued)	
Optima™ L-90K ultracentrifuge	Beckman Coulter
Ultracentrifuge rotor SW 60 Ti	Beckman Coulter
Ultracentrifuge rotor SW 41 Ti	Beckman Coulter
Sorvall® RC 6™ Plus Superspeed Centrifuge	Thermo Scientific
Rotor Sorvall F14S-6x250Y	Thermo Scientific
Rotor Sorvall F10S-6x500Y	Thermo Scientific
Rotor Sorvall SS-34	Thermo Scientific
Sorvall® RC12BPT™ Low-Speed Centrifuge	Thermo Scientific
Rotor Sorvall H-12000	Thermo Scientific
Equipment for electrophoresis and blotting	
EPS 601 power supply	GE Healthcare
Hoefer SE600 Ruby Blue native system	GE Healthcare
Mini-PROTEAN® 3 Cell	Bio-Rad
Mini-Sub® Cell GT Cell	Bio-Rad
Minifold® II Slot-Blot Manifold System	Whatman
PowerPac™ HC Power Supply	Bio-Rad
Semi Dry Blotting chamber	PEQLAB Biotechnologie
Scanners and gel documentation systems	
Agfa Curix 60 Developing machine	AGFA
Autoradiography Storage Phosphor Screen	GE Healthcare
LAS 1000	FujiFilm
Starion FLA-9000	FujiFilm
Storm 820 Phosphorimager	GE Healthcare
UVsolo TS transilluminator	Biometra
Other equipment	
Autoclave Systec DX-200	Systec
Balance BP 3100P	Sartorius
Electronic Digital Balance Kern ABJ 220-4M	KERN & Sohn
EmulsiFlex C5	Avestin
Excella® E10 platform shaker	New Brunswick Scientific
G 25 Shaker Incubator	New Brunswick Scientific
Gradient Master	BioComp Instruments
iMark™ Microplate Absorbance Reader	Bio-Rad
Innova® 44 Incubator Shaker	New Brunswick Scientific
GeneQuant™ 1300 Spectrophotometer	GE Healthcare
Magnetic stirrer MR 3001	Heidolph
Milli-Q-water purification system	Millipore
NanoVue™ Spectrophotometer	GE Healthcare
pH-meter	inoLab
Pipettes (different volumes)	Gilson
Potter S Homogenizer	Sartorius
SpeedVac concentrator	Savant
SPR Biosensor SR7000DC	XanTec bioanalytics
Thermomixer Comfort	Eppendorf
TPersonal 48 thermocycler	Biometra
Vortex-Genie 2	Scientific Industries

2.1.4. Software

Software used for data analysis and image processing is listed in Table 2.7.

Table 2.7. Software used in this study

Software	Purpose	Company
Adobe Illustrator CS3	Image processing	Adobe
Adobe Photoshop CS3	Image processing	Adobe
DataGraph 3.0	Creation of plots and graphs	Visual Data Tools
Geneious Pro 4.8.3	DNA and protein sequence analysis	Biomatters Ltd.
ImageQuant TL v 7.0	Quantification of Western blot signals	GE Healthcare
IMAGIC-5	Electron microscopy image processing	Image Science
Scrubber 2.0	Analysis of SPR data	BioLogic Software
SPRAutolink Version 1.1.2-E	Control of the SPR Biosensor SR7000DC	Reichert, Inc.
UCSF Chimera 1.3	Visualization of 3D structures	Resource for Biocomputing, Visualization, and Informatics
UNICORN	Control of the ÄKTA FPLC system	GE Healthcare

2.2. Cultivation of *E. coli*

2.2.1. Media and growth conditions for *E. coli*

E. coli strains BL21 and XL1-Blue (Stratagene) were grown on LB-agar plates or cultivated in LB medium at 37°C with vigorous shaking (170-220 rpm). For cultivation of ampicillin-resistant *E. coli* strains, 100 µg/ml ampicillin was added to the plates and media. Cell density was monitored by measuring light absorbance at 600 nm (OD₆₀₀).

For long-term storage, glycerol cryo-stocks were prepared by adding 20% of sterile glycerol to logarithmic-phase *E. coli* culture and freezing the mixture at -80°C. When needed, the cells were seeded on LB-agar plates containing appropriate antibiotic and then used for inoculating liquid cultures.

Ampicillin	100 mg/ml stock, sterile filtered
LB medium	1% (w/v) tryptone, 0.5% (w/v) yeast extract, 1% (v/w) NaCl, sterilized by autoclaving (20 min, 120°C)
LB+Amp medium	1% (w/v) tryptone, 0.5% (w/v) yeast extract, 1% (v/w) NaCl, sterilized by autoclaving. 100 µg/ml ampicillin was added to cold medium before use
LB-agar	LB medium with 1.5% (v/w) agar, sterilized by autoclaving (20 min, 120°C)
LB-agar+Amp	LB-agar was prepared as above, cooled down to 50°C, then 100 µg/ml ampicillin added

2.2.2. Preparation of transformation competent *E. coli* cells

Chemically competent *E. coli* BL21 and XL1-Blue cells were prepared using CaCl₂ method (Sambrook & Russell, 2000). For this, *E. coli* cells grown on LB-agar plates were used for inoculating 5 ml of LB medium. This culture was grown overnight with vigorous shaking, next day diluted 1:100 with pre-warmed LB medium and grown until OD₆₀₀ reached 0.5 (corresponding to mid-log phase). The cells were collected by centrifugation for 10 minutes (2000 g, 4°C) and resuspended in 250 ml of cold sterile 50 mM CaCl₂ solution. After 15 minutes incubation on ice, the cells were pelleted again and resuspended in 25 ml of cold sterile 50 mM CaCl₂. For storage, 15% glycerol was added and the cells were kept in single-use aliquots at -80°C.

CaCl ₂	50 mM in H ₂ O, sterilized by autoclaving
-------------------	--

2.2.3. Transformation of *E. coli*

100-300 µl of transformation competent *E. coli* XL1-Blue or BL21 cells were thawed on ice, 50-200 ng of DNA were added and gently mixed. The cells were incubated on ice for 30 minutes, followed by heat shock for 2 minutes at 42°C and cooling down on ice for 2 minutes. After that, 900 µl of LB medium pre-warmed to 37°C without antibiotics were added and the cells were incubated at 37°C with intense shaking for 1 hour. 200 µl of the cell suspension were plated on LB-agar plates containing appropriate selection antibiotic and grown at 37°C until single colonies became visible.

2.3. Molecular biology techniques

2.3.1. DNA isolation from *E. coli*

1-3 ml of LB medium containing 100 µg/ml ampicillin were inoculated with single *E. coli* colonies, grown overnight at 37°C with vigorous shaking and collected by centrifugation at 10 000 g for 5 minutes. DNA was isolated from the pelleted *E. coli* cells using PureYield™ Plasmid Miniprep System kit (Promega), according to the manufacturer's instructions. Purified DNA was stored frozen in water at -20°C.

Amount of isolated DNA was estimated by measuring light absorption at 260 nm using NanoVue spectrophotometer (GE Healthcare). One optical density unit at 260 nm (OD₂₆₀) was assumed to correspond to 50 µg/ml DNA. Quality of DNA preparation was estimated

by comparing light extinction at 260 nm (OD_{260} , absorption maximum for nucleic acids) and 280 nm (OD_{280} , typical absorption maximum for aromatic amino acids in proteins).

If DNA concentration in the sample was not sufficiently high or OD_{260}/OD_{280} ratio was lower than 1.85, DNA was precipitated with ethanol (based on Sambrook & Russell, 2000). For this, DNA solution was supplemented with sodium acetate (final concentration 0.3 M) and absolute ethanol was added to a final concentration of 70%. The sample was kept at -20°C for 30 minutes and the precipitated DNA was collected by centrifugation for 30 minutes at 20 000 g. The DNA pellet was washed once with 1 ml of 70% ethanol, dried and resuspended in appropriate volume of DNase-free water.

Sodium acetate	3 M in DNase-free water
-----------------------	-------------------------

2.3.2. Polymerase chain reaction (PCR)

Specific DNA fragments were amplified by polymerase chain reaction (PCR) using KOD Hot Start DNA polymerase (Novagen). Reaction mix (containing 100-200 ng of template DNA, 1.5 mM MgSO_4 , 0.2 mM dNTP mix, 0.3 μM forward and reverse primers and 0.02 units/ μl KOD polymerase in 1x KOD reaction buffer) was prepared according to the manufacturer's protocol. Cycling profile of the reaction started with initial DNA denaturation (combined with activation of the enzyme) for 2 minutes at 95°C , followed by 35 cycles, consisting of denaturation (20 s, 95°C), primer annealing (10 s, temperature dependent on primers) and chain elongation (20 s at 70°C) steps. Efficiency and specificity of the reaction were assessed by agarose gel electrophoresis with ethidium bromide staining.

2.3.3. Agarose gel electrophoresis

Electrophoresis of nucleic acids in agarose gels was used to separate and visualize DNA fragments of different lengths. 1% agarose was prepared freshly by dissolving agarose in boiling TAE buffer. After agarose was completely dissolved, the solution was cooled down to approximately 50°C , supplemented with 1 $\mu\text{g}/\text{ml}$ ethidium bromide and allowed to solidify in a form of a gel. DNA sample was mixed with DNA loading dye, loaded on the gel and ran at 8 V/cm in Mini-Sub® Cell GT Cell (Bio-Rad) filled with TAE buffer. DNA fragments were visualized by illuminating the gel with ultraviolet light (UV)

2. Materials and Methods

in UVsolo TS transilluminator (Biometra). If necessary, the bands containing fragments of interest were excised from the gel for preparative purposes under low-energy UV light.

TAE buffer	40 mM Tris-acetate, pH 8.0, 2 mM EDTA
DNA loading dye	10% sucrose, 0.25% OrangeG

2.3.4. Molecular cloning

A vector for expression of His-tagged Tim50^{CORE} (amino acids 164-361) in *E. coli* was generated by cloning corresponding fragment of *Saccharomyces cerevisiae* Tim50 into pPROEX HTa vector (Invitrogen). The fragment was amplified by PCR using forward primer (5'-ATATGGATCCCCCTTCAACTCAATGTTTCACCTACTTCC-3') and reverse primer (5'-ATATGCGGCCGCTTATTTTTTTCACACGATGATCAAATTCTTC-3'), containing sites for restriction enzymes BamHI and NotI, respectively. The PCR product was digested by corresponding restriction enzymes (BamHI-HF and NotI-HF, in NEB buffer 4, New England Biolabs) for 1 hour at 37°C, followed by agarose gel electrophoresis in 1% agarose gel containing 1 µg/ml ethidium bromide. Corresponding bands were cut from the gel under mild UV illumination, and the DNA was extracted by Wizard® SV Gel and PCR Clean-Up System. pPROEX HTa vector was linearized by double cleavage by BamHI-HF and NotI-HF (3 hours, 37°C, in NEB buffer 4) and purified from the agarose gel in the same way. 200 ng of the linearized vector were mixed with 150 ng of the purified insert and ligated by Rapid DNA Ligation Kit (Fermentas) for 1 hour at 23°C. 10 µl of the ligation reaction were directly used for transformation of competent XL1-Blue *E. coli* cells. Single colonies appearing on the LB-Amp plate after transformation were used for inoculating 2 ml of LB-Amp medium for subsequent DNA isolation. Isolated DNA was tested for the presence of the insert by digesting 500 ng with BamHI-HF and NotI-HF in NEB buffer 4 for 1 h at 37°C and agarose gel electrophoresis. To confirm identity of the sequence and absence of mutations, positive clones were sequenced in both directions with forward and reverse primers used for cloning, as described in section 2.3.6.

2.3.5. Site-directed mutagenesis

Site-directed mutagenesis using QuikChange™ Site-Directed Mutagenesis Kit (Agilent Technologies) was used for introducing C128S substitution in Tim21^{IMS} according to the instructions of the kit supplier. pProEX HTa-based vector encoding for Tim21^{IMS} (Albrecht et al., 2006) was used as a template. 20-50 ng of the DNA template was mixed with 125 ng of forward (5'- ATAAGAAGTTTGTACAGAGCGACGATGGCATTACGG-3') and reverse (5'- CCGTAATGCCATCGTCGCTCTGTAACAACTTCTTAT-3') primer and with reaction components provided in the kit in final reaction volume 50 µl. The reaction was started by adding 1 µl of *PfuTurbo* DNA polymerase (2.5 U/µl) and initial denaturation for 30 s at 95°C, followed by mutagenesis PCR, consisting of 16 cycles (30 s at 95°C, 1 min at 55°C and 6 min at 68°C). After completion of the reaction, it was cooled down on ice and unmodified parental DNA was digested by a methylation-sensitive restriction enzyme Dpn1 for 1 h at 37°C. Reaction product was directly used for transformation of competent XL1-Blue *E. coli* cells. Single colonies were picked; DNA was isolated and sequenced as described in sections 2.3.1 and 2.3.6, respectively.

2.3.6. Sequencing of DNA

DNA was sequenced at the facilities of Göttinger Center for Molecular Biosciences (Göttingen, Germany) using Genetic Analyzer 3100 (Applied Biosystems) or was sent to GATC Biotech (Constance, Germany). In the former case, 400 ng of DNA was used per sequencing reaction. The DNA was mixed with components of the BigDye® Terminator v1.1 Cycle Sequencing Kit (Applied Biosystems), according to the manufacturer's instructions, and 8 pmol of the corresponding primer were added. The reaction mixture was subjected to 25 cycles of sequencing PCR, each consisting of 10 s at 95°C, 15 s at 55°C and 4 min at 60°C. DNA was mixed with 12.5 mM EDTA and 0.3 M sodium acetate and precipitated by adding 5 volumes of absolute ethanol. After 5 minutes of incubation, DNA was pelleted by centrifugation for 20 minutes at 20000 g, washed once with 70% ethanol, dried, resuspended in 15 µl of Hi-Di™ formamide and stored at 4°C ready for sequencing. For sequencing at GATC Biotech, 20 µl of plasmid DNA dissolved in water at concentration 30-100 ng/µl were sent to the company together with 10 pmol/ml primers.

All sequencing data were analyzed using software Geneious Pro 4.8.3 (Drummond et al., 2012).

2.4. Cultivation of *S. cerevisiae* and preparation of mitochondria

2.4.1. Yeast media and growth conditions

Media used for cultivating *S. cerevisiae* are listed below. For strains that did not require additional selection, YPD and YPG media were used. Synthetic media lacking tryptophane (SD-Trp and SG-Trp) supplemented with 2% glucose or 3% glycerol, respectively, were used for selecting strains bearing pFL39-based plasmids. All liquid cultures were grown at 30°C with vigorous shaking (170-220 rpm). Solid media were prepared by adding 2% agar to corresponding media before autoclaving.

Glycerol cryo-stocks were prepared for long-term storage of yeast strains by adding equal volume of 30% glycerol to liquid culture and freezing at -80°C.

YPD	1% yeast extract, 2% peptone, 2% glucose
YPG	1% yeast extract, 2% peptone, 3% glycerol
SD-Trp	0.67% yeast nitrogen base, 0.07% complete supplement mixture without tryptophane (CSM-Trp), 2% glucose
SG-Trp	0.67% yeast nitrogen base, 0.07% CSM-Trp, 3% glycerol

2.4.2. Yeast transformation

To transform yeast with exogenous plasmid DNA, lithium acetate/PEG transformation method was performed essentially as described in Gietz & Schiestl, 2007, with minor modifications. Corresponding yeast strains were pre-cultured in 2xYPAD medium overnight; next day, the main culture was inoculated to OD₆₀₀ approximately equal to 0.6 and cultured until OD₆₀₀ reached 1.5-2.5. The cells were harvested by centrifugation (3000 g, 10 min), washed with sterile water and 0.1M lithium acetate solution and resuspended in 0.1 M lithium acetate (2 ml solution per 100 ml of initial culture). 100 µl of the obtained suspension were used for one transformation reaction. For this, 120 µg of carrier DNA were added, followed by addition of 300 µg plasmid DNA. 600 µl of LiAc/PEG solution were added and the cells were incubated for 60 min at 30°C with moderate shaking. 68 ml of sterile DMSO were added, the cells were subjected to heat

2. Materials and Methods

shock at 42°C for 15 minutes, collected by centrifugation at 100 g for 2 minutes, resuspended in 1 M sorbitol and seeded on appropriate selection plates.

2xYPAD medium	2% yeast extract, 4% peptone, 4% glucose, 0.008% adenine hemisulphate, autoclaved
Carrier DNA	herring sperm DNA (10 mg/ml) in TE buffer
TE buffer	10 mM Tris, pH 8.0, 1 mM EDTA
LiAc/PEG	0.1 M lithium acetate, 40% polyethylene glycol 4000 in water, filter-sterilized

2.4.3. Preparation of mitochondria

Mitochondria were prepared from yeast cells by differential centrifugation (Meisinger, Pfanner, & Truscott, 2006). Yeast were cultured in sequential pre-cultures of increasing volumes (5 ml YPD, followed by 200 ml YPG overnight pre-cultures) and used for inoculating final cultures (typically, 6x1.6 L per strain). For yeast strains requiring selective media, the same procedure was followed using corresponding synthetic media. The cells were collected when OD₆₀₀ reached 1.6-2.5 by centrifugation at 7000 g for 15 minutes. Collected cells were washed with water and treated with 10 mM dithiothreitol (DTT) in 100 mM Tris-HCl, pH 9.4 for 30 min at 30°C with moderate shaking. Cells were collected by centrifugation (7000 g, 10 min), washed with 1.2 M sorbitol and zymolyase buffer and resuspended in zymolyase buffer (7 ml per 1 g of initial yeast pellet). In order to digest the cell wall and obtain spheroplasts, the cells were treated with zymolyase (4 mg/g yeast) for 1 hour at 30°C with moderate shaking. Obtained spheroplasts were washed with zymolyase buffer without the enzyme, resuspended in homogenization buffer and homogenized by 15 strokes at 700 rpm in Potter S glass-Teflon homogenizer (Sartorius AG). Cell debris, nuclei and unopened cells were removed by two centrifugation steps (2000 g for 5 minutes and 7000 g for 10 minutes). Mitochondria were pelleted by centrifugation at 17000 g for 15 minutes, washed once with SEM buffer containing 1 mM PMSF and resuspended in SEM buffer. Protein concentration was determined by Bradford assay (described in section 2.6.1), the suspension was diluted with SEM buffer to final protein concentration 10 mg/ml, flash-frozen as single-use aliquots in liquid nitrogen and stored at -80°C.

DTT buffer	10 mM DTT, 100 mM Tris/H ₂ SO ₄ , pH 9.4
-------------------	--

Zymolyase buffer	1.2 M sorbitol, 20 mM potassium phosphate, pH 7.4
Homogenization buffer	0.6 M sorbitol, 10 mM Tris/HCl (pH 7.4), 1 mM EDTA, 0.2% (w/v) fatty acid free BSA, 1 mM PMSF
SEM buffer	250 mM sucrose, 10 mM MOPS, 1 mM EDTA, pH 7.2
PMSF stock	0.2 M phenylmethylsulfonyl fluoride in ethanol

2.5. Purification of proteins and protein complexes

2.5.1. Expression of recombinant proteins in *E. coli*

For expression of heterologous proteins in *E. coli*, chemically competent *E. coli* BL21 cells were freshly transformed with a plasmid encoding for the protein of interest under the control of *lacZ* promoter (see section 2.1.4 for details). Alternatively, cells from a glycerol stock (if available) were seeded on solid media and afterwards used for inoculating liquid cultures. The cells were used for sequential inoculation of 5 ml, 50 ml and 1 L of LB medium supplemented with 0.1 mg/ml ampicillin. The final (1 L) culture was grown at 37°C to OD₆₀₀ between 0.6 and 1.0 and protein expression was induced by addition of 1 mM IPTG. Cells were grown with vigorous shaking at 37°C for additional 4 hours, collected by centrifugation at 5000 g for 20 minutes and the pellets were frozen until needed.

To open the cells, frozen pellets were thawed at room temperature and resuspended in lysis buffer, specific for each protein. The cells were opened using EmulsiFlex C5 (Avestin) and insoluble material was removed by centrifugation for 30 minutes at 20000 g and filtering the supernatant through cellulose acetate filters with 0.2 µm pore size.

If purified proteins were to be used for SPR (section 2.6.10) or *in vitro* cross-linking assays (section 2.6.2), they were dialyzed against corresponding buffers before use.

2.5.2. Immobilized metal affinity chromatography

Recombinant proteins bearing a 6xHis tag were purified using immobilized metal affinity chromatography on HisTrap HP columns (column volumes 1 ml and 5 ml) on ÄKTA Purifier 10 (GE Healthcare). Clarified and filtered *E. coli* lysates (see section 2.5.1) were loaded at a flow rate of 0.5 ml/min on the columns pre-equilibrated with 10 column volumes of HisTrap Buffer A (specific for each protein, see Table 2.8). The columns were washed with 20 column volumes of HisTrap Buffer A and eluted with a

2. Materials and Methods

linear gradient of HisTrap Buffer B containing 500 mM imidazole at default flow rate 1 ml/min. Collected fractions were analyzed by SDS-PAGE followed by Coomassie Brilliant Blue staining. Fractions containing reasonable amounts of protein of interest were pooled and dialyzed overnight against desired buffer. After dialysis, purified proteins could be further processed in one of the following ways: (1) aliquoted, snap-frozen in liquid nitrogen and stored at -80°C until needed; (2) further purified using size exclusion chromatography; (3) for proteins with a TEV-cleavable His tag only: 1 mg of His-tagged TEV protease was added per 10 mg of protein and incubated for 1 hour at 30°C; the procedure was repeated with a fresh portion of the protease; cleaved tag and TEV protease were removed by incubation with Ni-NTA slurry (1 ml slurry per 10 mg of protein) for 3-4 hours at 4°C. Protein purity and cleavage efficiency were assessed by SDS-PAGE and Coomassie Brilliant Blue staining, proteins were snap-frozen in liquid nitrogen and stored at -80°C in small aliquots.

Table 2.8. Specific conditions for purification of His-tagged proteins

Protein	Lysis buffer	HisTrap buffer A	HisTrap buffer B	Dialysis buffer
Tim21 ^{IMS} and Tim21 ^{IMS-C128S}	50 mM Na ₂ HPO ₄ pH 8.0, 300 mM NaCl, 5 mM imidazole, EDTA-free protease inhibitor cocktail (Roche), 1% Triton X-100	50 mM Na ₂ HPO ₄ pH 8.0, 300 mM NaCl, 5 mM imidazole	50 mM Na ₂ HPO ₄ pH 8.0, 500 mM NaCl, 5 mM imidazole	20 mM HEPES, pH 7.2, 100 mM NaCl
Tim50 ^{IMS}	20 mM Tris, pH 8.0, 500 mM NaCl, 15 mM imidazole, 0.1% Triton X-100, 1 mM PMSF	20 mM Tris, pH 8.0, 500 mM NaCl, 15 mM imidazole	20 mM Tris, pH 8.0, 500 mM NaCl, 500 mM imidazole	20 mM Tris, pH 8.0, 500 mM NaCl
Tim50 ^{CORE}	20 mM HEPES, pH 7.5, 150 mM NaCl, 15 mM imidazole, EDTA-free protease inhibitor cocktail (Roche)	20 mM HEPES, pH 7.5, 150 mM NaCl, 15 mM imidazole	20 mM HEPES, pH 7.5, 150 mM NaCl, 500 mM imidazole	20 mM HEPES, pH 7.5, 150 mM NaCl, 50 µM EDTA

2.5.3. Ion exchange chromatography

Recombinantly expressed b₂(167)_Δ-DHFR was purified by ion exchange on Resource S column (GE Healthcare), based on the protocol described in Dekker et al., 1997. Collected *E. coli* cells expressing the protein were washed once with 30% sucrose, 20 mM potassium phosphate, pH 8.0, 1 mM EDTA and 10 mM dithiothreitol. The cells were

opened by EmulsiFlex C5 (Avestin) in lysis buffer containing 20 mM MOPS-KOH, pH 8.0, 1 mM EDTA, 10 mM dithiothreitol, 0.1% (v/v) Triton X-100, 1 mM PMSF and Complete EDTA-free protease inhibitor mix (Roche). After centrifugation and filtering (described in section 2.5.1), the clarified lysate was loaded on Resource S column (GE Healthcare) pre-equilibrated with buffer A (20 mM MOPS-KOH, pH 8.0, 1 mM EDTA) at flow rate 0.5 ml/min. The column was washed with 10 column volumes of buffer A and bound proteins were eluted with a linear gradient of NaCl in buffer A (from 0 to 500 mM NaCl in 10 column volumes). Fractions containing purified protein were combined, concentrated using Amicon Ultra centrifugal filter units (Millipore), supplemented with 50% glycerol and frozen at -80°C in small aliquots.

Lysis buffer	20 mM MOPS-KOH, pH 8.0, 1 mM EDTA, 10 mM dithiothreitol, 0.1% (v/v) Triton X-100, 1 mM PMSF and Complete EDTA-free protease inhibitor mix (Roche)
Buffer A	20 mM MOPS-KOH, pH 8.0, 1 mM EDTA
Buffer B	20 mM MOPS-KOH, pH 8.0, 1 mM EDTA, 500 mM NaCl

2.5.4. Size exclusion chromatography

Size exclusion chromatography (gel filtration) on an FPLC system ÄKTA Purifier 10 (GE Helthcare) was used as a polishing step after purification of recombinant proteins (using HiLoad 16/60 Superdex 200 pg or HiLoad 16/60 Superdex 75 pg). In all cases, columns were equilibrated with at least 2 column volumes of corresponding buffer (depending on the protein) and the proteins were separated at flow rate 1 ml/min and default settings for each column type (as recommended by the manufacturer).

2.5.5. IgG affinity chromatography

IgG affinity chromatography was used to purify proteins and protein complexes carrying protein A tag (Nilsson et al., 1987). TIM22, TIM23 and TOM-TIM supercomplex were purified from Tim18^{ProtA}, Tim23^{ProtA} or Tim21^{ProtA} mitochondria essentially as described previously (Chacinska et al., 2005; Geissler et al., 2002; Rehling et al., 2003). Same procedure was used for purifying respiratory chain supercomplexes using tandem affinity purification (TAP)-tagged Cor1 (Vukotic et al., 2012; Wiedemann et al., 2007; van der Laan et al., 2006).

IgG sepharose beads were prepared by cross-linking purified human IgG to cyanobromide-activated Sepharose 4B (GE Healthcare). Before use, the beads were washed twice with 5 bed volumes of acetate buffer, pH 3.5, and twice with 1% digitonin solubilization buffer.

Mitochondria were solubilized as described in section 2.7.3, insoluble material was removed by centrifugation at 20000 g for 10 minutes and the clarified supernatant was incubated with IgG sepharose beads (50 μ l slurry per 10 mg of mitochondrial protein) for 3 hours at 4°C with end-over-end shaking. After incubation, the beads were washed 10 times with 5 bed volumes of washing buffer (identical to solubilization buffer, but containing 0.3% digitonin). For SDS-PAGE analysis, bound proteins were eluted with Laemmli SDS loading buffer and analyzed by immunoblotting or colloidal Coomassie staining. For isolation of native protein complexes, the tag was cleaved by adding His-tagged tobacco etch virus (TEV) protease (10 μ g of protease per 1 mg of initial mitochondrial protein, overnight incubation at 4°C). After incubation, the protease was removed by Ni-NTA beads (Qiagen) and the purified protein complex was eluted by centrifugation.

Digitonin solubilization buffer	1% digitonin, 20 mM HEPES-NaOH, pH 7.5, 100 mM NaCl, 10% glycerol, 1 mM PMSF, 1 mM EDTA, supplemented with complete EDTA-free protease inhibitor cocktail (Roche)
Washing buffer	0.3% digitonin, 20 mM HEPES-NaOH, pH 7.5, 100 mM NaCl, 10% glycerol, 1 mM PMSF, 1 mM EDTA, supplemented with complete EDTA-free protease inhibitor cocktail (Roche)

2.5.6. Coimmunoprecipitation

Coimmunoprecipitation experiments were performed according to Herrmann et al., 2001. Corresponding antibodies were coupled to Protein A Sepharose beads (GE Healthcare) by dimethyl pimelimidate cross-linking. The beads were pre-equilibrated with digitonin solubilization buffer and added to solubilized mitochondria (section 2.7.3) for 3 hours at 4°C. After washing the beads, bound proteins were eluted with 5 bed volumes of 0.1 M glycine, pH 2.5, neutralized with 0.1 M Tris, pH 7.4 and precipitated with TCA (section 2.5.7).

2.5.7. Protein precipitation by trichloroacetic acid (TCA)

To reduce sample volume for SDS-PAGE, protein precipitation with trichloroacetic acid (TCA) was performed. For this, samples were incubated with 14% TCA and 0.0125% sodium deoxycholate for 30 min on ice and pelleted by centrifugation for 30 minutes at 20 000 g, 4°C. To remove traces of TCA, the pellet was washed once with 500 µl of ice-cold acetone and dried at 37°C for 10-15 minutes. Dried protein pellet was resuspended in Laemmli SDS loading buffer by shaking at 65°C for 20 minutes and used for SDS-PAGE.

TCA	72% trichloroacetic acid (TCA) in water
Na-deoxycholate	1.25% sodium deoxycholate in water

2.6. Biochemical analysis of proteins and protein complexes

2.6.1. Determination of protein concentration

Protein amounts in isolated mitochondria were estimated using Roti®-Quant Bradford protein determination assay. First, calibration curve was prepared using different dilutions (0; 7.5; 15; 30; 60 µg/µl) of bovine immunoglobulin G (Bio-Rad) in water (final reaction volume 84 µl). Different volumes of mitochondrial suspension (5, 10 or 20 µl) were adjusted with water to the same volume, and 1 ml of 1x Roti®-Quant solution was added to all samples. After 5 minutes of incubation, optical density was measured at 595 nm, and protein amount for each dilution was calculated using a calibration curve.

To determine concentration of purified recombinant proteins, Bradford-based Bio-Rad protein assay was used. Calibration curve was prepared using increasing concentrations (2, 4, 8, 12 and 16 µg/ml) of bovine serum albumin (New England Biolabs) in 1 ml of 1x Bio-Rad protein assay reagent. The protein of interest was diluted in the same reaction volume (typically, 1:1000, 1:200 and 1:100) of the reagent, and after 10 minutes of incubation, optical density at 595 nm was measured in duplicates using iMark™ Microplate Absorbance Reader. Unknown protein concentrations were determined using calibration curve.

Alternatively, concentration of purified proteins was determined by measuring light extinction at 280 nm using NanoVue spectrophotometer (GE Healthcare). Molar extinction coefficient for a given protein was calculated using the method of Gill and Hippel (Gill & Hippel, 1989) by the Geneious Pro 4.8.3 software (Biomatters Ltd.) and used to calculate protein concentration.

2.6.2. Chemical cross-linking *in vitro*

Desired amounts of purified proteins or synthetic peptides were mixed in cross-linking buffer, reaction volumes were adjusted with corresponding buffers (so that all reactions had the same buffer conditions and same volume, typically 20 μ l), and incubated for 10 minutes on ice. For Cu^{2+} cross-linking, 1 mM CuSO_4 was added to induce disulfide formation. After 30 min incubation on ice, the reactions were quenched by addition of 10 mM EDTA and non-reducing Laemmli SDS loading buffer. 5% β -mercaptoethanol was added to not cross-linked samples before loading the gel. The samples were analyzed by SDS-PAGE (section 2.6.3) and subsequent colloidal Coomassie staining (section 2.6.6) or immunoblotting (section 2.6.7).

Cross-linking buffer	20 mM HEPES-NaOH, pH 7.2, 100 mM NaCl
EDTA	0.5 M EDTA, pH 8.0
CuSO_4	50 mM CuSO_4 in water, freshly prepared

2.6.3. SDS-PAGE

Denaturing discontinuous electrophoresis of proteins (Laemmli, 1970, with modifications) was performed using polyacrylamide gels (acrylamide:bisacrylamide ratio 37.5:1) containing 0.1% SDS. Tris-buffered 4% acrylamide gel, pH 6.8 was used for stacking, and 10-15% acrylamide, pH 8.8 was used for resolving gels. Before loading on the gel, proteins were mixed with SDS loading buffer and incubated for 5 minutes at 95°C. The gels were run in Mini-PROTEAN® Cell (Bio-Rad) or custom-made gel system in running buffer containing 0.1% SDS at 20 mA/gel (Bio-Rad system) or 30 mA/gel (custom-made system). SDS-PAGE Molecular Weight Standards, Broad Range (Bio-Rad) were used as a molecular weight marker.

2. Materials and Methods

SDS loading buffer	10% glycerol, 2% SDS, 0.01% bromophenol blue, 60 mM Tris-HCl, pH 6.8, with or without 0.5% β -mercaptoethanol
SDS running buffer	25 mM Tris, 191 mM glycine, 0.1% SDS
Stacking gel	4% acrylamide, 0.1% SDS, 380 mM Tris-HCl, pH 8.8, 0.1% ammonium peroxodisulphate, 0.05% tetramethylethylenediamine (TEMED)
Resolving gel	10-15% acrylamide, 80 mM Tris-HCl, pH 6.8, 0.1% SDS, 0.1% ammonium peroxodisulphate, 0.05% TEMED

2.6.4. BN-PAGE

Blue native polyacrylamide gel electrophoresis (BN-PAGE) was used to separate protein complexes under non-denaturing conditions (Schägger & von Jagow, 1991). Solubilized mitochondria (section 2.7.3) or purified protein complexes were mixed with BN sample loading buffer and loaded on a 6-16% gradient gel with a 4% stacking gel. Electrophoresis was performed at 200 V for 2 hours, followed by 100 V overnight or 600 V for 6-7 hours. To increase subsequent blotting efficiency, cathode buffer with Coomassie Brilliant Blue G-250 was replaced with Coomassie-free buffer after 2 hours of run. High molecular weight calibration kit (GE Healthcare) was used as marker.

BN sample loading buffer (1x)	0.5% Coomassie Brilliant Blue G-250, 50 mM 6-aminocaproic acid, 10 mM Bis-Tris, pH 7.0
BN gel buffer (1x)	67 mM 6-aminocaproic acid, 50 mM Bis-Tris, pH 7.0
BN anode buffer	50 mM Bis-Tris, pH 7.0
BN cathode buffer	50 mM Tricine, 15 mM Bis-Tris, with or without 0.2% Coomassie Brilliant Blue G-250

2.6.5. Coomassie Brilliant Blue staining

Proteins in acrylamide gels and on PVDF membranes were stained with Coomassie Brilliant Blue (CBB) R-250 by incubating them in staining solution containing 2.5 g/l CBB R-250, 40% ethanol and 10% acetic acid at room temperature for 5 minutes (PVDF membranes) or 1-3 hours (acrylamide gels). Background staining was removed by washing in 30% ethanol, 10% acetic acid.

Coomassie staining solution	2.5 g/l CBB R-250, 40% ethanol and 10% acetic acid
Destaining solution	30% ethanol, 10% acetic acid

2.6.6. Colloidal Coomassie staining

Staining of proteins in acrylamide gels with colloidal Coomassie was performed based on the protocol described in Neuhoﬀ et al., 1988. The gels were fixed overnight in fixation solution (50% methanol, 2% phosphoric acid), washed with water (3 times, 0.5 hour each) and stained with staining solution containing 0.1% (w/v) CBB G-250 in 2 % (w/v) phosphoric acid, 10 % (w/v) ammonium sulfate and 20% methanol until protein bands became visible.

Fixation solution	50% methanol, 2% phosphoric acid
Colloidal Coomassie staining solution	0.1% (w/v) Coomassie Brilliant Blue G-250, 2 % (w/v) phosphoric acid, 10 % (w/v) ammonium sulfate and 20% methanol.

2.6.7. Western blotting and immunodecoration

After separation by SDS-PAGE or BN-PAGE, proteins were transferred to polyvinylidene fluoride (PVDF) membranes by semi-dry blotting using PEQLAB chambers. The membranes were activated by methanol and assembled underneath the gel between layers of Whatman paper soaked in blotting buffer. Blotting was performed at 250 mA for 2 hours.

Alternatively, direct transfer of proteins to the PVDF membrane using Minifold* II Slot-Blot Manifold System (Whatman) was used for proteins that could not be separated by electrophoresis after cross-linking by GraFix procedure (section 2.8.1). The membrane was subsequently treated in the same way as for conventional Western blotting.

After transfer, the membrane was stained with Coomassie R-250, completely destained with methanol, blocked with 5% milk in TBS-T and incubated with primary antibodies for 1 hour at room temperature or overnight at 4°C. The membrane was washed 3 times for 5 minutes with TBS-T and incubated with HRP or fluorescent dye-coupled secondary antibodies (section 2.1.3). After 3 more washing steps, the signal was detected either by scanning the membrane with Starion FLA-9000 (for fluorescently labeled antibodies) or by enhanced chemiluminescence detection (GE Healthcare) using X-ray films or LAS 1000 camera (Fujifilm).

2. Materials and Methods

Blotting buffer	20 mM Tris, 150 mM glycine, 0.02% SDS, 20% ethanol
TBS-T (Tris-buffered saline with Tween-20)	125 mM NaCl, 20 mM Tris-HCl, pH 7.5, 0.1% Tween-20

2.6.8. Digital autoradiography

Radioactively labeled proteins were detected in dried SDS-PAGE or BN-PAGE gels by exposing them to Storage Phosphor Screens (GE Healthcare) and detecting the signal with Storm820 scanner (GE Healthcare).

2.6.9. Glycerol density gradient centrifugation

10-30% glycerol density gradients were prepared by mixing low density buffer (containing 10% glycerol) and high density buffer (30% glycerol) using Gradient Master (BioComp Instruments) with pre-programmed conditions for 10-30% glycerol density gradients. Isolated protein complexes (section 2.5.5) or solubilized mitochondria (section 2.7.3) were loaded onto pre-cooled gradients in a maximal volume of 200 μ l and separated by ultracentrifugation in a SW60Ti rotor (Beckman-Coulter). Fractions (0.5 ml each) were collected from the top of the gradients, proteins were TCA precipitated (see section 2.3.11) and analyzed by SDS-PAGE and immunoblotting.

10% glycerol buffer	(unless otherwise indicated) 10% glycerol, 20 mM HEPES-NaOH, pH 7.4, 100 mM NaCl, 1 mM EDTA, 0.3% digitonin
30% glycerol buffer	(unless otherwise indicated) 30% glycerol, 20 mM HEPES-NaOH, pH 7.4, 100 mM NaCl, 1 mM EDTA, 0.3% digitonin
Solubilization buffer	(unless otherwise indicated) 1% digitonin, 20 mM HEPES-NaOH, pH 7.5, 100 mM NaCl, 10% glycerol, 1 mM PMSF, 1 mM EDTA, supplemented with complete EDTA-free protease inhibitor cocktail (Roche)

2.6.10. Surface plasmon resonance (SPR) measurements

Specific interactions between purified recombinant proteins or synthetic peptides were measured using Reichert SPR Biosensor SR7000DC with Ni²⁺ chelator sensorchip NiHC500m (XanTec bioanalytics), in running buffer containing 50 mM HEPES, pH 7.4, 150 mM NaCl and 50 μ M EDTA, at 20°C, flow rate 40 μ l/min. First, chip surface was conditioned with 0.5 M EDTA, pH 8.5 (3 times, 5 minutes each, at flow rate 50 μ l/min), followed by wash with running buffer for 5 minutes at 50 μ l/min. Left (sample) channel

2. Materials and Methods

was activated with 0.3 M NiSO₄ for 5 minutes (same flow rate), washed with immobilization buffer for 5 minutes, and 200 nM solution of a His-tagged ligand was injected for 7 minutes at 30 µl/min flow. To test interaction of the immobilized ligand with other proteins, increasing concentrations of analyte in the running buffer were injected for 270 s to both channels, and dissociation was followed for 12 minutes. Response difference between sample and reference channels was recorded. Affinity and kinetic data analyses were done by Scrubber 2.0 (BioLogic Software).

Conditioning buffer	0.5 M EDTA, pH 8.5
Ni²⁺ solution	0.3 M NiSO ₄ in immobilization/running buffer
Immobilization/running buffer	50 mM HEPES, pH 7.4, 150 mM NaCl, 50 µM EDTA, filter-sterilized

2.6.11. Mass-spectrometry

Mass-spectrometry analysis of proteins excised from SDS-PAGE gels stained with colloidal Coomassie was performed at the facilities of Biochemistry II department (University of Göttingen) using MALDI-TOF/TOF mass spectrometer (Ultraflextreme; Bruker Daltonics).

2.7. Assays in isolated mitochondria

2.7.1. *In vitro* translation of ³⁵S radiolabeled proteins

Proteins were translated *in vitro* in the presence of [³⁵S] methionine using TNT SP6 Quick Coupled Transcription/Translation system (Promega). 1 µg of plasmid containing open reading frame of interest under the control of the SP6 promoter was mixed with 50 µl of rabbit reticulocyte lysate and 50 µCi [³⁵S] methionine and incubated for 90 min at 30°C. The reaction was quenched with 20 mM non-radioactive methionine and 250 mM sucrose was added to the lysate before freezing it for storage at -80°C.

2.7.2. Protein import into isolated mitochondria

Radiolabeled or purified recombinant proteins were imported in mitochondria as described in (N Wiedemann, Pfanner, & Rehling, 2006). Mitochondria (75 µg per sample) were thawed on ice and resuspended in import buffer supplemented with ATP, NADH and, in case of importing recombinant proteins, creatine phosphate (CP) and creatine

2. Materials and Methods

kinase (CK). Membrane potential was dissipated in “ $-\Delta\psi$ ” samples by addition of 1% (v/v) AVO mix. All other samples were treated with equal volume of ethanol. Radiolabeled precursor was added and mitochondria were incubated for desired time at 25°C. The import was stopped by adding 1% AVO and putting the samples on ice. If necessary, unimported precursor was digested by treatment with 40 $\mu\text{g/ml}$ proteinase K for 15 minutes on ice with subsequent inactivation of the proteinase by 2 mM PMSF. Mitochondria were pelleted by centrifugation, washed with SEM buffer and resuspended in SDS loading buffer for SDS-PAGE analysis.

Import buffer	3% BSA, 250 mM sucrose, 80 mM potassium chloride, 5 mM magnesium chloride, 2 mM potassium phosphate, 5 mM methionine, 10 mM MOPS-KOH, pH 7.2, 2 mM ATP, 2 mM NADH, with or without 100 $\mu\text{g/ml}$ creatine kinase and 5 mM creatine phosphate
AVO mix	1 mM antimycin A, 0.1 mM valinomycin, 2 mM oligomycin in ethanol
SEM buffer	250 mM sucrose, 10 mM MOPS-KOH, pH 7.2, 1 mM EDTA
PMSF	0.2 M PMSF in ethanol
Proteinase K	1 mg/ml in water, stored at -80°C in aliquots.

2.7.3. Mitochondrial membrane solubilization

Isolated yeast mitochondria were thawed on ice, pelleted by centrifugation (20 000 g, 4°C , 10 min) and resuspended in solubilization buffer containing desired concentration of digitonin or another detergent (1 ml of buffer per 1 mg of mitochondrial protein). After 30 minutes of incubation at 4°C , insoluble material was removed by centrifugation (20000 g, 4°C , 10 min) and the cleared supernatant was used for further assays, such as BN-PAGE (section 2.6.4), size exclusion chromatography (2.5.4), glycerol density gradient centrifugation (2.6.9), immunoprecipitation (2.5.6) and IgG affinity chromatography (2.5.5).

Solubilization buffer	1% digitonin, 20 mM HEPES-NaOH, pH 7.5, 100 mM NaCl, 10% glycerol, 1 mM PMSF, 1 mM EDTA, supplemented with complete EDTA-free protease inhibitor cocktail (Roche)
------------------------------	---

2.7.4. Precursor arrest and formation of TOM-TIM23 supercomplex

Formation of TOM-TIM23 supercomplex was achieved by arresting a tightly folded precursor during its transport across outer and inner mitochondrial membranes

(Rassow et al., 1989). To achieve this, recombinantly expressed fusion protein b₂(167) Δ -DHFR (containing 167 N-terminal residues of the cytochrome b₂, but lacking residues 47-65 responsible for lateral sorting, fused to complete mouse DHFR sequence) was imported in mitochondria as described in section 2.7.2 in the presence of 5 μ M methotrexate for 15 minutes at 25°C.

MTX	10 mM stock in water, used as 2000x, stored frozen at -20°C in single-use aliquots
------------	--

2.7.5. Preparation of mitoplasts by osmotic swelling of mitochondria

To disrupt outer mitochondrial membrane, mitochondria were osmotically swollen in hypotonic buffer. For this, frozen mitochondrial aliquots were thawed on ice, pelleted by centrifugation (20 000 g, at 4°C) and resuspended in EM buffer (1 ml of buffer per 10 mg of mitochondrial protein) by pipetting up and down for approximately 20 times. EM buffer was added to final ratio of 1 ml buffer per 1 mg of mitochondrial protein and the mitochondrial suspensions were left on ice for 20 minutes with occasional vortexing. After that, mitoplasts were collected by centrifugation and used for further assays.

If necessary, swelling efficiency was tested by protease protection assay. For this, mitoplasts were treated with increasing concentrations of proteinase K (0, 30, 60 or 90 μ g/ml) for 10 min at 4°C. The reaction was stopped by adding 1 mM PMSF, mitoplasts were pelleted, resuspended in SDS Laemmli loading dye and analyzed by conventional SDS-PAGE and Western blotting.

EM buffer	10 mM MOPS-KOH, pH 7.2, 1 mM EDTA
PMSF	0.2 M PMSF in absolute ethanol
Proteinase K	1 mg/ml in water, stored at -80°C in aliquots.

2.7.6. Chemical cross-linking in mitochondria

Prepared mitochondria stored at -80°C were thawed on ice, pelleted by centrifugation and resuspended in isotonic SH buffer. For cross-linking experiments in mitoplasts, mitochondria were first subjected to osmotic swelling in EM buffer for 20 minutes on ice, as described in section 2.7.5, centrifuged and resuspended in hypotonic cross-linking buffer. Typically, 100 μ g of mitochondrial protein per sample were used. If necessary, the

samples were treated with corresponding purified proteins or synthetic peptides for 10 minutes on ice. After that, cross-link formation was induced by adding CuSO₄ to final concentration of 1 mM. The samples were incubated for 30 minutes on ice, and the reaction was quenched by adding 10 mM EDTA. Mitochondria were collected by centrifugation, resuspended in Laemmli SDS loading buffer without β -mercaptoethanol and analyzed by conventional SDS-PAGE and immunoblotting.

EM buffer	10 mM MOPS-KOH, pH 7.2, 1 mM EDTA
SH buffer	0.6 M sorbitol, 20 mM HEPES-KOH, pH 7.2
Cross-linking buffer	20 mM HEPES-NaOH, pH 7.2, 100 mM NaCl
EDTA	0.5 M EDTA, pH 8.0
CuSO₄	50 mM CuSO ₄ in water, freshly prepared

2.8. Electron microscopy

2.8.1. Gradient fixation (GraFix) of purified protein complexes

Gradient fixation (GraFix) of purified complexes was performed according to Kastner et al., 2008. This method implies stabilization of the isolated protein complexes by combining high-speed centrifugation in a glycerol density gradient with gradual fixation in a concentration gradient of glutaraldehyde or another chemical cross-linker. Glycerol density gradients were prepared essentially as described in section 2.6.9, with the only exception that 0.3% glutaraldehyde was added to the lower (30% glycerol) buffer. After centrifugation, fractions were collected from the top of the centrifuge tube and analyzed by slot blotting (section 2.6.7) and electron microscopy.

Upper GraFix buffer	10% glycerol, 20 mM HEPES-NaOH, pH 7.4, 100 mM NaCl, 1 mM EDTA, 0.3% digitonin
Lower GraFix buffer	0.3% glutaraldehyde, 30% glycerol, 20 mM HEPES-NaOH, pH 7.4, 100 mM NaCl, 1 mM EDTA, 0.3% digitonin
Glutaraldehyde	25% solution, EM grade

2.8.2. Preparation of negatively stained electron microscopy samples

Negatively stained samples for electron microscopy were prepared using uranyl acetate (based on Leberman, 1965). 2.5% uranyl acetate solution was prepared freshly in water, 25 mM NaOH was added and insoluble material was removed by centrifugation

for 30 minutes at 20 000 g. Approximately 120 μ l of this solution were placed in a well of a Teflon block and used for staining EM grids.

Two approaches for sample preparation using supporting carbon films with different properties were applied. For the first method (further referred to as “floating film technique”), carbon film-coated mica was cut into small pieces (approximately 0.4x0.4 cm) and inserted in a well of a Teflon block containing 25-50 μ l of a sample, in a way that carbon film detached and floated on the surface of the solution. The film was carefully covered with a copper EM sample grid and left on the sample surface for binding (typically, for 2-15 minutes). After that, the grid was briefly washed with a droplet of water and stained with uranyl acetate for 30 s. Excess of the stain was removed by blotting on a filter paper, the grid was air-dried at room temperature and directly used for EM.

For the second method, pre-made carbon film-coated grids (Fukami & Adachi, 1965) were glow-discharged for 2 minutes directly before use, placed on the surface of a sample in a Teflon block well and then processed as described above for the floating films.

For detergent removal by γ -cyclodextrin, grids were washed on a drop of 100 mM cyclodextrin and double distilled water prior to uranyl acetate staining.

Preparation of all negatively stained samples and subsequent electron microscopy analyses were performed at the facilities of 3D Electron Cryo-Microscopy group at Max Planck Institute for Biophysical Chemistry, Göttingen, Germany.

2.8.3. Transmission electron microscopy

All images of negatively stained samples were recorded at acceleration voltage 160 kV using CM200 FEG transmission electron microscope (Philips) with a 4Kx4K charge-coupled device (CCD) camera (Tietz Video Systems, Gauting, Germany) with 2-fold binning. Images destined for single-particle analysis were recorded as series of non-overlapping 4x4 spotscans.

2.8.4. Image processing and analysis

Processing of raw images and image analysis were performed by Dr. F. Hauer at the Max Planck Institute for Biophysical Chemistry, Göttingen, Germany. In brief, images of each series were combined in a larger micrograph and single particles were selected semi-automatically using the EMAN 1.9 software (Ludtke, Baldwin, & Chiu, 1999). Images were aligned and classified in a reference-free manner to obtain 2D class averages (Dube, Tavares, Lurz, & Heel, 1993). 3D reconstitution was done by the angular reconstitution technique (Van Heel, 1987). Image processing was done using the IMAGIC-5 software (van Heel et al., 1996). For visualization of 3D volumes, UCSF Chimera was used (Pettersen et al., 2004).

3. Results

3.1. Analysis of protein-protein interactions in the TIM23 translocase

3.1.1. Identification of Tim50 cross-linking adducts

Tim50 is an essential component of the TIM23 complex, also called presequence translocase. It fulfills a number of important functions, most of which are attributed to its C-terminal intermembrane space domain (Tim50^{IMS}, Fig. 3.1A). This domain is involved in numerous interactions with the other components of the translocation machinery: it serves as a presequence receptor (Qian, Gebert, Höpker, Yan, Li, Wiedemann, van der Laan, Pfanner, & Sha, 2011a; Schulz et al., 2011), regulates channel activity of the TIM23 complex (Meinecke et al., 2006) and transiently interacts with TOM (Shiota et al., 2011).

A crystal structure of the Tim50^{CORE} fragment (amino acids 164-361, Fig. 3.1B) revealed the presence of a large groove containing several negatively charged residues, which was hypothesized to be the presequence-binding region of Tim50 (Qian, Gebert, Höpker, Yan, Li, Wiedemann, van der Laan, Pfanner, & Sha, 2011a). However, based on a photocrosslinking approach, a C-terminal fragment, absent in the X-ray structure, was found to form a presequence-binding domain (PBD) of Tim50 (Schulz et al., 2011). To investigate the role of the groove and to identify potential interaction partners of Tim50 binding in this region, we used a cross-linking approach, taking advantage of a single cysteine residue located at the bottom of the groove.

Mitochondria were subjected to chemical cross-linking using CuSO₄ as an oxidizing agent and cross-linking products were resolved by non-reducing SDS-PAGE followed by Western blotting with anti-Tim50 antibodies. CuSO₄ treatment induced the formation of several prominent cross-linking adducts (Fig. 3.2A). Their specificity was confirmed by performing the same procedure in mitochondria bearing an HA tag on Tim50 (Tim50^{HA}) and immunodecoration with anti-HA antibodies, which resulted in a size shift of most cross-linking adducts.

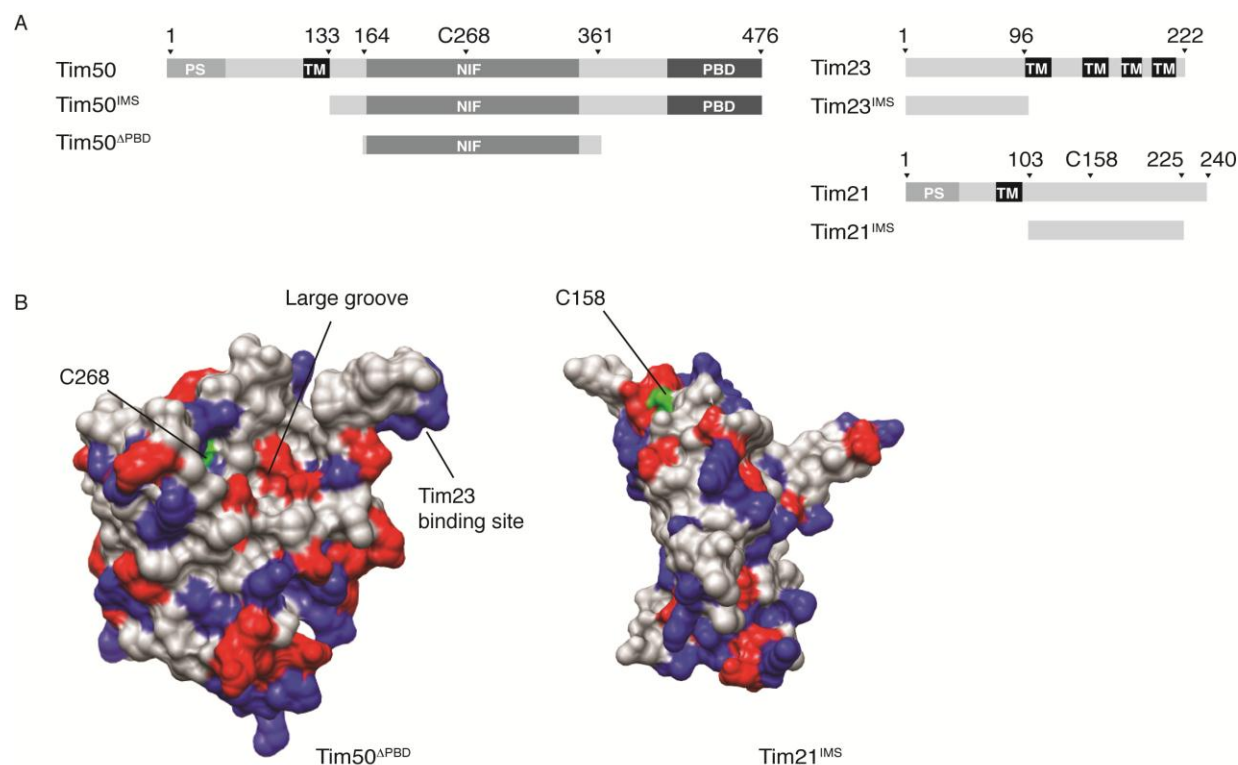


Figure 3.1. Structures of the Tim21, Tim23 and Tim50 fragments

(A) Schematic representations of Tim21, Tim50, Tim23 and their fragments used in this study. Presequences (PS), transmembrane domains (TM), NIF domain of Tim50 and relevant cysteine residues are indicated. Positively charged residues are blue, negative are red. (B) X-ray structures of Tim21^{IMS} (protein data bank accession number 2CIU) (Albrecht et al., 2006) and Tim50^{CORE} (protein data bank accession number 3QLE) (Qian et al., 2011). Negatively charged residues are red, positive are blue, cysteines are green. Positions of the cysteines, as well as large groove and Tim23-binding site of Tim50 are indicated.

To identify the interacting proteins, cross-linking was performed in mitochondria with tagged versions or deletions of selected TOM, TIM22 and TIM23 components. Tagging proteins of the TOM, PAM and TIM22 complexes did not cause any detectable changes in the cross-linking pattern of Tim50 (Fig. 3.2B, lanes 1-10). However, in Tim21^{ProtA} mitochondria one of the prominent cross-links of approximately 80 kDa was shifted compared to wild type (Fig. 3.2B, lanes 11-12, black mark). Expression of wild-type Tim21 from a plasmid in Tim21^{ProtA} mitochondria rescued the missing adduct (Fig. 3.2C, lane 4), excluding the possibility that the protein A tag interfered with binding of another unknown protein to Tim50. The same cross-linking adduct was missing in *tim21Δ* mitochondria and expression of Tim21 from a plasmid completely restored it (Fig. 3.2C, lanes 2 and 5). Based on this, we identify the 80 kDa cross-link as Tim21-Tim50 adduct.



Tim23 is a well-known interaction partner of Tim50. To check for the presence of a Cu²⁺-induced cross-link between the two proteins, the same cross-linking experiment was performed in mitochondria containing HA- or protein A-tagged versions of Tim23 (Tim23^{HA} and Tim23^{ProtA}, respectively). One of the adducts was specifically shifted in

both strains, remaining intact in Tim21^{ProtA} mitochondria, which allowed its identification as Tim23-Tim50 cross-linking product (Fig. 3.2D).

From this, we conclude that Tim21 and Tim23 are in close proximity to Tim50 in mitochondria (<3Å).

3.1.2. The IMS domains of Tim21 and Tim50 interact *in vitro*

Both Tim21 and Tim50 are integral membrane proteins with single transmembrane spans and large soluble domains exposed to IMS (Fig. 3.1A). To find out, if anchoring to the inner mitochondrial membrane is required for the interaction, we performed *in vitro* cross-linking experiments with purified IMS domains of Tim21 and Tim50.

His-tagged Tim21^{IMS} (amino acids 103-225), Tim50^{IMS} (aa 132-476) and Tim50^{CORE} (aa 164-361, corresponding to the crystallized fragment in Qian et al., 2011) were expressed in *E. coli* and purified by Ni²⁺ affinity chromatography (Fig. 3.3). If necessary, the tag was removed by cleavage with tobacco etch virus (TEV) protease. In addition, we expressed and purified mutated version of Tim21^{IMS}, which contained a cysteine to serine substitution (Tim21^{IMS-C128S}) and served as a negative control for Cu²⁺ cross-linking experiments (Fig. 3.3.B).

To confirm the interaction between Tim21^{IMS} and Tim50^{IMS} in an *in vitro* approach, purified IMS domains of both proteins were subjected to Cu²⁺ cross-linking and analyzed by SDS-PAGE with subsequent colloidal Coomassie staining. The cysteine-free version of Tim21^{IMS} was used to confirm the specificity of Cu²⁺ cross-linking. Addition of Cu²⁺ induced dimerization of Tim21^{IMS}, but not of Tim21^{IMS-C128S} (Fig. 3.4A, lanes 4-5). The formation of a Tim50^{IMS} dimer was also observed (Fig. 3.4A, lane 6), consistent with previous observations (Gevorkyan-Airapetov et al., 2009). When Tim21^{IMS} (but not Tim21^{IMS-C128S}) and Tim50^{IMS} were combined in the same reaction, an additional cross-linking adduct appeared, corresponding to the Tim21^{IMS}-Tim50^{IMS} heterodimer (Fig. 3.4A, lane 8).

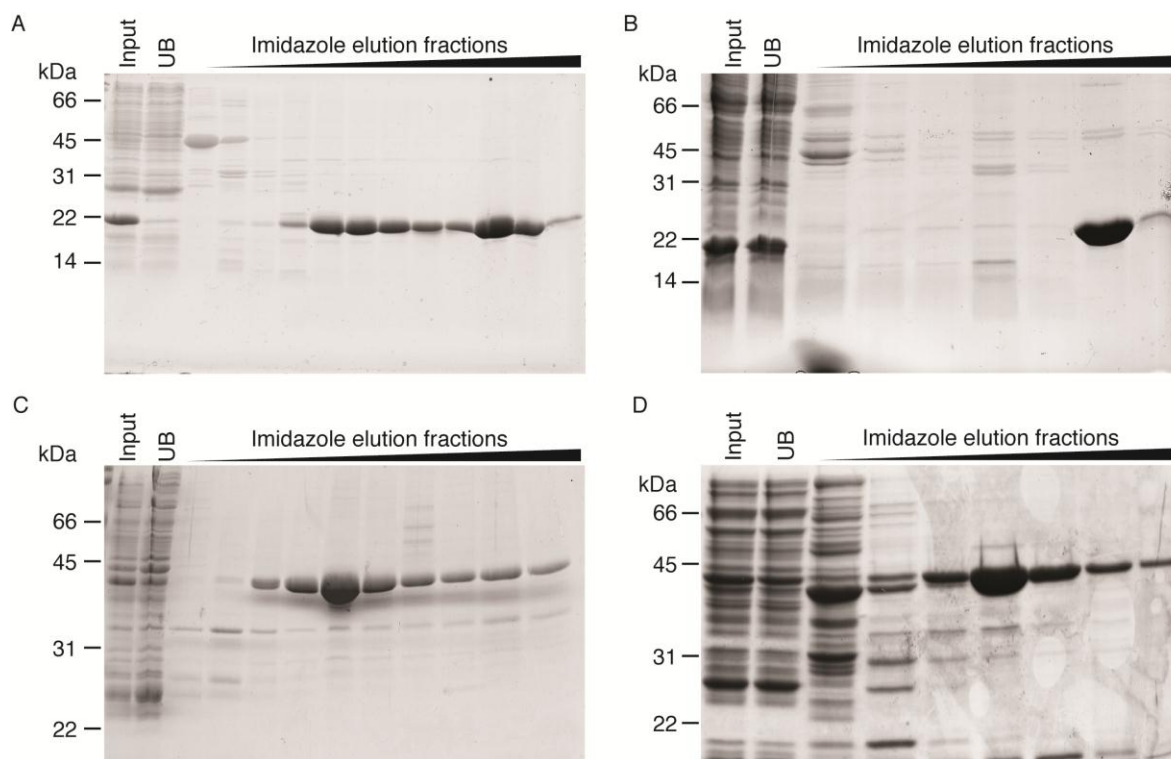


Figure 3.3. Protein purification from *E. coli*

(A) Tim21^{IMS} was purified on a HisTrap HP 1 ml column and eluted with a linear 0–500 mM imidazole gradient, as described in section 2.5.2. Loading, 5 μ l fraction material per lane. The gel is stained with Coomassie Brilliant Blue R-250. UB, unbound material. (B) The same for Tim21^{IMS-C128S}. (C) The same for Tim50^{IMS}. (D) The same for Tim50^{CORE}.

To confirm the specificity of the cross-linking, a similar experiment was performed, in which increasing concentrations of purified Tim50^{IMS} or bovine serum albumin (BSA) were added to purified Tim21^{IMS} in the presence of Cu²⁺. As expected, Tim50^{IMS} was efficiently cross-linked to Tim21^{IMS}, whereas no cross-linking product was appearing in BSA-containing samples (Fig. 3.4B). Based on this, we conclude that Tim21 and Tim50 directly interact via their IMS domains and their transmembrane domains are dispensable for this interaction.

Two functionally distinct fragments were described within the IMS domain of Tim50: Tim50^{PBD}, which is responsible for presequence binding, and the core Tim50^{CORE}, to which Tim23 binding has been attributed (Qian et al., 2011; Schulz et al., 2011; see Fig. 3.1). The only cysteine residue in Tim50 is located at the bottom of the large groove in the Tim50^{CORE} fragment (Fig. 3.1), suggesting that interaction with Tim21 occurs in this region.

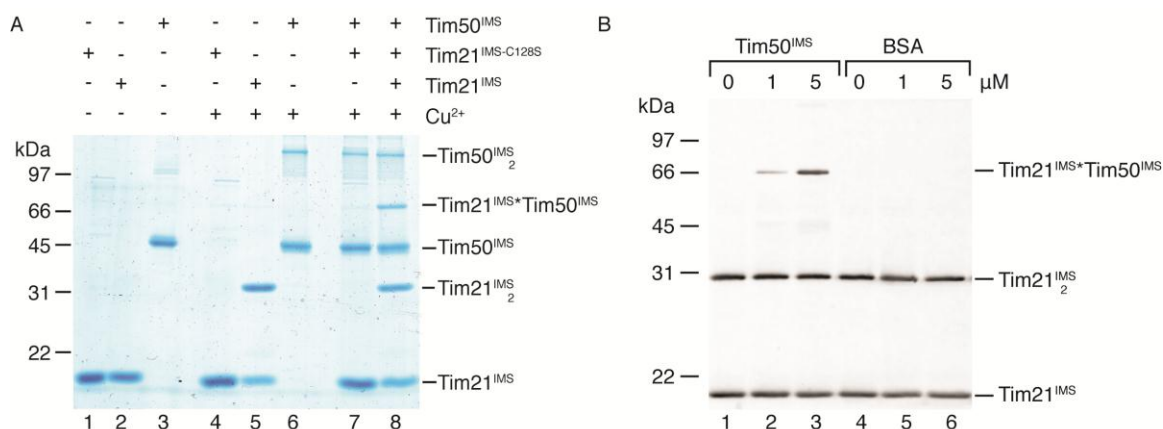


Figure 3.4. IMS domains of Tim21 and Tim50 interact *in vitro*

(A) Purified recombinant proteins (25 μM Tim21^{IMS} or Tim21^{C128S} and 10 μM Tim50^{IMS}) were cross-linked with 5 mM CuSO₄. Cross-linking products were visualized in the gel by staining with colloidal Coomassie. (B) Indicated amounts of purified Tim50^{IMS} or bovine serum albumin (BSA) were mixed with recombinant Tim21^{IMS} (final concentration 1 μM) and cross-linked by adding 1 mM CuSO₄, followed by Western blotting and decoration with anti-Tim21 antibody.

However, this does not exclude the role of Tim50^{PBD} for interaction with Tim21. To find out, if the PBD fragment is needed for the interaction, we performed *in vitro* cross-linking experiments as above with purified Tim50^{CORE}. Similarly to Tim50^{IMS}, Tim50^{CORE} formed dimers upon treatment with CuSO₄ (Fig. 3.5A, lane 4) and was efficiently cross-linked to Tim21^{IMS} added in increasing concentrations (Fig. 3.5A, lanes 5-7), showing that presequence-binding domain of Tim50 is dispensable for interaction with Tim21^{IMS}.

In order to obtain additional information about physical nature of the interaction, Tim21^{IMS} was cross-linked with Tim50^{CORE} by Cu²⁺ in the presence of increasing NaCl concentrations (Fig. 3.5B). Based on the observation that increasing salt concentration had no effect on cross-link formation, we conclude that the interaction is predominantly of a non-ionic nature.

Until now, all the evidence about physical interaction between Tim21 and Tim50 relied solely on cross-linking experiments. However, such experiments cannot provide quantitative information about affinity of this interaction. We used surface plasmon resonance (SPR) measurements to confirm interactions between the analyzed proteins by an independent approach and in a quantitative manner.

3. Results

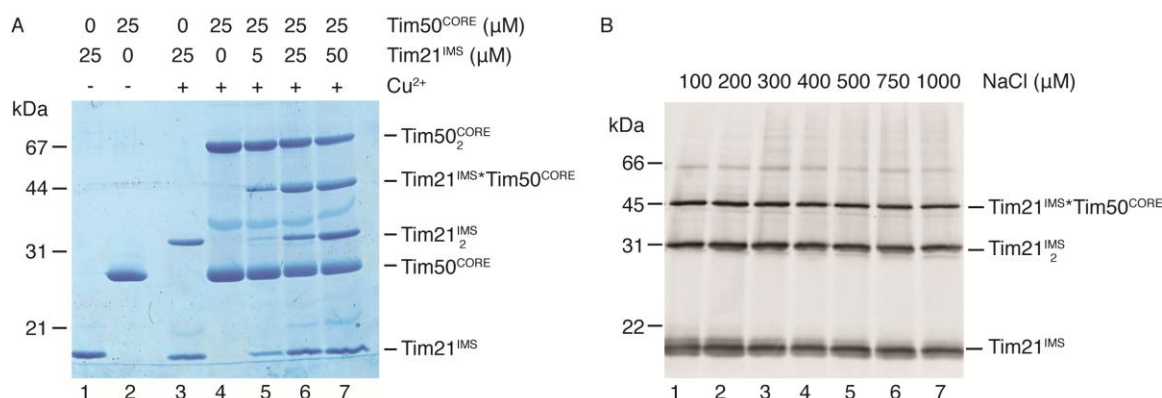


Figure 3.5. PBD of Tim50 is not required for interaction with Tim21

(A) Indicated amounts of Tim21^{IMS} and Tim50^{CORE} were cross-linked with 1 mM CuSO₄, separated on non-reducing SDS-PAGE and stained with colloidal Coomassie. (B) Tim21^{IMS} and Tim50^{CORE} were mixed (at final concentration 1 μM each) and subjected to CuSO₄ cross-linking in the presence of increasing NaCl concentrations. Cross-linking products were detected by anti-Tim21 immunoblotting.

Table 3.1. Parameters of protein-protein interactions measured by SPR

SPR data presented in Fig. 3.6 and Fig. 3.7 were analyzed by Scrubber 2.0 and interaction parameters were determined based on association/dissociation kinetics (k_a , k_d and K_D) and on equilibrium data (K_D). Data are presented as mean±standard error of the mean (n=3).

Ligand-analyte	Kinetic parameters			Equilibrium parameters
	k_a , mM ⁻¹ s ⁻¹	k_d , s ⁻¹	K_D , μM	K_D , μM
Tim50 ^{IMS} -Tim21 ^{IMS}	64.6±6.7	0.016±0.001	0.26±0.03	0.29±0.05
Tim50 ^{IMS} -pALDH	12.9±1.4	0.048±0.002	3.79±0.22	3.76±0.25
Tim50 ^{PBD} -pALDH	6.3±0.7	0.044±0.010	6.94±1.18	12.5±2.56
Tim50 ^{CORE} -pALDH	14.7±3.0	0.055±0.006	3.94±0.47	4.02±0.34

His-tagged Tim50^{IMS} was immobilized on a Ni²⁺ chelator sensorchip and concentration-dependent binding of Tim21^{IMS} was monitored. A typical sensogram is shown on Fig. 3.6A. Fitting affinity data (right panel) strongly argued for a single binding site model, with the K_D of approximately 290 nM. Kinetic data analysis under the assumption of a simple bimolecular interaction was in a good agreement with the affinity data, determining the K_D of the interaction at 260 nM (Table 3.1). To exclude the possibility of an experimental mistake due to unspecific binding of proteins to Tim50^{IMS}-His, we performed the same experiment adding comparable concentrations of BSA to immobilized Tim50^{IMS}. No binding could be observed in the entire concentration range, supporting specificity of Tim50^{IMS} interaction with Tim21^{IMS} (Figure 3.6B).

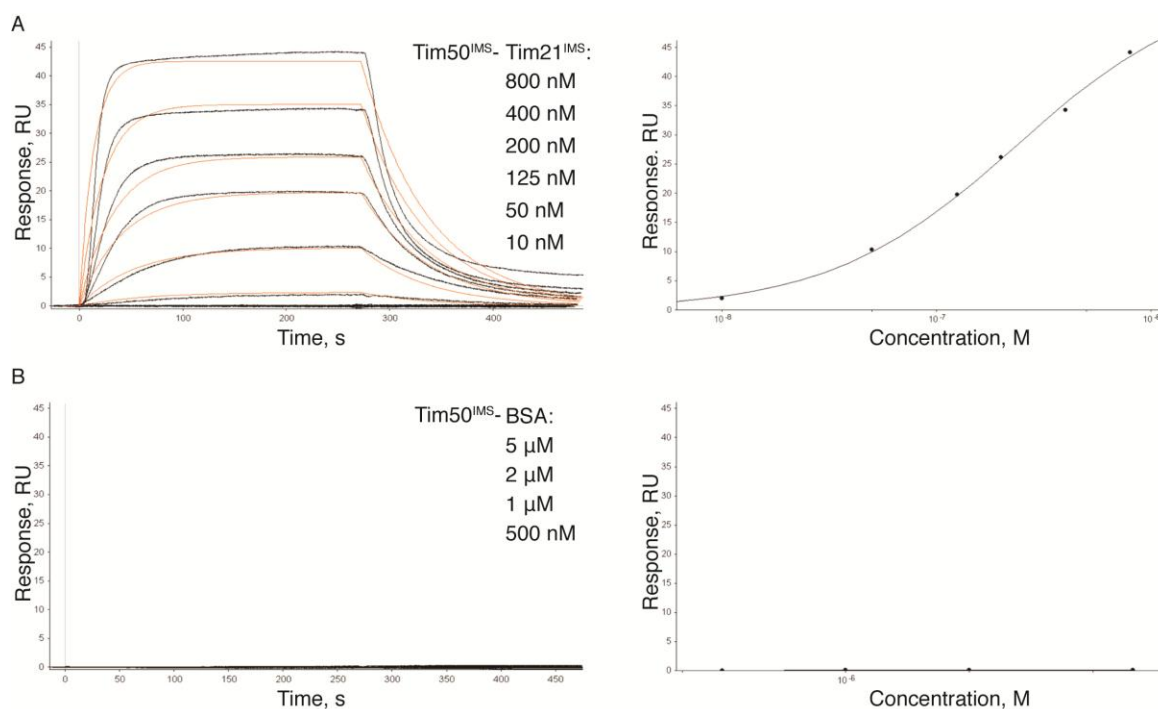


Figure 3.6. SPR analysis of Tim21^{IMS}-Tim50^{IMS} interaction

Tim50^{IMS-His} was immobilized on a chip and SPR response was recorded after adding indicated concentrations of Tim21^{IMS} (A) or BSA (B), as described in section 2.6.10. Left panels: typical sensograms. Black lines, observed binding; red, calculated k_a/k_d fitting of the kinetic data. Right panels: equilibrium analysis (data fitting based on a model of simple bimolecular interaction).

3.1.3. Presequence binding to Tim50 is independent of Tim21

We have shown that Tim21 binds to Tim50 close to its cysteine residue at the bottom of the large groove, which was previously hypothesized to represent a presequence-binding region (Qian, Gebert, Höpker, Yan, Li, Wiedemann, van der Laan, Pfanner, & Sha, 2011a). This finding raises two important questions: (1) do presequences also bind to this region, and (2) if so, do they compete with Tim21 for binding? The first question has been addressed previously by cross-linking approach (Schulz et al., 2011), which did not reveal presequence binding to the Tim50 fragment lacking the PBD (amino acids 162-365). We decided to verify this finding by an independent method, not relying on any cross-linking. In order to directly probe interaction of presequence peptides with Tim50, we immobilized His-tagged Tim50^{IMS}, Tim50^{PBD} and Tim50^{CORE} on a Ni²⁺ chelator sensorchip and recorded SPR response after addition of rat ALDH presequence peptide (pALDH) or its scrambled version pALDH-s (Fig. 3.7 and Table 3.1).

3. Results

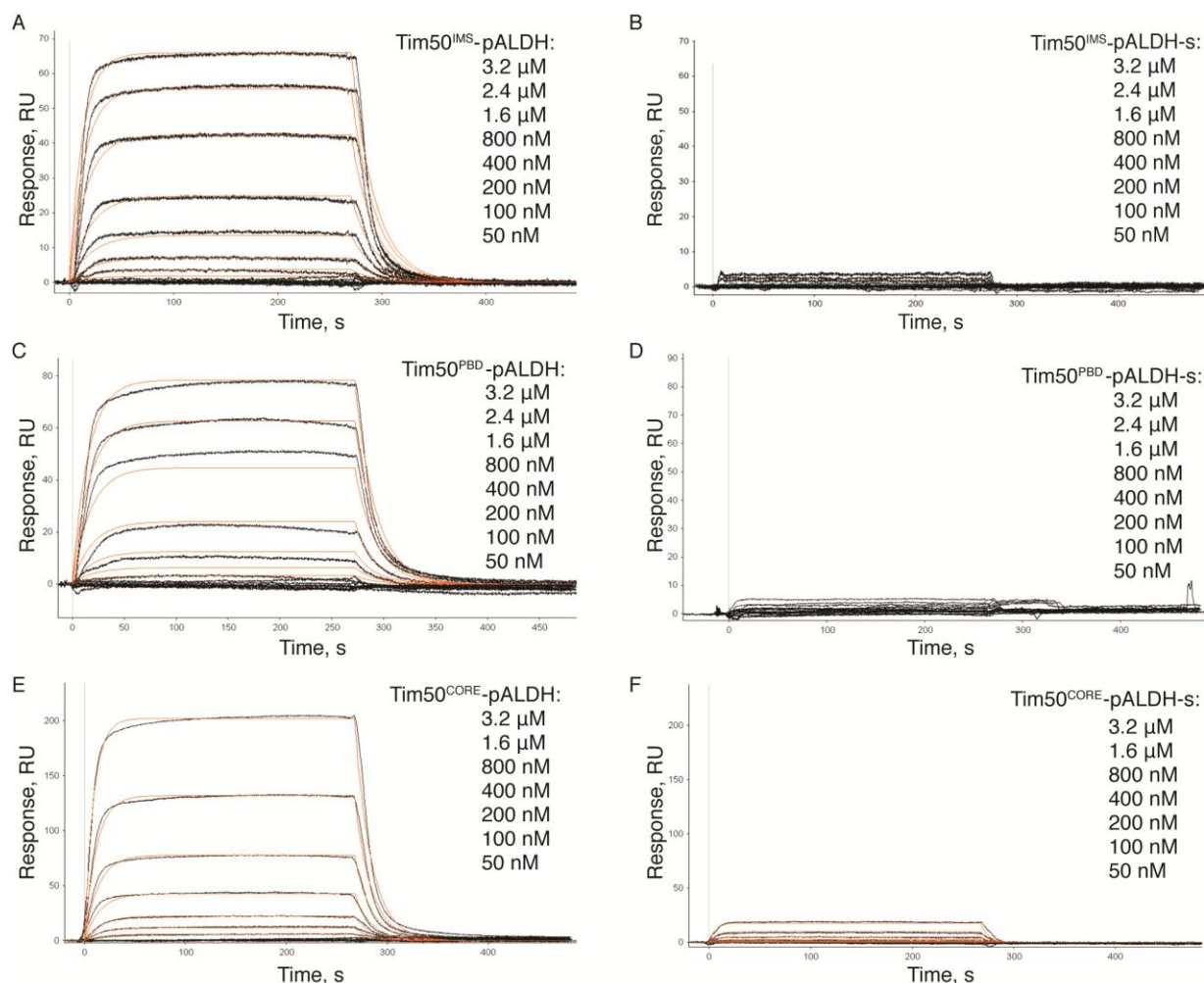


Figure 3.7. SPR analysis of presequence interaction with Tim50 fragments

Typical sensograms are shown for Tim50^{IMS}-pALDH (A), Tim50^{PBD}-pALDH (C) and Tim50^{CORE}-pALDH interactions (E). Corresponding measurements with pALDH-s are shown in (B), (D) and (F). Black lines, observed binding; red, calculated k_a/k_d fitting of the kinetic data. (Fitting kinetic data for the Tim50^{IMS}-pALDH-s and Tim50^{PBD}-pALDH-s interactions was not possible). Details are in the text.

As expected, the presequence peptide specifically interacted with Tim50^{IMS} with a K_D of approximately 3.8 μ M, whereas the import-inactive peptide pALDH-s showed almost no interaction (Fig. 3.7, A-B).

Next, we investigated presequence binding to Tim50^{PBD}-His. This domain was specifically binding the pALDH peptide, although with slightly lower affinity than full-length Tim50^{IMS} (Fig. 3.7C-D). Different affinities are attributed to different association kinetics of the presequence peptide, which was approximately two times slower for Tim50^{PBD} compared to Tim50^{IMS} (Table 3.1).

To our surprise, we also observed strong specific binding of the presequence peptide to Tim50^{CORE-His}, with affinity and kinetics similar to Tim50^{IMS} (Fig. 3.7E-F and Table 3.1). Interestingly, fitting equilibrium data for Tim50^{IMS}-pALDH binding (Fig. 3.7A, right panel) strongly supported model of a single presequence-binding site, which would imply cross talk between different domains.

Presequences and Tim21^{IMS} interact with the same fragment of Tim50, but is their binding mutually exclusive? To answer this question, Tim21^{IMS} and Tim50^{IMS} were cross-linked by Cu²⁺ in the presence of increasing concentrations of pALDH or pALDH-s and analyzed by Western blotting (Fig. 3.8A). No differences in the cross-linking efficiencies were observed even at 50-fold excess of the presequence peptide, suggesting that Tim21^{IMS} binding to Tim50 is independent of the presequence. The same experiment was repeated with another presequence peptide, pCox4, yielding the same result (Fig. 3.8B, lanes 1-3). To rule out the possibility that in the full-length Tim50^{IMS} presequence binding was affected by the presence of the PBD, the same experiment was performed using Tim50^{CORE} (Fig. 3.8B). As with Tim50^{IMS}, pCox4 had no effect on Tim21 binding to Tim50^{CORE}, suggesting that these interactions take place at different regions of Tim50.

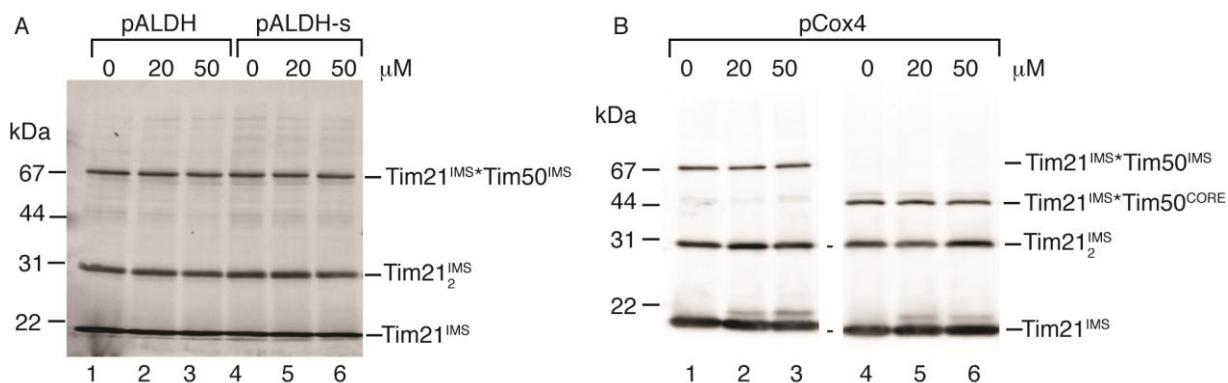


Figure 3.8. Presequences do not affect Tim21^{IMS}-Tim50^{IMS} interaction *in vitro*

(A) Purified 1 μ M Tim21^{IMS} and Tim50^{IMS} were cross-linked with Cu²⁺ in the presence of increasing amounts of pALDH or pALDH-s and analyzed by immunoblotting against Tim21. (B) Purified Tim21^{IMS} and Tim50^{IMS} (lanes 1-3) or Tim21^{IMS} and Tim50^{CORE} (lanes 4-6) were cross-linked in the presence of indicated concentrations of pCox4 and analyzed as in (A).

3.1.4. Dynamics of Tim50 interactions in response to presequence

Tim50 is one of the first components that recognize presequences appearing at the IMS side of the outer mitochondrial membrane (Mokranjac et al., 2003; Yamamoto et al., 2002). To follow dynamics of Tim50 interactions during translocation cycle, we treated isolated mitochondria with an excess of a presequence peptide, followed by Cu^{2+} -induced cross-linking and immunoblotting with anti-Tim50 antibody. We observed a concentration-dependent increase of the Tim50-Tim23 cross-link (up to 80% compared to the control sample) accompanied by significant decrease (down to 30% of initial level) of Tim21-Tim50 cross-linking adduct (Fig. 3.9A-B). At the same time, treatment with a control peptide had no significant effect on either of the interactions.

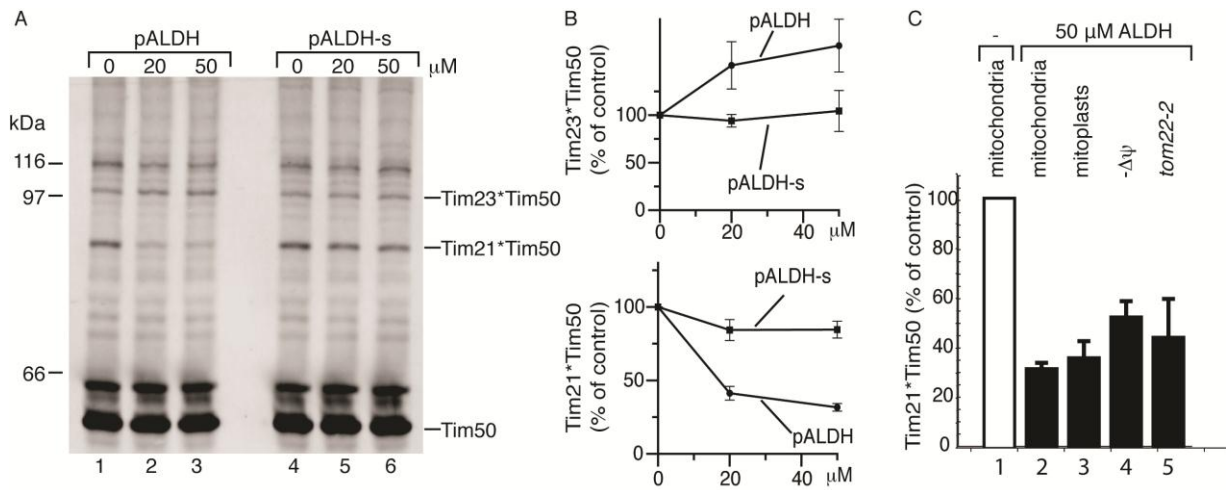


Figure 3.9. Presequence peptides affect interactions between Tim21, Tim23 and Tim50 *in organello*

(A) Mitochondria were pre-treated with indicated concentrations of the pALDH presequence peptide or its scrambled version (pALDH-s), cross-linked with CuSO_4 and analyzed by immunodecoration against Tim50. (B) Signals from the corresponding cross-links were quantified, normalized to buffer-treated control (set as 100%) and presented as mean \pm standard error of the mean ($n=6$). (C) The same experiment as in (A) was performed in normal wild type mitochondria (white bar), osmotically swollen mitochondria (mitoplasts), mitochondria with dissipated membrane potential ($-\Delta\psi$) and *tom22-2* mitochondria ($n=4$ for all). Intensity of Tim21-Tim50 cross-link after treatment with 50 μM pALDH peptide is shown, in comparison to mock treatment.

The observed decrease of Tim21-Tim50 cross-link apparently contradicted our observation that presequences do not affect Tim21-Tim50 interaction *in vitro*, suggesting that the *in organello* effect was mediated by another component of the translocation machinery. Since both Tim50 and Tim21 are known to interact with components of the

TOM complex, we checked if intactness of the outer membrane or the IMS domain of Tom22 were required for the presequence-induced loss of the Tim21-Tim50 interaction. Presequence treatment after osmotic swelling (to disrupt the outer membrane) of wild type mitochondria or the use of *tom22-2* mitochondria (lacking the IMS domain of Tom22) caused similar changes in Tim21-Tim50 cross-linking as in wild-type mitochondria (Fig. 3.9C, bars 3 and 5). Moreover, a membrane potential across the inner membrane was also not required (Fig. 3.9C, bar 4), confirming that this loss of cross-link took place at early stages of the translocation process.

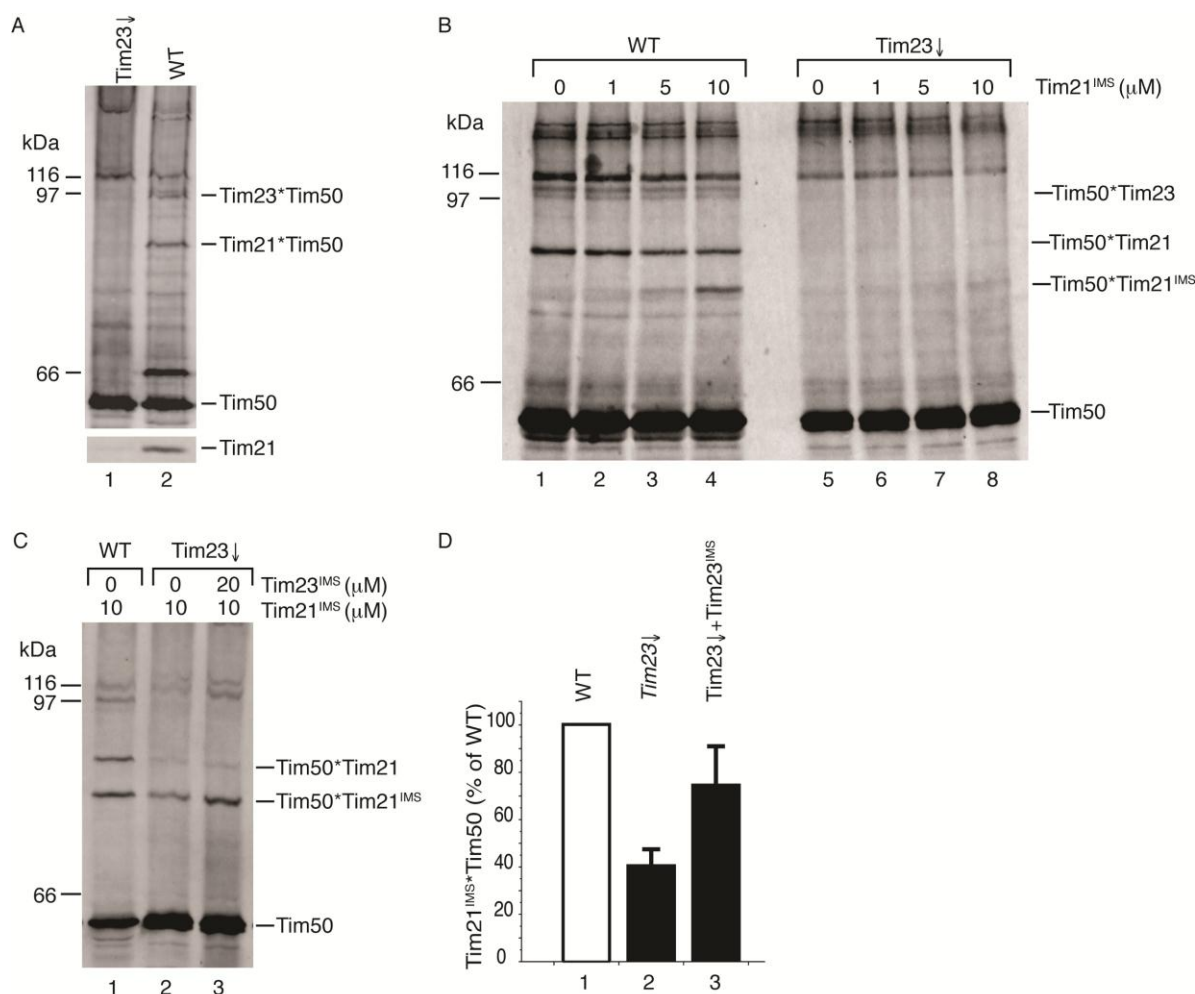


Fig. 3.10. IMS domain of Tim23 affects Tim21^{IMS}-Tim50 interaction in mitoplasts

(A) Cu²⁺-induced cross-linking in Tim23^Δ mitochondria, followed by immunoblotting against Tim50. Below: Level of Tim21 in Tim23^Δ mitochondria, detected by immunoblotting. (B) Mitoplasts derived from wild type or Tim23^Δ mitochondria were subjected to cross-linking after incubation with indicated concentrations of Tim21^{IMS}. (C) Treatment of wt and Tim23^Δ mitoplasts with indicated concentrations of Tim21^{IMS} and Tim23^{IMS} was followed by Cu²⁺ cross-linking and immunoblotting against Tim50. (D) Quantification of Tim21^{IMS}-Tim50 signals in (C) normalized to control. Data are presented as mean±standard error of the mean (n=5).

If outer membrane proteins do not mediate the presequence effect on the Tim21-Tim50 interaction, can Tim23, being the only remaining presequence receptor in the IMS, affect it? To address this question, we analyzed Tim50 cross-links in mitochondria with depleted Tim23 (Tim23 \downarrow) (Schulz et al., 2011) and found no Tim21 and Tim23 adducts (Fig. 3.10A, upper blot). This lack of adduct formation was due to significantly reduced levels of Tim23 and Tim21 in these mitochondria (Fig. 3.10A, anti-Tim21 decoration). To overcome this problem, recombinant Tim21^{IMS} was added to mitoplasts and cross-linked to Tim50, as described in Section 2.7.6. Surprisingly, the amount of Tim21^{IMS}-Tim50 cross-linking product was still significantly lower in Tim23 \downarrow mitochondria, despite comparable levels of Tim50 in both strains (Fig. 3.10B). Addition of recombinant Tim23^{IMS} to the reaction rescued, at least partially, the cross-link between Tim21^{IMS} and Tim50, supporting the assumption of a regulatory role of Tim23^{IMS} for this interaction *in organello* (Fig. 3.10C).

3.1.5. Dynamics of the TIM23 complex

Presequence-induced changes in the cross-linking pattern of Tim50 can have different explanations. One scenario would imply structural rearrangements or conformational changes of proteins within the translocase, so that distances between the cross-linked cysteine residues become unfavorable for cross-link formation. Alternative explanation could be that one or both proteins leave the TIM23 complex. To distinguish between these two possibilities, we performed co-immunoprecipitation (co-IP) experiments after mitochondrial treatment with presequences.

Mitochondria were incubated with presequence peptide pCox4 or its inactive counterpart SynB2, solubilized in digitonin-containing buffer and used for co-IP with antibodies directed against Tim50, Tim23 and, as a negative control, Ylh47. The results shown in Fig. 3.11 strongly favor the model implying mobility of the translocase components, predicting that the amounts of co-immunoprecipitated proteins differ after presequence-treatment. Indeed, the amount of Tim21 that co-precipitated with Tim50 and Tim23 was significantly reduced in mitochondria treated with presequence peptide. At the same time, association of Tim50 with Tim23, judged by Tim23 co-immunoprecipitation with Tim50, was slightly promoted. Interestingly, association of

Pam17, a non-essential constituent of the PAM complex, with the TIM23 complex increased after addition of presequence.

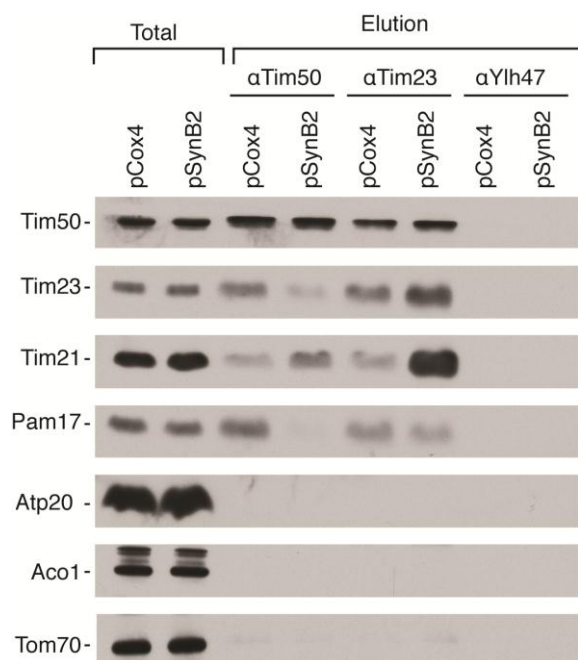


Figure 3.11. Co-immunoprecipitation experiments after presequence-treatment

Mitochondria were treated with 50 μ M pCox4 or SynB2 peptides for 20 minutes and, after solubilization in 1% digitonin, used for immunoprecipitation experiments with indicated antibodies. Immunoprecipitated proteins were analyzed by non-reducing SDS-PAGE and Western blotting. Total, 20%; Eluate, 100%.

These results support the model of a highly dynamic translocase, switching between different forms during the translocation cycle. In order to directly monitor association of proteins with different forms of the TIM23 complex, mitochondria treated with pCox4 or SynB2 were solubilized with digitonin and loaded on 10-30% glycerol density gradients. After centrifugation, fractions were collected from the top and distribution of proteins was analyzed by SDS-PAGE and Western blotting (Fig. 3.12A). Tim23 was detected predominantly in fraction 5 in both control and presequence-treated mitochondria, whereas the distribution of Tim50 and Tim21 changed in response to treatment with pCox4: The Tim50 peak was shifted from fraction 3 to fraction 5, and the Tim21 distribution became broader.

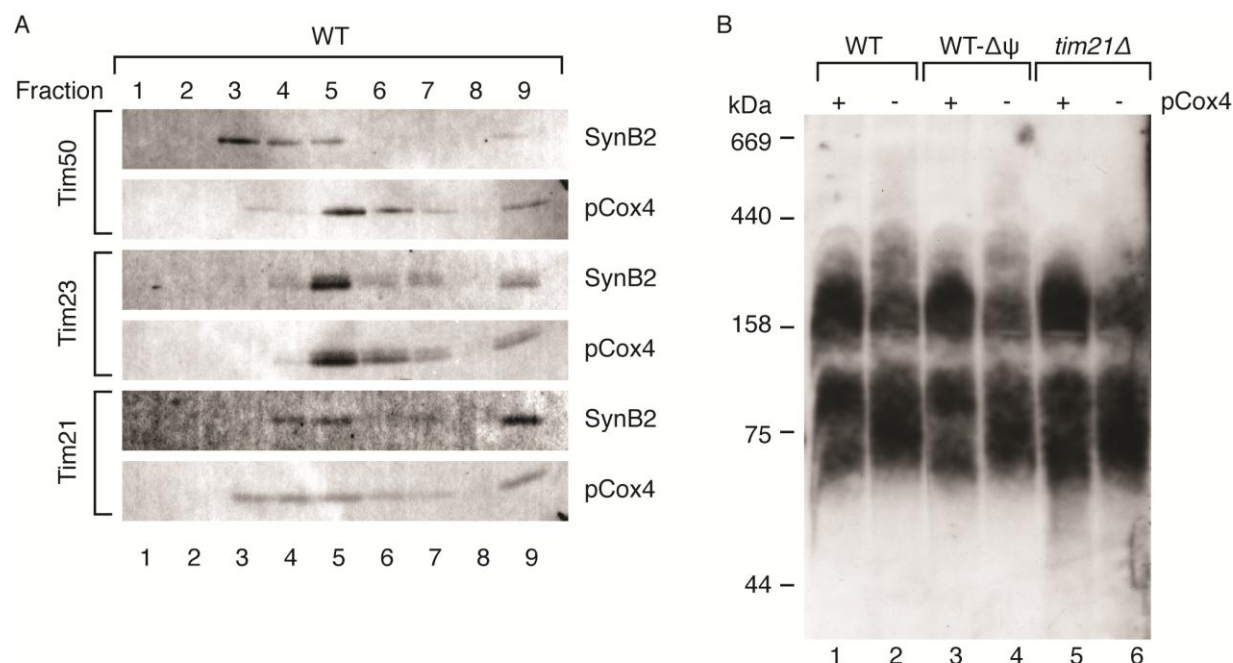


Figure 3.12. Non-denaturing analysis of the TIM23 complex

(A) Glycerol density gradient centrifugation. Mitochondria (150 μ g/sample) were incubated for 20 minutes in the presence of 50 μ M pCox4 or SynB2 peptides, solubilized by 1% digitonin and separated by glycerol gradient centrifugation for 16 hours at 215,000 \times g. 9 fractions were collected from the top, and after TCA precipitation analyzed by SDS-PAGE and immunoblotting. (B) BN-PAGE. Mitochondria (50 μ g/lane) were treated as in (A), solubilized in digitonin and loaded on a 6-16% BN-PAGE, followed by immunodecoration against Tim23. The same experiment was repeated in mitochondria with dissipated membrane potential (WT- $\Delta\psi$) and *tim21* Δ mitochondria.

The resolving power of the glycerol gradient centrifugation could be insufficient to separate different forms of the TIM23 translocase. To overcome this problem, we analyzed solubilized membrane complexes by BN-PAGE (Fig. 3.12B). Mitochondria were treated and solubilized as above; membrane complexes were separated by BN-PAGE and analyzed by immunoblotting against Tim23. TIM23 dissociates on BN-PAGE into three subcomplexes: the 90 kDa core complex and two higher molecular weight Tim21-containing forms. Presequence treatment shifted the equilibrium towards higher molecular weight complexes, which could reflect tighter association of the translocase components. The effect did not depend on Tim21 or membrane potential (Fig. 3.12B, lanes 3-6). In conclusion, we found that the TIM23 translocase undergoes significant changes during the translocation process, including association of some components (such as Pam 17) and dissociation of the others (such as Tim21).

3.2. Electron microscopy

3.2.1. Initial electron microscopy analysis of the TIM23 complex

In order to reveal the underlying mechanisms of protein translocation by the TIM23 translocase, a firm structural understanding is essential and can therefore be considered a prerequisite in the elucidation of its precise mode of action. Electron microscopy has been previously used to analyze structures of other mitochondrial membrane complexes (Dudkina et al., 2005, 2006; Lau et al., 2008; Model et al., 2002, 2008; Rehling et al., 2003; Rubinstein et al., 2003), making it a method of choice for the structural analysis of the TIM23 translocase.

The TIM23 complex was purified by IgG affinity chromatography (section 2.5.5) from mitochondria with a C-terminal protein A tag on Tim21 (Tim21^{ProtA}) or Tim23 (Tim23^{ProtA}). For a negative control, a mock purification from wild type mitochondria was performed according to the same procedure. Specificity and efficiency of protein complex purifications were confirmed by Western blotting (Fig. 3.13A) and mass-spectrometry analysis (Fig. 3.13B). Isolated complexes were directly used for preparation of EM samples negatively stained with uranyl acetate.

Electron microscopy revealed the presence of abundant, highly heterogeneous low-contrast particles (Fig. 3.13C). However, similar background was found in control samples, which contained no TIM23 complex (Fig. 3.13D). In order to separate particles of interest from contaminating components, while simultaneously improving sample homogeneity and image contrast, gradient fixation (GraFix) was applied (Kastner et al., 2008). This method combines ultracentrifugation in a glycerol density gradient with gradual fixation by glutaraldehyde. Purified TIM23 was subjected to this procedure; complex containing fractions were determined by slot blotting and immunodecoration against specific components of the translocase (Fig. 3.15A). In addition, gradient centrifugation was performed without fixation, allowing subsequent separation of proteins by SDS-PAGE (Fig. 3.15B). Both methods yielded similar results, detecting the majority of the complex in the lower third of the gradient (fractions 6-7 out of 9).

3. Results

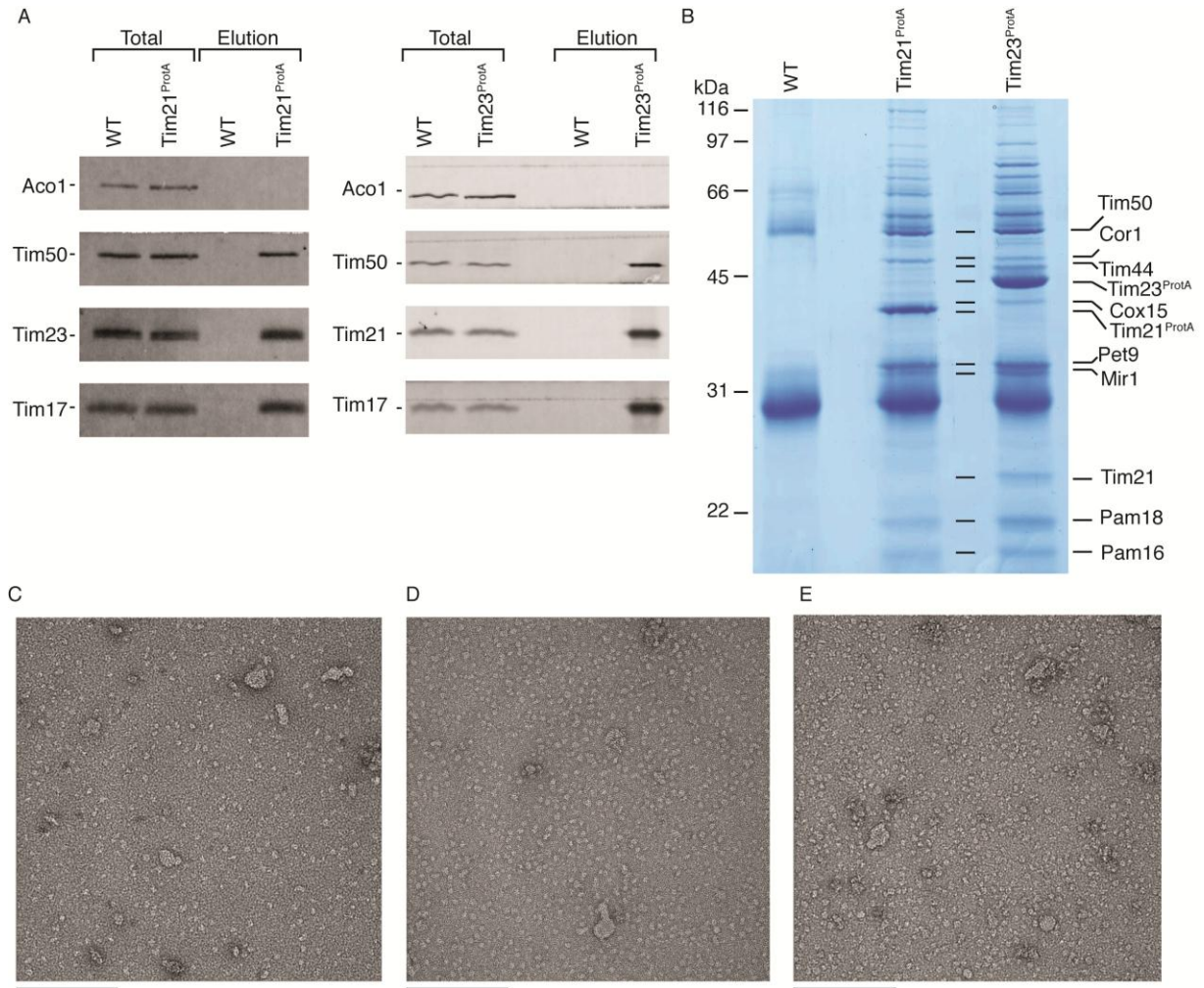


Figure 3.13. Purification and electron microscopy of the TIM23 complex

TIM23 was purified from Tim21^{ProtA} and Tim23^{ProtA} mitochondria by IgG affinity chromatography. Control purification from corresponding wild type mitochondria was done according to the same procedure. (A) SDS-PAGE - Western blotting analysis of the SDS-eluted proteins. Total, 5%; Elution, 100%. (B) Colloidal Coomassie staining of the complexes purified as in (A) on SDS-PAGE and the results of mass-spectrometric analysis of the complexes. (C-D) Representative negative stain images of the purified TIM23 complex from Tim21^{ProtA} mitochondria (C) and Tim23^{ProtA} (D). (E) A representative raw negative stain image of the mock purification. Scale bars, 100 nm.

Negative stain EM images of fraction 7 from the TIM23 GraFix gradient are shown in Fig. 3.14C. As expected, the procedure significantly improved both contrast and homogeneity of the sample, as compared to conventional sample preparation (Fig. 3.13B). However, the contaminations were similarly affected, as judged by the images of the negative control sample (Fig. 3.14D).

3. Results

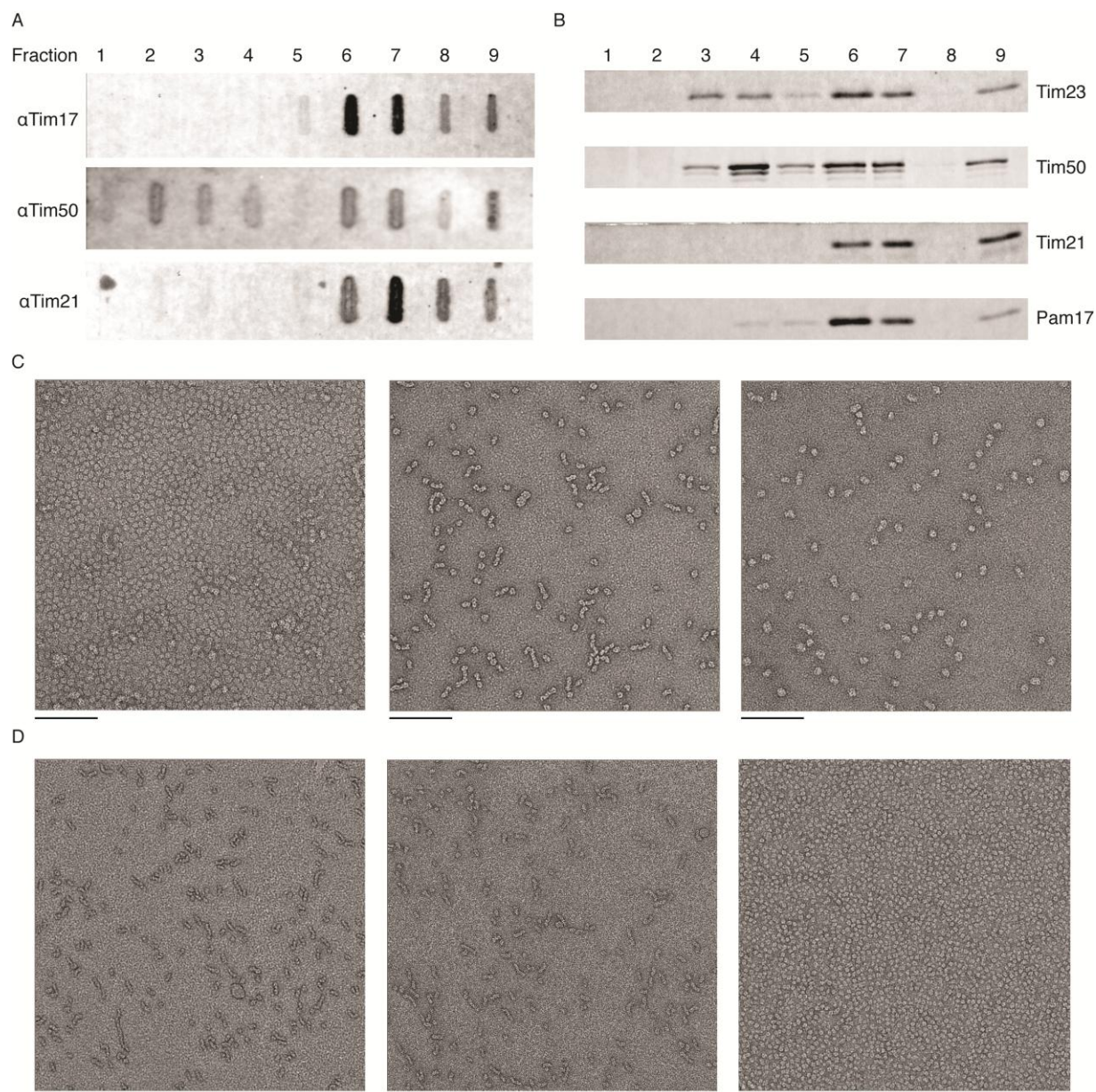


Figure 3.14. Gradient fixation of the purified TIM23 complex

TIM23 purified from 500 μg of Tim23^{ProtA} mitochondria was separated on a 10-30% glycerol gradient with (A) or without (B) 0-0.3% glutaraldehyde for 16 h at 215,000 g in a Beckman SW-60Ti rotor at 4°C. Fractions were collected from the top of the gradient and analyzed by slot blotting (A) or SDS-PAGE and Western blotting with immunodecoration against indicated components of the complex. (B). (C) Representative raw negative stain images of GraFix fraction 7. Scale bars, 100 nm. (D) Representative negative control images of GraFix fraction 7. Scale bars, 100 nm.

To determine the source of the background, negatively stained EM samples of buffers and solutions used in TIM23 complex purifications were prepared (Fig. 3.15). Digitonin, a mild non-ionic detergent required for the purification of TIM23, was found to be the

source of contaminating particles. In distilled water and digitonin-free elution buffer (Fig. 3.15A and Fig. 3.15C) almost no particles were present, whereas digitonin-containing buffers displayed severe contamination problems (Fig. 3.15B). To overcome this problem, three independent ways to optimize sample quality were tested: (1) extensive purification of commercially available digitonin; (2) detergent removal via γ -cyclodextrin (Signorell et al., 2007), and (3) replacing digitonin with other detergents as well as reducing its concentration. The first two approaches will be discussed below, while biochemical optimizations will be reviewed in section 3.2.4.

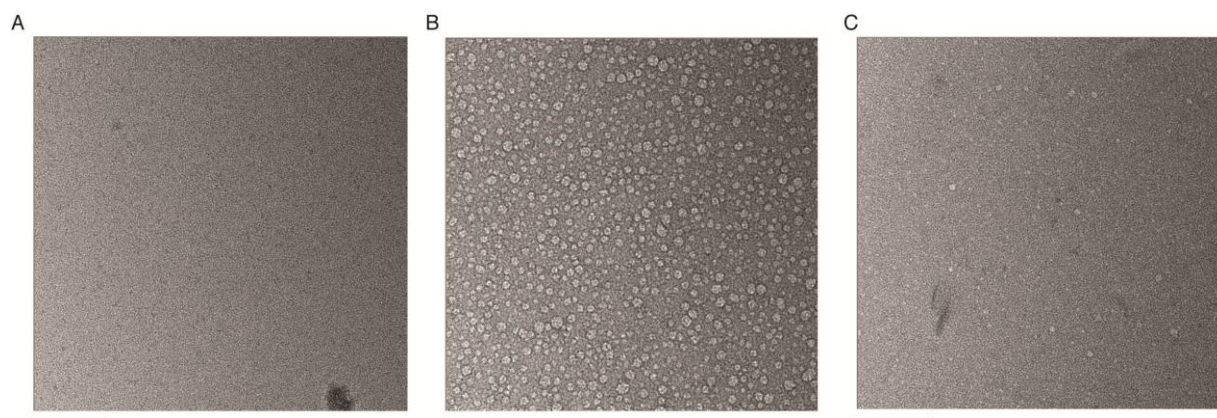


Figure 3.15. Typical contaminations found in buffers and solutions

Raw images of EM grids prepared with: (A) pure water, (B) TIM23 elution buffer, and (C) TIM23 elution buffer without digitonin. Scale bar, 100 nm.

3.2.2. Reduction of contaminations and background in EM samples

Purification of digitonin was achieved by re-crystallization in ethanol, dissolving the dried precipitate in water and removing charged components by passing the solution through ion-exchange columns HiTrap Q FF and HiTrap SP FF (GE Healthcare) (Herrmann et al., 2001). This procedure appeared to be highly efficient in removing gross contaminations (Fig. 3.16A) and was employed in all subsequent experiments. However, the remaining granulous background was strong enough to significantly impair contrast in negatively stained images, therefore extensive optimization was required for efficient EM analysis of the relatively small TIM23 complex.

Cyclodextrins are ring-shaped molecules with a hydrophilic exterior and hydrophobic interior environment, enabling the enclosure of detergents and other small amphiphilic

molecules (Degrip & Vanoostrum, 1998; Signorell et al., 2007). Washing EM grids with 100 μ M γ -cyclodextrin solution resulted in the complete removal of all unspecific background (Fig. 3.16B). Cyclodextrin also removed most of the low-contrast structures in samples of the TIM23 purification (Fig. 3.16C). However, the abundance, contrast and homogeneity of the remaining particles were insufficient for single-particle analysis, and therefore required further optimization.

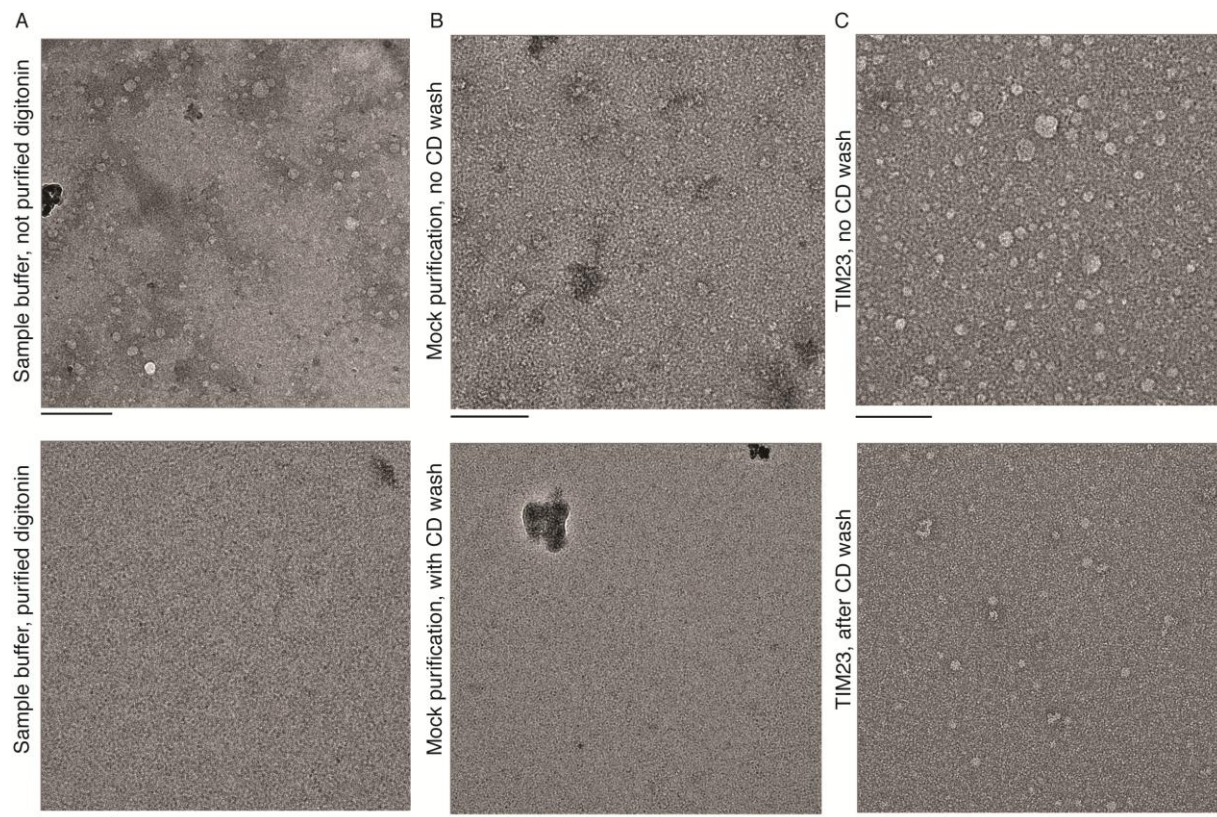


Figure 3.16. Removal of EM contaminations

(A) Digitonin was purified as described in the text. Negatively stained samples were prepared from the TIM23 elution buffer containing non-purified (above) and purified (below) digitonin. (B) Mock purification or (C) Tim21^{ProtA} purification of the TIM23 complex was done using non-purified digitonin. EM grids were prepared from the GraFix fractions conventionally (above) or were additionally washed with a drop of 100 μ M γ -cyclodextrin and double distilled water (below). Scale bars, 100 nm.

3.2.3. Preparation of TIM22 and respiratory chain complexes for EM

Having established general conditions for the preparation of negatively stained EM samples, we decided to test them on a relatively large and stable protein complex of known structure. Respiratory chain complexes, which fulfill all these requirements, were selected for initial testing. Complex III was purified by IgG affinity chromatography from

digitonin-solubilized mitochondria with a tandem affinity purification (TAP) tag on Cor1 (Cor1^{TAP}), a core subunit of the ubiquinol-cytochrome c reductase complex. The negative control sample was prepared according to the same procedure with wild-type mitochondria. Re-crystallized and purified digitonin was used in all experiments. Specificity and efficiency of the purification were confirmed by immunoblotting (Figure 3.17A). The eluate from the mock purification contained almost no analyzed proteins at detectable levels. In the Cor1^{TAP} purification, components of complex III (Rip1 and Qcr6) were confirmed in the eluate, while other non-associated proteins (Tom40 and Tom70) could not be detected.

Purified complexes were directly used to prepare negatively stained EM grids (Figure 3.17B-C). Almost no particles were found in the negative control sample (Fig. 3.17B), whereas preparations from Cor1^{TAP} mitochondria (Fig. 3.17C) yielded significant amounts of high-contrast particles, corresponding in shape and size to the published structures of respiratory chain supercomplexes (Mileykovskaya et al., 2012). The effect of the γ -cyclodextrin wash was also tested (Fig. 3.17D). Although the amount of particles attached to the carbon film was only insignificantly reduced, their shape and contrast were affected, suggesting deleterious effect of the washing step on complex integrity. Based on this observation, cyclodextrin was not used in subsequent EM sample preparations.

Successful purification and EM visualization of respiratory chain supercomplexes indicated that the established conditions for electron microscopy could be, in principle, applied in the analysis of purified complexes of the inner mitochondrial membrane. However, TIM23 is significantly smaller and less abundant than respiratory chain supercomplexes. For further optimization steps, TIM22 was selected, as it is a protein complex of the inner mitochondrial membrane of known 2D structure (Rehling et al., 2002), and is comparable to TIM23 in size and abundance.

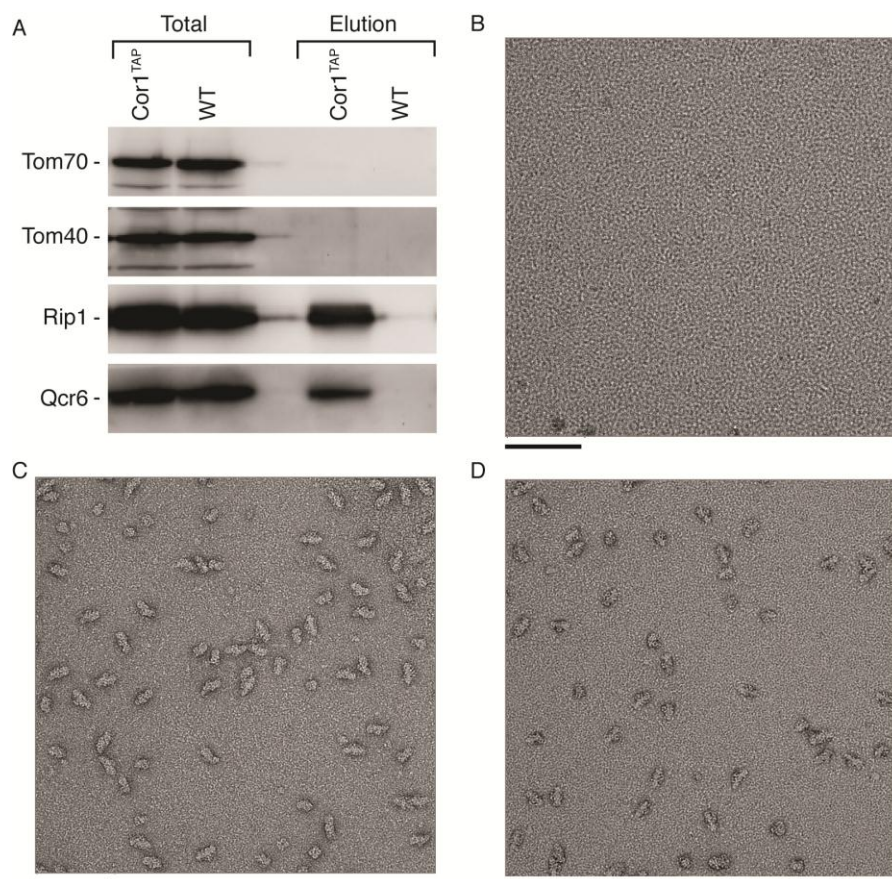


Figure 3.17. Purification and EM of respiratory chain supercomplexes

(A) Purification of RC complexes. 10 mg of wild-type or Cor1^{TAP} mitochondria were purified by IgG affinity chromatography with TEV protease cleavage of the tag and analyzed by Western blotting. Loading: Total, 20%; Eluate, 100%. (B-D). Electron microscopic analysis of purified RC complexes. Uranyl acetate-stained EM samples were prepared from the negative control sample (B) or purified complexes (C) using glow-discharged grids. Additional washing step with 100 μM cyclodextrin prior to uranyl acetate staining was applied in (D). Scale bar, 100 nm.

Purification of TIM22 was achieved utilizing the same strategy, using IgG affinity purification from a strain bearing protein A tag on Tim18 (Tim18^{ProtA}). Purification efficiency and specificity were estimated by immunoblotting (Fig. 3.18A). Purified complexes were subjected to GraFix followed by slot blotting (Fig. 3.18B). Fractions containing the majority of the complex (6 and 7 out of 9) were used for preparation of negatively stained EM samples. Despite sufficient purification efficiency, as well as high biochemical purity, EM analysis of the complex was hindered by a strong granular background (Fig. 3.18C). However, complexes were clearly distinguishable and of sufficient abundance, contrast and quality (Fig. 3.18D), suggesting that the optimized

sample preparation conditions were applicable to the analysis of small membrane complexes in digitonin-containing buffers.

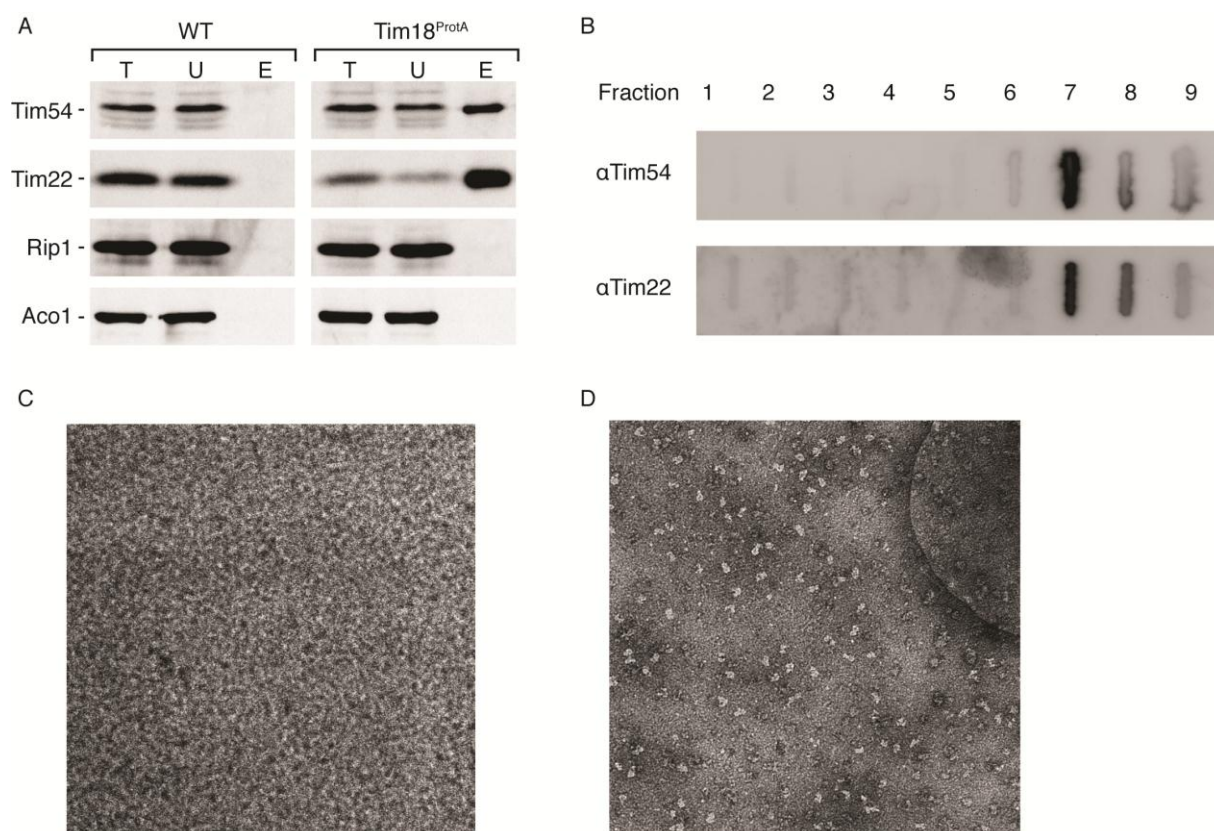


Figure 3.18. Purification and negative stain EM of the TIM22 complex

The TIM22 complex was purified from Tim18^{ProtA} mitochondria by IgG affinity chromatography with TEV protease cleavage of the tag. Wild type mitochondria were used in the negative control purification following the same procedure. **(A)** Western blotting analysis. T, Total (10%); U, unbound (10%); E, Elution (100%). **(B)** The purified complex was loaded on a 10–30% glycerol gradient with 0–0.3% glutaraldehyde and centrifuged at 215,000 g in a Beckman SW60 Ti rotor for 16 hours. 9 fractions were collected from the top of the gradient and analyzed by slot blotting. Fractions 6 and 7 were used for subsequent electron microscopy. **(C)** Raw negative stain images of negative control fraction 7. **(D)** Negative stain images of fraction 7 of the purified TIM22 complex.

3.2.4. Optimization of conditions for TIM23 complex purification

EM analysis of the TIM23 complex was expected to be the most challenging task, due to its small size, instability and functional heterogeneity. However, most of the critical problems throughout all stages of analysis were caused by strong background present in all digitonin-containing samples. Replacing digitonin by other surfactants would be the most straightforward solution, but, to date, digitonin is the only published detergent suitable for the purification of the TIM23 complex. To overcome this limitation, the

GraFix procedure might be helpful, as it provides additional stability to purified complexes through high hydrostatic pressure in conjunction with chemical fixation (Stark, 2010).

To test the possibility of replacing digitonin by n-dodecyl- β -D-maltoside (dodecylmaltoside, DDM), another detergent commonly used in EM analysis of membrane complexes, the TIM23 complex was purified by IgG affinity chromatography from the Tim23^{ProtA} mitochondria (Fig. 3.13A and 3.13B) and subjected to GraFix on a glycerol gradient containing 0.02% DDM (Fig.3.19A, lane 2). Under these conditions, the complex was shifted towards lower molecular weight fractions, as compared to a digitonin-based gradient (Fig.3.19A, lane 1), indicating its complete dissociation.

To make the detergent exchange more gradual, a modified GraFix procedure was tested, in which conventional glycerol and glutaraldehyde gradients were combined with opposing 0–0.02% DDM and a reverse 0.3–0% digitonin gradient (Fig.3.19A, lane 3). The distribution of the TIM23 complex in the digitonin–DDM gradient was similar to that of 0.3% digitonin, suggesting the retainment of complex integrity. Negative stain electron microscopy revealed the presence of structured particles in the corresponding fractions of the gradient (Fig. 3.19C), which could not be detected in the negative control (Fig. 3.19B). However, the background remained strong enough to make subsequent single-particle analysis impossible.

If the background problem is caused by the detergent, can its concentration in the sample be reduced? To test this, purified TIM23 complex was analyzed by centrifugation in glycerol gradients with increasing digitonin concentrations (Fig. 3.20A). The optimal digitonin concentration for biochemical stability of the complex was determined to be 0.3%. Above this concentration, dissociation of proteins from the complex was observed, indicated by their accumulation in fractions corresponding to lower molecular weight. Conversely, reducing the digitonin concentration below 0.3% led to aggregation and pelleting of the complex, making it undetectable in the gradient fractions.

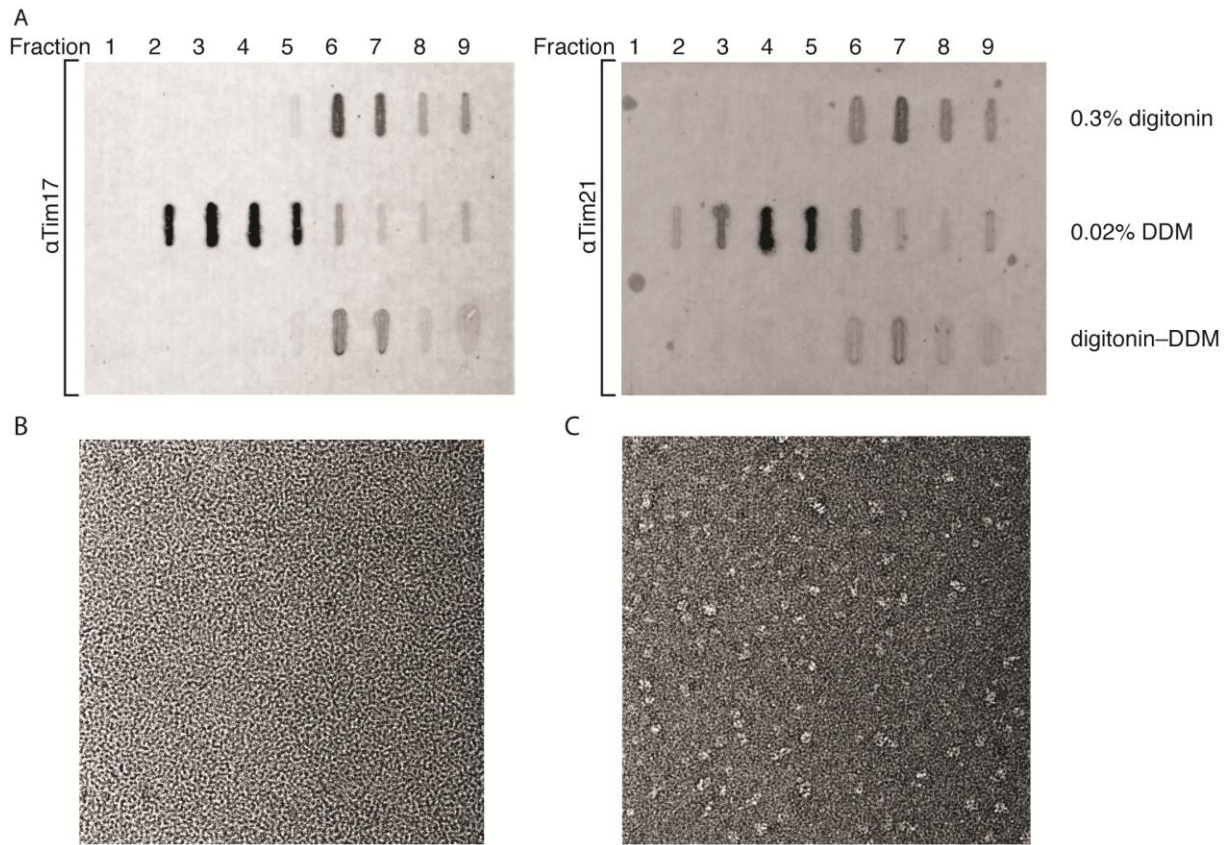


Figure 3.19. Detergent exchange in GraFix

(A) Purified TIM23 complex was subjected to GraFix in glycerol gradients containing 0.3% digitonin (upper lane), 0.02% DDM (middle lane) and in a combined digitonin to DDM gradient (lower lane). After 16 hours of centrifugation at 45,000 rpm in a Beckman SW60Ti rotor, collected fractions were analyzed by slot blotting and immunodecoration against Tim17 and Tim21. (B-C) EM images of the negative control (B) and sample (C), corresponding to fraction 7 of the digitonin-DDM gradient described in (A). Scale bar, 100 nm.

Amphipols (amp*h*i*p*athic polymers), mild non-detergent surfactants, allow purification of membrane complexes in a detergent-free system, which is compatible with EM (Flötenmeyer et al., 2007; Gohon et al., 2008; Popot, 2010). To test their compatibility with the TIM23 complex, a gradient centrifugation assay was used in the presence of increasing concentrations of A8-35, one of the most commonly used amphipols (Tribet et al., 1996). Unfortunately, even extremely low concentrations of A8-35 caused complete dissociation of the TIM23 complex, which can be judged by the shift of complex components to higher fractions (Fig. 3.20B).

A new class of amphiphiles, maltose-neopentyl glycols (MNGs), having favorable biochemical properties for integral membrane proteins, have been recently introduced

(Chae et al., 2010). However, using these detergents with the purified TIM23 complex also caused its dissociation (Fig. 3.20C), confirming that digitonin is, to date, the only detergent suitable for TIM23 complex purification.

Additional optimization of other buffer properties was done using the same method. The complex stability was tested by gradient centrifugation and subsequent analysis of TCA-precipitated fractions by SDS-PAGE and Western blotting. Three parameters have been tested: pH (in the range between 6.5 and 8.5), NaCl concentration (50-500 mM) and the buffering system (imidazole, HEPES and phosphate-buffered saline). However, these experiments did not allow any improvement of the complex stability compared to the default conditions (100 mM NaCl, 20 mM HEPES, pH 7.5) (data not shown).

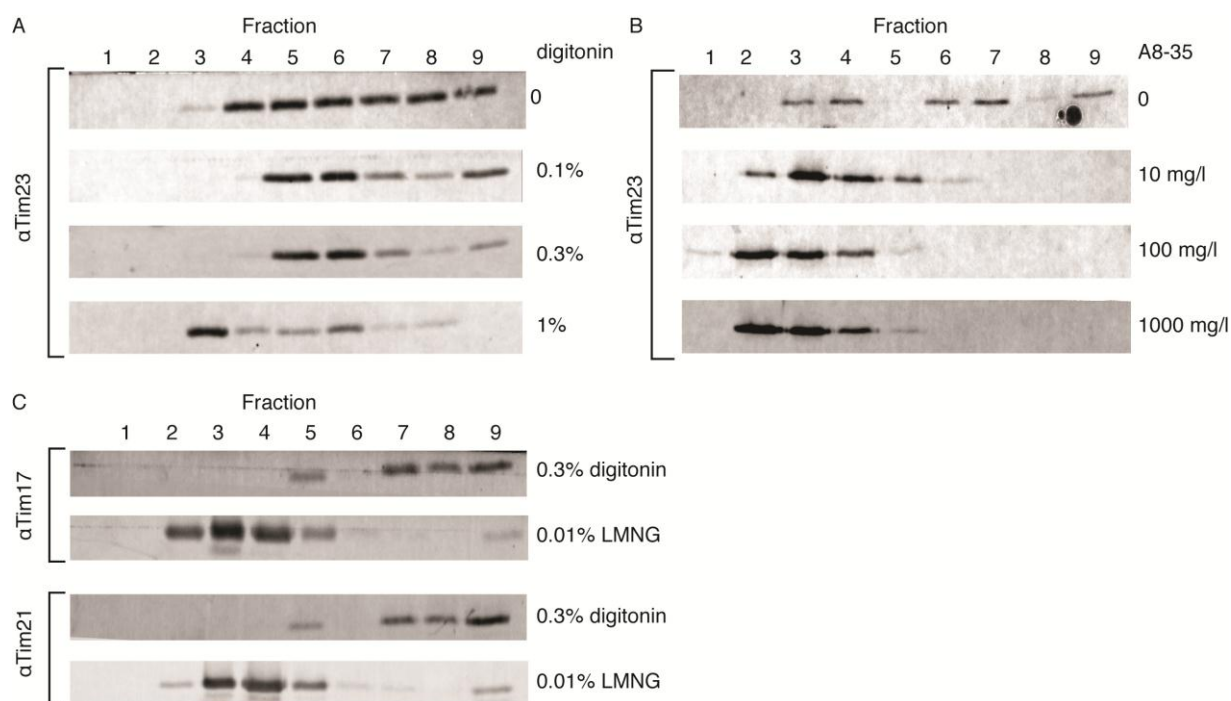


Figure 3.20. Optimizing detergent conditions

(A) Digitonin-solubilized mitochondria were separated on glycerol gradients with indicated digitonin concentrations for 10 hours at 50,000 rpm in a Beckman SW60Ti rotor. Fractions were collected from the top, TCA precipitated and analyzed by SDS-PAGE and Western blotting. Immunodecoration against Tim23 is shown. (B) TIM23 complex purified in digitonin was analyzed by centrifugation for 16 hours at 45,000 rpm in a Beckman SW60Ti rotor in glycerol gradients containing the indicated concentrations of the A8-35 amphipol. After TCA precipitation, fractions were analyzed by SDS-PAGE and immunoblotting. Tim23 decoration is shown. (C) The same as in and (B) for MNG-containing gradients. Immunodecorations against Tim21 and Tim17 are shown.

3.2.5. EM structure of the TOM-TIM supercomplex

One of the main difficulties in EM analysis of the TIM23 complex is its small size, making single particle EM impossible in the presence of a strong background, caused by the presence of detergent. To overcome this problem, an indirect solution was found enabling the analysis of larger complexes containing TIM23 as a constituent. The TOM-TIM23 supercomplex is formed in the presence of an arrested precursor *in transit* (Rassow et al., 1989), allowing for the indirect increase in particle size.

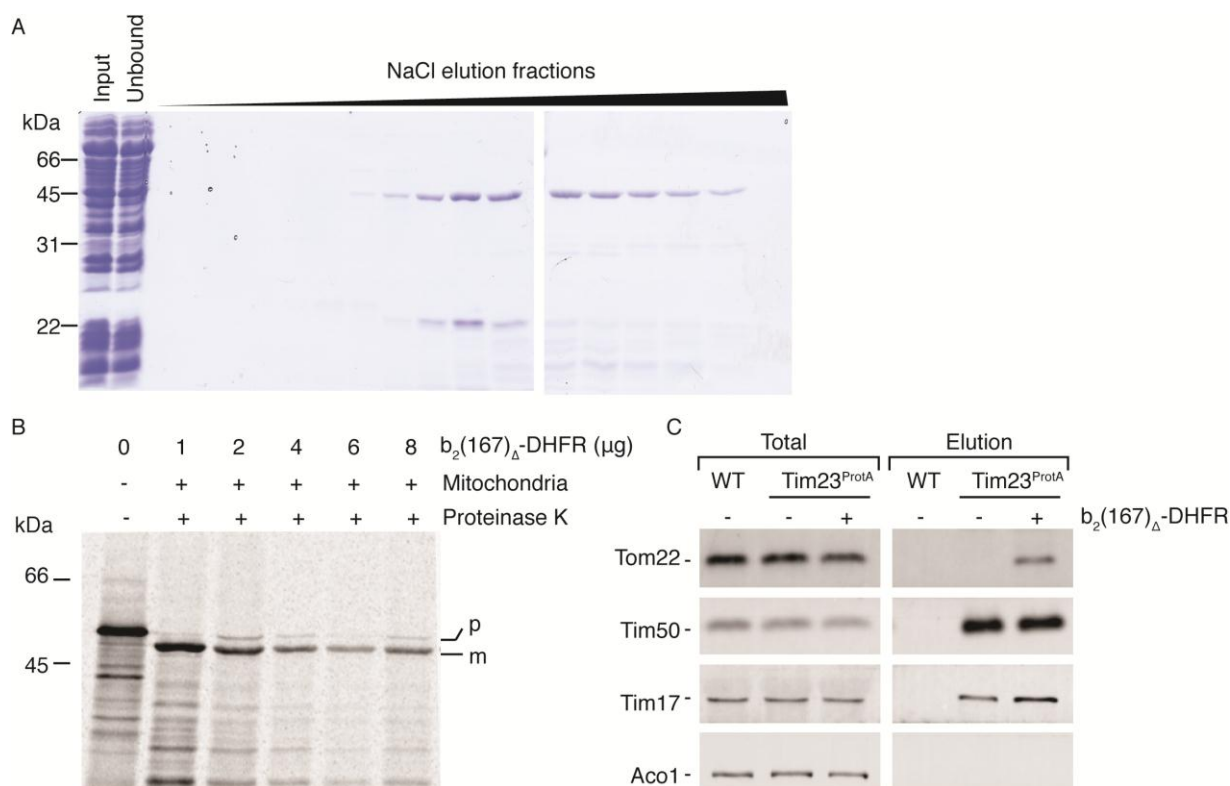


Figure 3.21. Import arrest of the $b_2(167)_\Delta$ -DHFR precursor and formation of the TOM-TIM supercomplex

(A) Purification of $b_2(167)_\Delta$ -DHFR from *E. coli* by ion exchange chromatography. For details see section 2.5.3. (B) [35 S]-labeled F1 β precursor was imported into isolated mitochondria at 25°C in the presence of 5 μ M MTX and increasing concentrations of $b_2(167)_\Delta$ -DHFR; with proteinase K treatment, followed by SDS-PAGE and autoradiography. p, precursor; m, mature (processed) form. (C) IgG affinity purification was used to isolate complexes from Tim23^{ProtA} mitochondria (for control, from wild type) with or without $b_2(167)_\Delta$ -DHFR arrest. After TEV cleavage, eluted complexes were analyzed by SDS-PAGE and immunoblotting. Total, 5%; elution, 100%.

A fusion precursor protein containing the mitochondrial targeting signal of cytochrome b_2 was fused to mouse dihydrofolate reductase ($b_2(167)_\Delta$ -DHFR) and

expressed in *E. coli* and purified by ion exchange chromatography (Fig. 3.20A and section 2.5.3). It was tested for its ability to block import of a [^{35}S]-labeled precursor in the presence of the irreversible dihydrofolate reductase inhibitor, methotrexate (MTX) (Fig. 3.20B), which showed its accumulation in the translocation machinery. Finally, IgG affinity complex purification from Tim23^{ProtA} mitochondria in the presence of arrested b₂(167) Δ -DHFR confirmed co-purification of the TOM complex components with TIM23 (Fig. 3.20C). These results confirm successful formation and isolation of the TOM-TIM supercomplex.

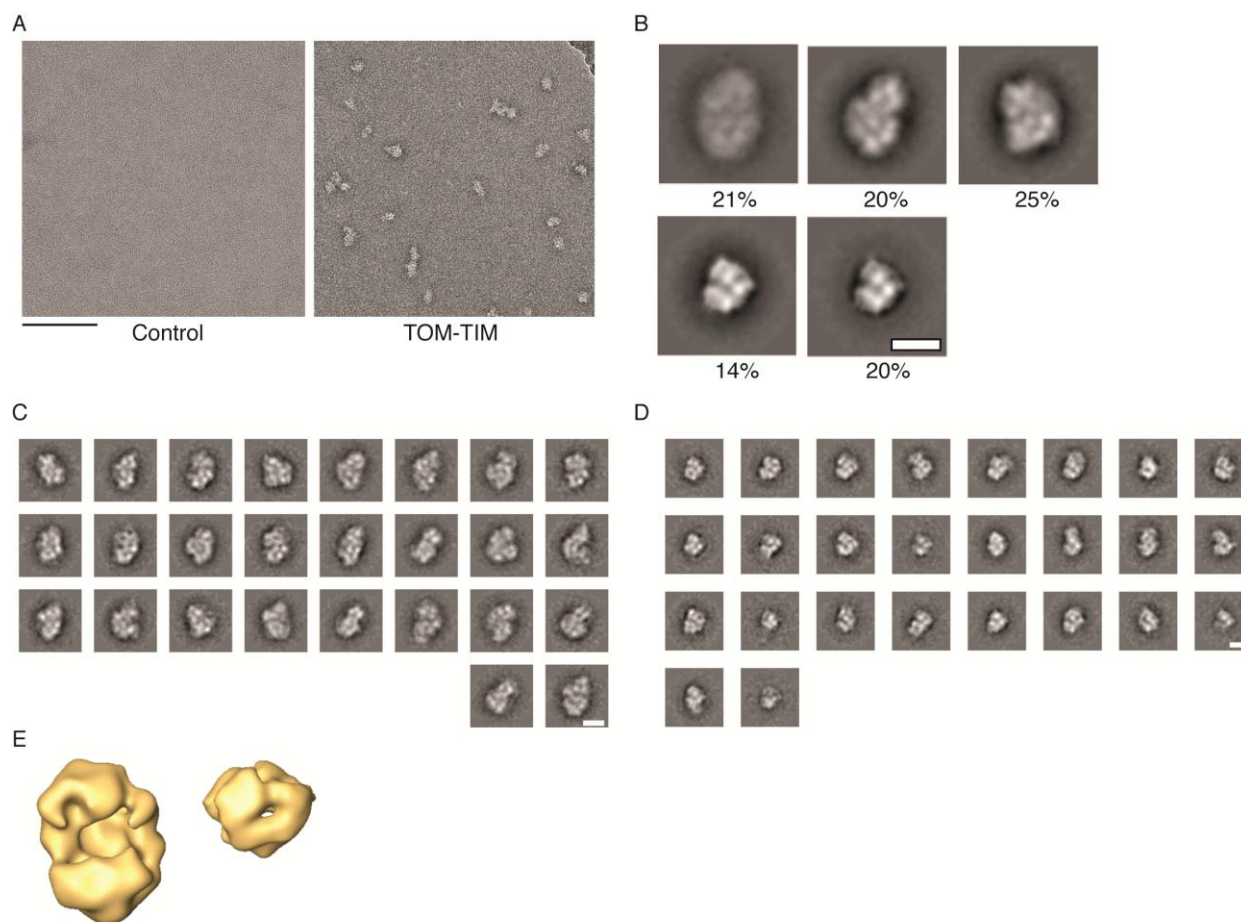


Figure 3.22. Single particle EM analysis of the isolated TOM-TIM supercomplex

(A) Negative stain images of the TOM-TIM supercomplex after GraFix. The images were recorded at an electron dose of 20-40 $\text{e}^-/\text{\AA}^2$, acceleration voltage 160 kV and 121,000-fold magnification. Left, negative control, right, TOM-TIM supercomplex. Scale bar, 100 nm. (B) Subsets of particles constructed from semiautomatically selected particles after 4-6 rounds of reference-free alignment and classification. Percentages indicate representation of the particular subset among all particles. Scale bar, 10 nm. (C) Selected class averages of the larger subset of particles. Scale bar, 10 nm. (D) Selected class averages of the smaller subset of particles. Scale bar, 10 nm. (E) 3D volumes of the supercomplex were obtained using the angular reconstitution technique. Images courtesy of Dr. F. Hauer.

The isolated supercomplex was subjected to GraFix and analyzed by single particle electron microscopy (Fig. 3.21A). Reference-free multiple sequence alignment and classification of the TIM-TOM complex images revealed the presence of several subsets of particles (Fig. 3.21B), some of them being significantly larger than the others. Similar particle distribution between the subsets showed no preference in purification or binding to the grid. Selected class averages of the larger and the smaller subsets of particles are shown in Fig. 3.21C and Fig. 3.21D, respectively. Preliminary 3D reconstructions, obtained by the angular reconstitution technique (Van Heel, 1987) are presented in Fig. 3.22E.

It can be suggested that the larger structure corresponds to the TOM-TIM supercomplex, whereas the smaller particles are TIM23 complexes co-purified with the supercomplex due to the presence of the tag on a Tim23 component. Further refinement of the structure and its verification by random conical tilt analysis (Radermacher, 1988) are ongoing processes.

4. Discussion

4.1. Dynamic interactions within the TIM23 complex

4.1.1. Interactions of Tim50 *in organello* and *in vitro*

Tim50 is the first component of the TIM23 complex to contact the preprotein as it enters the IMS after translocation through the Tom40 channel (Geissler et al., 2002; Mokranjac et al., 2003; Yamamoto et al., 2002). This initiates a chain of protein-protein interactions that mediate the activation of the Tim23 channel and presequence translocation to the matrix (Chacinska et al., 2009; Mokranjac & Neupert, 2010; Schmidt et al., 2010). The details of these early import stages are poorly understood. This study investigated protein interactions in the TIM23 complex in response to presequences, focusing on Tim50 as a primary presequence receptor (Qian et al., 2011; Schmidt et al., 2010; Schulz et al., 2011).

Taking advantage of the single cysteine residue located within the Tim50 core domain (Qian et al., 2011), Cu²⁺ cross-linking was applied for studying its interactions. One of the Tim50's cross-linking adducts was identified as Tim23, its well-known interaction partner (Alder et al., 2008; Geissler et al., 2002; Gevorgyan-Airapetov et al., 2009; Mokranjac et al., 2009; Tamura et al., 2009). Another prominent cross-linking adduct was formed between Tim50 and Tim21 (section 3.1.1).

Cu²⁺ cross-linking suggests very close proximity of the interacting proteins of the translocase; however, it cannot serve as proof of their direct physical interaction. Cross-linking experiments performed with purified IMS domains of both proteins strongly support the *in organello* findings. These experiments also suggested a hydrophobic nature of interaction, due to its insensitivity to high salt concentrations.

In addition, complex formation between Tim21^{IMS} and Tim50^{IMS} was confirmed by an independent method, surface plasmon resonance (section 3.1.2). The K_D of this interaction was found to be approximately 250-300 nM. This value is at least two orders of magnitude lower than the published K_D's of the Tim23-Tim50 and Tim50-pHsp60 presequence interactions (approximately 60 μM for both), evaluated by the same

method (Gevorkyan-Airapetov et al., 2009; Marom et al., 2011). In order to directly compare binding affinities of Tim21 and presequences to Tim50 under the same experimental conditions, SPR was used to determine the binding parameters of a presequence peptide used in this study, pALDH, to Tim50. The K_D of this interaction was about 5 μ M, whereas pALDH-s, a scrambled version of the same peptide, displayed only insignificant binding to Tim50. Although this value was significantly lower than the published Tim50-pHsp60 interaction (which can be explained by intrinsic differences between different presequences), the K_D of the Tim21-Tim50 interaction was still one order of magnitude less.

Interestingly, these SPR measurements also contributed towards the investigation of the controversial question of Tim50 presequence binding sites (section 3.1.3). Schulz et al., 2011 have shown that presequence peptides interact with the very C-terminal portion of Tim50, termed Tim50^{PBD} (for presequence-binding domain). On the other hand, presequence binding to a conserved negatively charged groove on the Tim50 core fragment has been proposed (Qian et al., 2011). SPR confirmed the specific binding of the pALDH presequence to both the full-length IMS domain of Tim50 (amino acids 132-476) and the Tim50^{PBD} (amino acids 395-476) fragment, although with slightly lower affinity for the latter. Surprisingly, presequence binding was also detected for the Tim50^{CORE} fragment (amino acids 164-361), with affinity and specificity similar to the full-length IMS fragment. Three explanations can be suggested for this seemingly controversial observation. The first option would be that both sites are active in the full-length Tim50. However, fitting affinity data strongly argued for a single presequence-binding site in Tim50^{IMS}. Moreover, if both sites were functional Tim50^{PBD} would be dispensable for presequence binding *in vivo*, which contradicts to the results of Schulz et al., 2011. The second possibility would imply that in the full-length Tim50^{IMS} one of the domains blocks presequence interaction with the other. However, also in this case Tim50^{PBD} would be non-essential. Finally, the third possible explanation would be that both sites contribute to the formation of a presequence-binding site *in vivo*. Till now, this model fits the experimental data better than the other two, although there is no direct evidence for such cooperation between domains. If this is the case, one can speculate that

presequence binding to Tim50^{PBD} occurs via the hydrophobic side of the amphipathic helix, whereas the interaction with the core involves charged residues in the large groove of Tim50. Further studies are required to clarify this question.

In conclusion, we identified a Tim21-Tim50 cross-link adduct in mitochondria and confirmed the direct physical interaction between these proteins by two independent methods, chemical cross-linking and SPR.

4.1.2. Presequence-induced changes in Tim50 interactions

Treating mitochondria with presequence peptides allows for the investigation of early stages in the presequence import pathway (Schulz et al., 2011; Shiota et al., 2011). Analysis of Tim50 interactions under these conditions by chemical cross-linking revealed a presequence-dependent increase in the Tim23-Tim50 cross-link and a significant decrease of the Tim21-Tim50 adduct (section 3.1.4).

The promotion of the Tim23-Tim50 interaction was in agreement with the cross-linking data obtained previously (Alder et al., 2008b). The presequence effect on the Tim21-Tim50 cross-link was quite surprising. Considering a comparably low K_D value of the Tim21^{IMS}-Tim50^{IMS} interaction, it could be expected that these proteins interact in a non-dynamic manner, fulfilling a scaffold function within the translocase. Moreover, comparison of Tim21 and pALDH affinities to Tim50 predicts that the presequence would not efficiently compete with Tim21 for Tim50 binding, even if they share the same binding site. Indeed, *in vitro* cross-linking experiments showed that addition of presequence peptide, even in significant excess, did not affect the amount of Tim21-Tim50 product.

These results show that the effect of presequences on Tim21-Tim50 interaction is indirect and needs to be mediated by other components of the translocation machinery. Although unambiguous identification of these components was not possible, we suggest that Tim23 could be one of them based on the following considerations.

The stage of the import pathway at which the dissociation of the Tim21-Tim50 cross-link takes place can be determined quite precisely. On the one hand, this effect does not depend on the presence of the outer mitochondrial membrane or the IMS domain of

Tom22, suggesting that known interactions of both Tim21 and Tim50 with the TOM components do not play a role in this process (Albrecht et al., 2006; Chacinska et al., 2005; Mokranjac et al., 2005; Shiota et al., 2011; Tamura et al., 2009).

On the other hand, in the absence of a membrane potential, presequence transport is blocked at a stage after its binding to Tim50 and Tim23, but before translocation across the membrane (Mokranjac & Neupert, 2010; Schmidt et al., 2010). The observation that the presequence effect on the Tim21-Tim50 cross-link does not require membrane potential confirms that this dissociation occurs at one of the early import stages.

These considerations point to Tim23 as the only remaining known protein in the IMS that is able to bind presequences downstream of Tom22 and Tim50 (Bauer et al., 1996; Chacinska et al., 2009; Marom et al., 2011; Schmidt et al., 2010; de la Cruz et al., 2010). This suggestion implies that Tim23 is able to influence the interaction between Tim21 and Tim50 *in organello*. Indeed, although the intermembrane space domains of Tim21 and Tim50 are sufficient for their interaction *in vitro*, in mitochondria this interaction strongly depends on the presence of Tim23^{IMS}.

Based on this, we conclude that Tim21 and Tim50 interact *in organello* in a presequence-sensitive and Tim23-dependent manner.

4.1.3. Dynamics and mobility of TIM23 components

The effects on Tim50 cross-links observed after presequence treatment can have different explanations. One of the options would imply structural rearrangements within the TIM23 complex, leading to changes in protein orientation unfavorable for cross-linking. On the other hand, it can be explained by the association and dissociation of particular components with the presequence translocase. Our co-immunoprecipitation experiments (section 3.1.5) strongly argue for the second option.

In fact, the presequence-induced increase of the Tim23-Tim50 cross-link is in agreement with higher amounts of Tim23 coimmunoprecipitated with Tim50; the decrease in the Tim21-Tim50 cross-link correlates with the reduced amount of Tim21 precipitated with Tim50. Besides that, the amount of Pam17 after presequence treatment was significantly increased in both Tim23 and Tim50 co-IPs.

What could be the explanation for these changes? Tim21 and Pam17 are well-known dynamic components of the translocase (Chacinska et al., 2005, 2010; Popov-Čeleketić et al., 2008; Hutu et al., 2008). Their antagonistic behavior is in correspondence with both models of the translocase organization (Chacinska et al., 2009). As was expected, Tim21 dissociated from the core of the translocase after presequence treatment in order to allow for Pam17 binding for subsequent motor assembly needed for matrix-targeted import. This was, at least to some extent, reflected in the reduced Tim21-Tim50 cross-link and significantly reduced amounts of Tim21 precipitated with both Tim50 and Tim23 after presequence treatment.

Tim50 has been shown to be only partially associated with the core of the TIM23 translocase or loosely associated (Geissler et al., 2002; Mokranjac & Sichtung, 2009; Yamamoto et al., 2002). Although it is difficult to distinguish between these two options, the essential role of Tim50 in maintaining the permeability barrier of the Tim23 channel (Meinecke et al., 2006) would require some part of it to be at least transiently associated with the rest of the TIM23 complex in the absence of presequences. In this case, different amounts of Tim23 precipitated with Tim50 can be explained by differential stability of Tim50's association with TIM23 with and without presequences. However, recruitment of new Tim50 molecules to the TIM23 complex after the addition of presequence cannot be excluded.

4.1.4. A model of preprotein import

The results of this study contribute to the general model of the presequence pathway (Chacinska et al., 2009; Dudek et al., 2012; Marom et al., 2011; Mokranjac & Neupert, 2010; Schmidt et al., 2010). Based on this, the following model of the early steps of matrix import by TIM23 can be suggested (Fig. 4.1).

In the default state of the translocase (Fig. 4.1A) the IMS domain of Tim50 interacts with the IMS domain of Tim21. Its transient interaction with Tim23 is also required to maintain the permeability barrier of the membrane (Meinecke et al., 2006). The association of Tim50 with the TIM23 complex at this stage is relatively weak, allowing for partial dissociation of Tim50 from the translocase during complex purification or co-

immunoprecipitation procedures. It also cannot be excluded that a significant part of Tim50 is not associated with the TIM23 complex (Geissler et al., 2002; Mokranjac & Sichtung, 2009; Yamamoto et al., 2002). The IMS domain of Tim23 is in a dimeric form when the channel is closed (Bauer et al., 1996; Meinecke et al., 2006). PAM is not associated with the TIM23 complex; Tim21 may be responsible for preventing its binding (Chacinska et al., 2005). At the same time, interaction with the respiratory chain in a Tim21- and Mgr2-dependent manner is promoted (Gebert et al., 2012; Nils Wiedemann et al., 2007; van der Laan, Wiedemann, et al., 2006). It is not clear, if the IMS domains of Tim50 and Tom22 also interact at this stage, but this interaction might be beneficial to maintain close contacts between the TIM23 and TOM complexes, and would explain *in vivo* cross-linking data by Shiota et al., 2011.

When a presequence appears from the Tom40 channel, it induces significant rearrangements in the translocation machinery (Fig. 4.1B). First, it binds to Tim50, releasing its block of the Tim23 channel (Alder et al., 2008a, 2008b; Meinecke et al., 2006). The Tim21-Tim50 interaction is weakened, but Tim21 remains at the translocase; dissociation of Tim21 from Tim50 allows for the formation of the Tim23-Tim50 cross-link (Alder et al., 2008b). The association of Tim50 with TIM23 at this state is strengthened, and new Tim50 molecules can be recruited to the complex. Recognition of presequences by Tim50 serves for both specificity and efficiency of their subsequent transfer to Tim23. At this stage, a presequence binding role of the IMS domain of Tom22 and its subsequent release, facilitated by Tim21, has been suggested (Albrecht et al., 2006; Chacinska et al., 2005, 2009; Mokranjac et al., 2005; Mokranjac & Sichtung, 2009; Tamura et al., 2009).

In the next stage of the presequence pathway (Fig. 4.1C), Tim21 dissociates from the rest of the translocase, leading to the partial dissociation of respiratory chain complexes from TIM23 and allowing for the association of Pam17 (Popov-Čeleketić et al., 2008; Schiller, 2009; Nils Wiedemann et al., 2007; van der Laan et al., 2006). Importantly, although assembly of Pam17 occurs at this early stage (Schiller, 2009) and is not membrane-potential dependent, other motor components are not yet associated with the translocase.

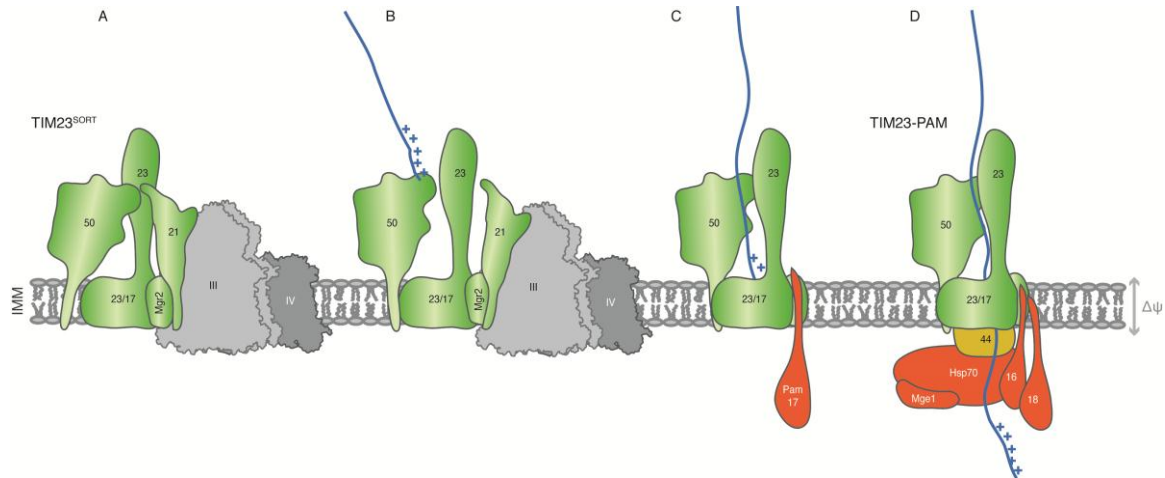


Figure 4.1. A model of matrix-targeted preprotein import

The details are in the text. IMM, inner mitochondrial membrane. III and IV, respiratory chain complexes III and IV. $\Delta\psi$, membrane potential.

After that, presequences bind to the IMS domain of Tim23, leading to the dissociation of its dimer and thereby allowing for presequence passage through the channel in a membrane-potential dependent manner (Alder et al., 2008a, 2008b; Bauer et al., 1996; de la Cruz et al., 2010). All steps, preceding presequence interaction with Tim23 and its transmembrane passage, are considered to be membrane potential-independent (Chacinska et al., 2009; Marom et al., 2011; Mokranjac & Neupert, 2010; Schmidt et al., 2010).

When presequences appear on the matrix side of the inner membrane (Fig. 4.1D), dissociation of Pam17 occurs, followed by sequential association of Pam16-Pam18 and Tim44-mtHsp70; the fully assembled motor drives further translocation of preproteins in an ATP-dependent manner (D'Silva et al., 2004; Hutu et al., 2008; Popov-Čeleketić et al., 2008; Wiedemann et al., 2007).

This model tries to accommodate different views on the organization of the translocase (the “single-entity” and the “modular” concepts), although not always possible. It cannot be considered final and completely non-controversial; however, it combines most of the available observations and can be updated accordingly and modified with new emerging data.

4.2. Structural analysis of the TIM23 translocase

4.2.1. The background problem

Electron microscopy has proven to be a valuable tool for the structural investigation of mitochondrial membrane complexes (Dudkina et al., 2010; Rubinstein, 2007). This method has significantly contributed to the field of mitochondrial protein translocation by providing structures of the TOM and TIM22 complexes (Model et al., 2002, 2008; Rehling et al., 2003). Hence, one would assume that TIM23 would be a promising candidate for single particle EM analysis; nevertheless its small size, instability and intrinsic heterogeneity have made its EM investigation exceedingly difficult and therefore extensive sample preparation optimization was required.

As no gross TIM23 complex structural information was available, it was of the highest importance to distinguish between specific signal and artifacts on EM images. In order to investigate the background staining contribution of the individual components we prepared negatively stained EM samples of buffers and solutions used for TIM23 complex purifications and compared them to the images of the purified TIM23 complex (section 3.2.1). To our surprise, abundant particles with clearly discernable structures of high contrast were found in most of the control samples. Digitonin, a mild non-ionic detergent required for the purification of TIM23, was determined to be the major background contamination source. A significant part of this work has been devoted towards the resolution of background staining in the EM images.

The observed digitonin-related artifacts were of two types. Contaminations of the first type were represented by clearly defined, high-contrast particles, between 100 and 200 nm in size. The other type of unspecific signal was a poorly defined grainy background, most probably attributed to digitonin micelles (Smith & Pickels, 1940). Commercially available digitonin is purified from the *Digitalis purpurea* plant and is known to be of exceedingly low purity (Herrmann et al., 2001; Ryan et al., 2001). Additional purification by re-crystallization and ion exchange chromatography successfully removed most of the high-contrast particles from EM preparations, while the background structures of the second type remained. This background, which did not interfere with EM imaging of

larger particles such as respiratory chain supercomplexes, was detrimental for single particle analysis of small complexes such as the TIM23 translocase.

Digitonin has been known for a long time to form large homogenous micelles with a sedimentation coefficient of approximately 5.8 S, corresponding to a molecular weight between 75 and 400 kDa (Smith & Pickels, 1940), which is in the same range as the TIM23 complex. This fact explains the inability of GraFix (Kastner et al., 2008) to solve the background problem for TIM23, while concomitantly being highly advantageous for larger complexes such as TOM-TIM supercomplex and TIM22.

Washing EM grids with γ -cyclodextrin, which complexes with detergent molecules inside a ring-shaped cavity (Degrip & Vanoostrum, 1998; Signorell et al., 2007), appeared to be highly efficient in removing the micellar background. However, this treatment significantly reduced image quality of the respiratory chain complexes, therefore its use in TIM23 grid preparation would not be suitable due its highly instable nature as compared to respiratory chain complexes (section 3.2.3).

As all attempted approaches of removing the deleterious characteristics of digitonin in negative stain EM sample preparation have failed, in regards to the TIM23 complex, other detergent substitution methods were explored. As a detergent-free sample preparation of the TIM23 translocase is impossible, using mild non-detergent surfactants could provide an alternative to conventional detergents (Popot, 2010). Amphipol A8-35, an amphipatic polymer, which was previously used in electron microscopy of membrane proteins and complexes (Althoff et al., 2011; Cvetkov et al., 2011; Flötenmeyer et al., 2007; Gohon et al., 2008), could be the surfactant of choice. Although amphipols are generally not capable of membrane solubilization, they have been shown to assist in the stabilization of hydrophobic proteins in detergent-free environments (Gohon et al., 2008; Popot, 2010; Tribet et al., 1996), therefore being ideal for EM analysis. However, A8-35 was shown to be destructive to the purified TIM23 complex, causing its complete dissociation during detergent exchange (section 3.2.4). Maltose-neopentyl glycol-based amphiphiles, which have recently been introduced, are considered to be promising tools for protein crystallization and electron microscopy, due to their very low critical micelle

concentrations (Chae et al., 2010); however, they were also not suitable for maintaining TIM23 complex stability (section 3.2.4).

Promising results were obtained by combining the GraFix methodology with gradual detergent exchange during centrifugation. Although dodecylmaltoside (DDM) caused dissociation of the TIM23 complex under normal conditions, it could partially replace digitonin in GraFix gradients when its concentration was increased gradually. Detergent exchange was helpful for the EM analysis, slightly reducing the digitonin background noise, although the benefit gained was not sufficient enough to allow for the EM analysis of the TIM23 complex (sections 3.2.4 and 3.2.2).

In summary, we tried to approach the problem from multiple directions, but did not find a way to efficiently remove the digitonin background, while at the same time maintain TIM23 integrity. However, the list of tested optimization techniques is not comprehensive. Other potential ways to resolve the digitonin background issue exist, such as the utilization of nanodiscs, lipoprotein particles consisting of a lipid patch surrounded by stabilizing proteins (Civjan et al., 2003; Popot, 2010). Other non-detergent surface-active molecules, such as fluorinated surfactants (Park et al., 2007) and amphipatic peptides (Schafmeister et al., 1993; Tribet et al., 1996) can be tested for their ability to replace digitonin in the TIM23 complex purifications. Interestingly, presequences, being amphipatic peptides, are also TIM23 substrates. Their high affinity to the translocase, combined with their surface activity, could provide the desired stabilization of the complex in aqueous solutions at relatively low peptide concentrations.

4.2.2. Biochemical approaches to improve sample quality

Further challenges in EM of the TIM23 include its biochemical instability, functional heterogeneity and high dynamics. In this study, solving the background problem was of the highest priority, although the aforementioned problems have not been neglected.

The TIM23 translocase has been shown to exist as at least two different isoforms, these being the Tim21-containing TIM23^{SORT} and the PAM-associated TIM23^{CORE} (Chacinska et al., 2005, 2010; Wiedemann et al., 2007; van der Laan et al., 2006, 2007).

Moreover, the physical association of the TIM23^{SORT} isoform with the respiratory chain has been shown (Gebert et al., 2012; Nils Wiedemann et al., 2007; van der Laan, Wiedemann, et al., 2006), adding another level of heterogeneity to the sample. However, slight modification of the purification strategy allows for the specific isolation of one of the two TIM23 isoforms. Purification via Tim21^{ProtA} allows for specific isolation of the TIM23^{SORT} form, whereas purification via an affinity tag on Tim23 from a *tim21Δ* strain would enrich the TIM23^{CORE} isoform. Purification via Tim23^{ProtA} in a Tim21 containing strain yields a mixture of both isoforms. Two of these purification strategies were tested (Fig. 3.13) and directly compared via EM.

Although the existence of different TIM23 isoforms has been questioned (Popov-Čeleketić et al., 2008; Popov-Čeleketić et al., 2011), all models of the presequence translocase point towards its highly dynamic nature (Chacinska et al., 2009; Dudek et al., 2012). This dynamic nature has important consequences in regards to the structural analysis of the complex. First, conformational changes will directly increase the heterogeneity of the sample, as particles representing different translocation stages will be present in one sample. A potential solution to this issue would be to shift the equilibrium towards one of the forms, for example, by arresting a substrate (such as b₂(220)_Δ-DHFR) in the translocase (Chacinska et al., 2010).

Another consequence of the highly dynamic nature of TIM23 might be its inherent instability. Indeed, dynamics imply transient protein interactions, leading to their fragility upon complex solubilization and isolation. The GraFix technique was designed to help resolve this issue by cross-linking loosely associated components under favorable conditions (Kastner et al., 2008; Stark, 2010). In addition, the optimizing of biochemical purification conditions can provide additional means of increasing general stability. This project compared various biochemical conditions such as salt concentration, pH and buffer system, which all failed to increase sample quality, as determined by gradient centrifugation analysis (section 3.2.4 and data not shown). However, the number of conditions that can be tested via this laborious manner is limited. The development of high-throughput screening assays (for example, based on

ThermoFluor® technology) (Cummings et al., 2006) will provide additional means to find optimal purification conditions for fragile complexes.

4.2.3. Low-resolution structure of the TOM-TIM supercomplex

In this study, preliminary negative stain EM images of the TOM-TIM supercomplex are presented (section 3.2.5). Initial image classification revealed the existence of two particle subsets, one of which included small round-shaped particles of approximately 10 nm in diameter. The second subset was represented by elongated particles, with average dimensions of approximately 10x20 nm. In this Tim23^{ProtA} isolation, one could speculate that the larger particles are TOM-TIM supercomplexes, whereas the smaller ones are individual TIM23 complexes, highlighting the resolution limitation of the GraFix technique.

Preliminary 3D reconstruction was done via angular reconstitution (van Heel et al., 1996). While this technique has been shown to be sub-optimal for small non-symmetrical particles (Rubinstein, 2007), it allows for the ascertainment of a rough overview of the spatial organization of the complexes. The conclusions of this analysis suggest that the two parts of the putative supercomplex are tightly bound and that the isolated smaller particles are likely the lesser particle found in the supercomplex, corresponding to TIM23.

4.2.4. Perspectives and outlook

To date, a significant amount of data has been accumulated concerning the structures of the individual components of the mitochondrial protein import system (Endo et al., 2011). Important insights into the higher ordered structural organization of the translocation machinery can be deduced from cross-linking experiments (Alder et al., 2008; Herrmann et al., 2001; Hutu et al., 2008; Popov-Čeleketić et al., 2011; Shiota et al., 2011). However, these individual pieces of data need a basis by which they can be combined, therefore even a low-resolution EM structure will have a high impact on the field by providing a platform for the integration of structural and functional information.

The resulting structure of the TOM-TIM supercomplex, while being an important step forward, it does not provide significant functional data. Further work is required to

reveal structural details, which in combination with the information obtained by other methods will lead to a comprehensive mechanistic model of the presequence translocase.

Localization of subunits within the TOM-TIM supercomplex can be achieved by immunogold labeling and genetic tagging or deleting particular complex components. This additional complex mapping data will enable a more in-depth understanding of the structural basis of protein-protein interactions.

Isolating complexes using affinity tags on different subunits (such as Tim21 and Tim23) will allow for the isolation of different supercomplex forms (Chacinska et al., 2010). This approach can also be indirectly applied for subunit localization studies, for example allowing for the identification of the PAM and/or Tim21 positions within the overall structure.

Random conical tilt analysis (Radermacher, 1988) can allow for the verification of the 3D structure, being a more reliable method for 3D reconstruction of low-symmetry particles, as compared to angular reconstitution (Rubinstein, 2007). Cryo-EM analysis can supplement negative stain microscopy, especially within the interior of the translocase, while at the same time excluding the possibility of staining artifacts (Dubochet, 2012; Rubinstein, 2007).

Combining electron microscopy with carbon film-assisted endoprotease digestion (Richter et al., 2010) can provide further higher order structure data of the translocase machinery.

Together, these and other approaches will lead to a comprehensive structural and mechanistic model of TIM23 action, which will raise new challenging questions in the field of mitochondrial biogenesis.

5. Summary and Conclusions

This study was devoted to structural and functional investigations of the inner mitochondrial membrane translocase, TIM23. In the first part of this work, a previously unknown interaction between two components of the translocase, Tim21 and Tim50, was identified. The main conclusions of this project are summarized below:

- Tim21 and Tim50 can be cross-linked by Cu^{2+} , suggesting close proximity of the two proteins *in organello*.
- Intermembrane space (IMS) domains of both proteins are sufficient for their interaction *in vitro*.
- The K_D of the Tim21^{IMS}-Tim50^{IMS} interaction is about 250 – 300 nM.
- The interaction is predominantly hydrophobic.
- The C-terminal presequence-binding domain of Tim50 is not required for their interaction.
- Tim21 and presequence binding to Tim50 are independent of each other.
- However, in mitochondria, the Cu^{2+} -induced cross-link between Tim21 and Tim50 is reduced after presequence treatment.
- This effect does not depend on the presence of the outer mitochondrial membrane or the membrane-potential across the innermembrane.
- In the absence of Tim23, the interaction between Tim50 and Tim21^{IMS} *in organello* is reduced.
- Presequences trigger Tim21 release from the core of the TIM23 complex, promoting PAM association.

The structural investigation of the presequence translocase was done by negative stain electron microscopy. Extensive optimization was performed, leading to a low-resolution negative stain structure of the TOM-TIM supercomplex. The main outcomes of this project are summarized below.

- Commercial digitonin contains contaminating particles, which can be removed by re-crystallization and ion exchange chromatography.
- However, the remaining granular background, attributed to digitonin micelles, makes negative stain analysis of the TIM23 complex impossible.
- Washing electron microscopy grids with γ -cyclodextrin prior to the uranyl acetate staining efficiently removes the background, however, it negatively affects the integrity of the translocase.
- The GraFix procedure in most cases improves sample homogeneity and stability; however, it does not resolve the background problem.
- The established sample preparation conditions could be successfully used for single particle electron microscopy of TIM22 and respiratory chain complexes, but not for the TIM23 complex.
- However, isolated TOM-TIM supercomplex, formed after the $b_2(167)_\Delta$ -DHFR arrest in mitochondria, could be analyzed by electron microscopy after the GraFix procedure. Two subsets of particles could be identified, one of them potentially being the co-isolated TIM23 complex. 3D volumes of both subsets were obtained by angular reconstitution.

In conclusion, the results of the first part contribute to the general mechanistic TIM23 import model. The electron microscopic section of the study establishes a technical basis for further structural investigation of the mitochondrial presequence translocase.

6. References

- Abe, Y., Shodai, T., Muto, T., Mihara, K., Torii, H., Nishikawa, S., Endo, T., et al. (2000). Structural basis of presequence recognition by the mitochondrial protein import receptor Tom20. *Cell*, 100(5), 551-560.
- Albrecht, R., Rehling, P., Chacinska, A., Brix, J., Cadamuro, S. a, Volkmer, R., Guiard, B., et al. (2006). The Tim21 binding domain connects the preprotein translocases of both mitochondrial membranes. *EMBO reports*, 7(12), 1233-8.
- Alder, N. N., Jensen, R. E., & Johnson, A. E. (2008a). Fluorescence mapping of mitochondrial TIM23 complex reveals a water-facing, substrate-interacting helix surface. *Cell*, 134(3), 439-50.
- Alder, N., Sutherland, J., & Buhring, A. (2008b). Quaternary structure of the mitochondrial TIM23 complex reveals dynamic association between Tim23p and other subunits. *Molecular biology of the cell*, 19, 159-170.
- Allison, D. S., & Schatz, G. (1986). Artificial mitochondrial presequences. *Proceedings of the National Academy of Sciences of the United States of America*, 83(23), 9011-5.
- Althoff, T., Mills, D. J., Popot, J.-L., & Kühlbrandt, W. (2011a). Arrangement of electron transport chain components in bovine mitochondrial supercomplex I1III2IV1. *The EMBO journal*, 30(22), 4652-64.
- Althoff, T., Mills, D. J., Popot, J.-L., & Kühlbrandt, W. (2011b). Arrangement of electron transport chain components in bovine mitochondrial supercomplex I(1)III(2)IV(1). *The EMBO journal*, 1, 1-13.
- Bauer, M. F., Sirrenberg, C., Neupert, W., & Brunner, M. (1996). Role of Tim23 as voltage sensor and presequence receptor in protein import into mitochondria. *Cell*, 87(1), 33-41.
- Becker, T., Böttlinger, L., & Pfanner, N. (2011). Mitochondrial protein import: from transport pathways to an integrated network. *Trends in biochemical sciences*, 37(3), 85-91.
- Bohnert, M., Pfanner, N., & van der Laan, M. (2007). A dynamic machinery for import of mitochondrial precursor proteins. *FEBS Letters*, 581(15), 2802-2810.
- Bolender, N., Sickmann, A., Wagner, R., Meisinger, C., & Pfanner, N. (2008). Multiple pathways for sorting mitochondrial precursor proteins. *EMBO reports*, 9(1), 42-9.
- Bonneaud, N., Ozier-Kalogeropoulos, O., Li, G. Y., Labouesse, M., Minvielle-Sebastia, L., & Lacroute, F. (1991). A family of low and high copy replicative, integrative and single-stranded S. cerevisiae/E. coli shuttle vectors. *Yeast*, 7(6), 609-15.
- Bonnefoy, N., Fiumera, H. L., Dujardin, G., & Fox, T. D. (2009). Roles of Oxal-related inner-membrane translocases in assembly of respiratory chain complexes. *Biochimica et biophysica acta*, 1793(1), 60-70.
- Brandon, M., Baldi, P., & Wallace, D. C. (2006). Mitochondrial mutations in cancer. *Oncogene*, 25(34), 4647-62.
- Bueler, S. A., & Rubinstein, J. L. (2008). Location of subunit d in the peripheral stalk of the ATP synthase from Saccharomyces cerevisiae. *Biochemistry*, 47(45), 11804-11810.
- Bömer, U., Meijer, M., Maarse, a C., Hönlinger, a, Dekker, P. J., Pfanner, N., & Rassow, J. (1997). Multiple interactions of components mediating preprotein translocation across the inner mitochondrial membrane. *The EMBO journal*, 16(9), 2205-16.

6. References

- Bömer, U., Rassow, J., Zufall, N., Pfanner, N., Meijer, M., & Maarse, a C. (1996). The preprotein translocase of the inner mitochondrial membrane: evolutionary conservation of targeting and assembly of Tim17. *Journal of molecular biology*, 262(4), 389-95.
- Carroll, J., Fearnley, I. M., Skehel, J. M., Shannon, R. J., Hirst, J., & Walker, J. E. (2006). Bovine complex I is a complex of 45 different subunits. *The Journal of biological chemistry*, 281(43), 32724-7.
- Chacinska, A., Koehler, C. M., Milenkovic, D., Lithgow, T., & Pfanner, N. (2009). Importing mitochondrial proteins: machineries and mechanisms. *Cell*, 138(4), 628-44.
- Chacinska, A., Lind, M., Frazier, A. E., Dudek, J., Meisinger, C., Geissler, A., Sickmann, A., et al. (2005). Mitochondrial presequence translocase: switching between TOM tethering and motor recruitment involves Tim21 and Tim17. *Cell*, 120(6), 817-29.
- Chacinska, A., Rehling, P., Guiard, B., Frazier, A. E., Schulze-Specking, A., Pfanner, N., Voos, W., et al. (2003). Mitochondrial translocation contact sites: separation of dynamic and stabilizing elements in formation of a TOM-TIM-preprotein supercomplex. *The EMBO journal*, 22(20), 5370-81.
- Chacinska, A., van der Laan, M., Mehnert, C. S., Guiard, B., Mick, D. U., Hutu, D. P., Truscott, K. N., et al. (2010). Distinct forms of mitochondrial TOM-TIM supercomplexes define signal-dependent states of preprotein sorting. *Molecular and cellular biology*, 30(1), 307-18.
- Chae, P. S., Rasmussen, S. G. F., Rana, R. R., Gotfryd, K., Chandra, R., Goren, M. A., Kruse, A. C., et al. (2010). Maltose-neopentyl glycol (MNG) amphiphiles for solubilization, stabilization and crystallization of membrane proteins. *Nature methods*, 7(12), 1003-1008.
- Civjan, N., Bayburt, T., Schuler, M., & Sligar, S. (2003). Direct solubilization of heterologously expressed membrane proteins by incorporation into nanoscale lipid bilayers. *Biotechniques*, 35(3), 556-560, 562-563.
- Correia, S., Santos, R., Perry, G., Zhu, X., Moreira, P., & Smith, M. (2012). Mitochondrial importance in Alzheimer's, Huntington's and Parkinson's diseases. *Advances in Experimental Medicine and Biology*, 724, 205-221.
- Couoh-Cardel, S. J., Uribe-Carvajal, S., Wilkens, S., & García-Trejo, J. J. (2010). Structure of dimeric F1F0-ATP synthase. *The Journal of biological chemistry*, 285(47), 36447-55.
- Cummings, M. D., Farnum, M. a, & Nelen, M. I. (2006). Universal screening methods and applications of ThermoFluor. *Journal of biomolecular screening*, 11(7), 854-63.
- Cvetkov, T. L., Huynh, K. W., Cohen, M. R., & Moiseenkova-Bell, V. Y. (2011). Molecular architecture and subunit organization of TRPA1 ion channel revealed by electron microscopy. *The Journal of biological chemistry*, 286(44), 38168-76.
- Davidov, Y., & Jurkevitch, E. (2009). Predation between prokaryotes and the origin of eukaryotes. *BioEssays : news and reviews in molecular, cellular and developmental biology*, 31(7), 748-57.
- Davies, K. M., Strauss, M., Daum, B., Kief, J. H., Osiewacz, H. D., Rycovska, A., Zickermann, V., et al. (2011). Macromolecular organization of ATP synthase and complex I in whole mitochondria. *Proceedings of the National Academy of Sciences of the United States of America*, 108(34), 14121-6.
- Degrip, W., & Vanoostrum, J. (1998). Selective detergent-extraction from mixed detergent/lipid/protein micelles, using cyclodextrin inclusion compounds: a novel generic approach for the preparation of proteoliposomes. *Biochemical Journal*, 674, 667-674.

6. References

- Dekker, P. J., Keil, P., Rassow, J., Maarse, a C., Pfanner, N., & Meijer, M. (1993). Identification of MIM23, a putative component of the protein import machinery of the mitochondrial inner membrane. *FEBS letters*, 330(1), 66-70.
- Dekker, P. J., Martin, F., Maarse, a C., Bömer, U., Müller, H., Guiard, B., Meijer, M., et al. (1997). The Tim core complex defines the number of mitochondrial translocation contact sites and can hold arrested preproteins in the absence of matrix Hsp70-Tim44. *The EMBO journal*, 16(17), 5408-19.
- Dolezal, P., Likic, V., Tachezy, J., & Lithgow, T. (2006). Evolution of the molecular machines for protein import into mitochondria. *Science*, 313(5785), 314-8.
- Donzeau, M., Káldi, K., Adam, a, Paschen, S., Wanner, G., Guiard, B., Bauer, M. F., et al. (2000). Tim23 links the inner and outer mitochondrial membranes. *Cell*, 101(4), 401-12.
- Drummond, A. J., Ashton, B., Buxton, S., Cheung, M., Heled, J., Kears, M., Moir, R., et al. (2012). Geneious v4.8.
- Dube, P., Tavares, P., Lurz, R., & Heel, M. V. (1993). The portal protein of bacteriophage SPP1: a DNA pump with 13-fold symmetry. *EMBO Journal*, 12(4), 1303-1309.
- Dubochet, J. (2012). Cryo-EM-the first thirty years. *Journal of Microscopy*, 245(3), 221-224.
- Dudek, J., Rehling, P., & van der Laan, M. (2012). Mitochondrial protein import: Common principles and physiological networks. *Biochimica et biophysica acta*, Epub ahead of print.
- Dudkina, Natalya V, Kouril, R., Bultema, J. B., & Boekema, E. J. (2010). Imaging of organelles by electron microscopy reveals protein-protein interactions in mitochondria and chloroplasts. *FEBS letters*, 584(12),
- Dudkina, Natalya V, Kouril, R., Peters, K., Braun, H.-P., & Boekema, E. J. (2010). Structure and function of mitochondrial supercomplexes. *Biochimica et biophysica acta*, 1797(6-7), 664-70.
- Dudkina, Natalia V, Eubel, H., Keegstra, W., Boekema, E. J., & Braun, H.-P. (2005). Structure of a mitochondrial supercomplex formed by respiratory-chain complexes I and III. *Proceedings of the National Academy of Sciences of the United States of America*, 102(9), 3225-9.
- Dudkina, Natalya V, Sunderhaus, S., Braun, H.-P., & Boekema, E. J. (2006). Characterization of dimeric ATP synthase and cristae membrane ultrastructure from *Saccharomyces* and *Polytomella* mitochondria. *FEBS letters*, 580(14), 3427-32.
- D'Silva, P., Liu, Q., Walter, W., & Craig, E. a. (2004). Regulated interactions of mtHsp70 with Tim44 at the translocon in the mitochondrial inner membrane. *Nature Structural & Molecular Biology*, 11(11), 1084-1091.
- Efremov, R. G., & Sazanov, L. a. (2011). Respiratory complex I: "steam engine" of the cell? *Current opinion in structural biology*, 21(4), 532-40.
- Endo, T., Yamano, K., & Kawano, S. (2011). Structural insight into the mitochondrial protein import system. *Biochimica et biophysica acta*, 1808(3), 955-70.
- Flötenmeyer, M., Weiss, H., Tribet, C., Popot, J.-L., & Leonard, K. (2007). The use of amphipathic polymers for cryo electron microscopy of NADH:ubiquinone oxidoreductase (complex I). *Journal of Microscopy*, 227(Pt 3), 229-35.
- Forner, F., Foster, L. J., Campanaro, S., Valle, G., & Mann, M. (2006). Quantitative proteomic comparison of rat mitochondria from muscle, heart, and liver. *Molecular & cellular proteomics : MCP*, 5(4), 608-19.

6. References

- Friedrich, T., & Böttcher, B. (2004). The gross structure of the respiratory complex I: a Lego System. *Biochimica et Biophysica Acta*, 1608(1), 1-9.
- Fukami, A., & Adachi, K. (1965). A New Method of Preparation of a Self-Perforated Micro Plastic Grid and its Application. *JOURNAL OF ELECTRON MICROSCOPY*, 14(2), 112-118.
- Gebert, M., Schrempp, S. G., Mehnert, C. S., Heißwolf, A. K., Oeljeklaus, S., Ieva, R., Bohnert, M., et al. (2012). Mgr2 promotes coupling of the mitochondrial presequence translocase to partner complexes. *The Journal of cell biology*, 197(5), 595-604.
- Geissler, A., Chacinska, A., Truscott, K. N., Wiedemann, N., Brandner, K., Sickmann, A., Meyer, H. E., et al. (2002). The mitochondrial presequence translocase: an essential role of Tim50 in directing preproteins to the import channel. *Cell*, 111(4), 507-18.
- Genova, M. L., & Lenaz, G. (2011). New developments on the functions of coenzyme Q in mitochondria. *BioFactors (Oxford, England)*, 37(5), 330-54.
- Gevorkyan-Airapetov, L., Zohary, K., Popov-Čeleketić, D., Mapa, K., Hell, K., Neupert, W., Azem, A., et al. (2009). Interaction of Tim23 with Tim50 Is essential for protein translocation by the mitochondrial TIM23 complex. *The Journal of biological chemistry*, 284(8), 4865-72.
- Gietz, R. D., & Schiestl, R. H. (2007). Quick and easy yeast transformation using the LiAc/SS carrier DNA/PEG method. *Nature protocols*, 2(1), 35-7.
- Gill, S., & Hippel, P. (1989). Calculation of protein extinction coefficients from amino acid sequence data. *Analytical Biochemistry*, 182, 319-326.
- Taylor, a B., Smith, B. S., Kitada, S., Kojima, K., Miyaura, H., Otwinowski, Z., Ito, a, et al. (2001). Crystal structures of mitochondrial processing peptidase reveal the mode for specific cleavage of import signal sequences. *Structure:1993*, 9(7), 615-25.
- Glancy, B., & Balaban, R. S. (2012). Role of mitochondrial Ca²⁺ in the regulation of cellular energetics. *Biochemistry*, 51(14), 2959-73.
- Gohon, Y., Dahmane, T., Ruigrok, R. W. H., Schuck, P., Charvolin, D., Rappaport, F., Timmins, P., et al. (2008). Bacteriorhodopsin/amphipol complexes: structural and functional properties. *Biophysical journal*, 94(9), 3523-37.
- Gray, M. W. (1999). Mitochondrial Evolution. *Science*, 283(5407), 1476-1481.
- Heinemeyer, J., Braun, H.-P., Boekema, E. J., & Kouril, R. (2007). A structural model of the cytochrome C reductase/oxidase supercomplex from yeast mitochondria. *The Journal of biological chemistry*, 282(16), 12240-8.
- Herrmann, J., Kauff, F., & Neuhaus, H. (2009). Thiol oxidation in bacteria, mitochondria and chloroplasts: common principles but three unrelated machineries. *Biochimica et biophysica acta*, 1793(1), 71-77.
- Herrmann, J. M., & Riemer, J. (2012). Mitochondrial Disulfide Relay: Redox-regulated Protein Import into the Intermembrane Space. *The Journal of biological chemistry*, 287(7), 4426-33.
- Herrmann, J., Westermann, B., & Neupert, W. (2001). Analysis of protein-protein interactions in mitochondria by coimmunoprecipitation and chemical cross-linking. *Methods in Cell Biology*, 65, 217-230.
- Hunte, C. (2003). Protonmotive pathways and mechanisms in the cytochrome bc₁ complex. *FEBS Letters*, 545(1), 39-46.

6. References

- Hutu, D., Guiard, B., & Chacinska, A. (2008). Mitochondrial protein import motor: differential role of Tim44 in the recruitment of Pam17 and J-complex to the presequence translocase. *Molecular biology of the cell*, 19, 2642-2649.
- Iacovino, M., Granycome, C., Sembongi, H., Bokori-Brown, M., Butow, R. a, Holt, I. J., & Bateman, J. M. (2009). The conserved translocase Tim17 prevents mitochondrial DNA loss. *Human molecular genetics*, 18(1), 65-74.
- Kastner, B., Fischer, N., Golas, M. M., Sander, B., Dube, P., Boehringer, D., Hartmuth, K., et al. (2008). GraFix : sample preparation for single-particle electron cryomicroscopy. *Nature methods*, 5(1), 53-55.
- Koll, H., Guiard, B., Rassow, J., Ostermann, J., Horwich, a L., Neupert, W., & Hartl, F. U. (1992). Antifolding activity of hsp60 couples protein import into the mitochondrial matrix with export to the intermembrane space. *Cell*, 68(6), 1163-75.
- Kutik, S., Stojanovski, D., Becker, L., Becker, T., Meinecke, M., Krüger, V., Prinz, C., et al. (2008). Dissecting membrane insertion of mitochondrial beta-barrel proteins. *Cell*, 132(6), 1011-24.
- Kutik, S., Stroud, D. a, Wiedemann, N., & Pfanner, N. (2009). Evolution of mitochondrial protein biogenesis. *Biochimica et biophysica acta*, 1790(6), 409-15. Elsevier B.V.
- Laemmli, U. (1970). Cleavage of structural proteins during the assembly of the head of bacteriophage T4. *Nature*, 227(5259), 680-685.
- Lane, N., & Martin, W. (2010). The energetics of genome complexity. *Nature*, 467(7318), 929-934.
- Lang, B., & Gray, M. (1999). Mitochondrial genome evolution and the origin of eukaryotes. *Annual review of genetics*, 33, 351-397.
- Lau, W. C. Y., Baker, L. a, & Rubinstein, J. L. (2008). Cryo-EM structure of the yeast ATP synthase. *Journal of molecular biology*, 382(5), 1256-64.
- Lau, W. C. Y., & Rubinstein, J. L. (2010). Structure of intact *Thermus thermophilus* V-ATPase by cryo-EM reveals organization of the membrane-bound V(O) motor. *Proceedings of the National Academy of Sciences of the United States of America*, 107(4), 1367-72.
- Lau, W. C. Y., & Rubinstein, J. L. (2012). Subnanometre-resolution structure of the intact *Thermus thermophilus* H⁺-driven ATP synthase. *Nature*, 481(7380), 214-8. Nature Publishing Group.
- Leberman, R. (1965). Use of uranyl formate as a negative stain. *J Mol Biol.*, 13(2), 606.
- Lee, H., & Wei, Y. (2012). Mitochondria and aging. *Advances in Experimental Medicine and Biology*, 942, 311-327.
- Lenaz, G., Baracca, A., Barbero, G., Bergamini, C., Dalmonte, M. E., Del Sole, M., Faccioli, M., et al. (2010). Mitochondrial respiratory chain super-complex I-III in physiology and pathology. *Biochimica et biophysica acta*, 1797(6-7), 633-40.
- Lenaz, G., & Genova, M. L. (2010). Structure and organization of mitochondrial respiratory complexes: a new understanding of an old subject. *Antioxidants & Redox Signaling*, 12(8), 961-1008.
- Lill, R., & Mühlenhoff, U. (2005). Iron-sulfur-protein biogenesis in eukaryotes. *Trends in biochemical sciences*, 30(3), 133-41.
- Lill, R., & Mühlenhoff, U. (2008). Maturation of iron-sulfur proteins in eukaryotes: mechanisms, connected processes, and diseases. *Annual review of biochemistry*, 77, 669-700.

6. References

- Lithgow, T., & Schneider, A. (2010). Evolution of macromolecular import pathways in mitochondria, hydrogenosomes and mitosomes. *Philosophical transactions of the Royal Society of London. Series B, Biological sciences*, 365(1541), 799-817.
- Ludtke, S. J., Baldwin, P. R., & Chiu, W. (1999). EMAN: semiautomated software for high-resolution single-particle reconstructions. *Journal of structural biology*, 128(1), 82-97.
- Ma, Z. A., Zhao, Z., & Turk, J. (2012). Mitochondrial dysfunction and β -cell failure in type 2 diabetes mellitus. *Experimental diabetes research*, 2012, ID: 703538.
- Mailloux, R. J., & Harper, M.-E. (2011). Uncoupling proteins and the control of mitochondrial reactive oxygen species production. *Free radical biology & medicine*, 51(6), 1106-15.
- Marom, M., Azem, A., & Mokranjac, D. (2011). Understanding the molecular mechanism of protein translocation across the mitochondrial inner membrane: still a long way to go. *Biochimica et biophysica acta*, 1808(3), 990-1001.
- Marom, M., Dayan, D., Demishtein-Zohary, K., Mokranjac, D., Neupert, W., & Azem, A. (2011). Direct interaction of mitochondrial targeting presequences with purified components of the TIM23 complex. *The Journal of biological chemistry*, 286(51), 43809-43815.
- Martin, W. F. (2011). Early evolution without a tree of life. *Biology direct*, 6(1), 36. BioMed Central Ltd.
- Martinez-Caballero, S., Grigoriev, S. M., Herrmann, J. M., Campo, M. L., & Kinnally, K. W. (2006). Tim17p Regulates the Twin Pore Structure and Voltage Gating of the Mitochondrial Protein Import Complex TIM23. *Journal of Biological Chemistry*, 282(6), 3584-93.
- Meinecke, M., Wagner, R., Kovermann, P., Guiard, B., Mick, D. U., Hutu, D. P., Voos, W., et al. (2006). Tim50 maintains the permeability barrier of the mitochondrial inner membrane. *Science*, 312(5779), 1523-6.
- Meisinger, C., Pfanner, N., & Truscott, K. (2006). Isolation of yeast mitochondria. *Methods Mol Biol*, 313, 33-39.
- Mick, D. U., Fox, T. D., & Rehling, P. (2011). Inventory control: cytochrome c oxidase assembly regulates mitochondrial translation. *Nature reviews. Molecular cell biology*, 12(1), 14-20.
- Mileyskovskaya, E., Penczek, P. a, Fang, J., Mallampalli, V. K. P. S., Sparagna, G. C., & Dowhan, W. (2012). Arrangement of the Respiratory Chain Complexes in *Saccharomyces cerevisiae* Supercomplex III₂IV₂ Revealed by Single Particle Cryo-electron Microscopy (EM). *The Journal of biological chemistry*, [Epub ahead of print].
- Model, K., Meisinger, C., & Kühlbrandt, W. (2008). Cryo-electron microscopy structure of a yeast mitochondrial preprotein translocase. *Journal of molecular biology*, 383(5), 1049-57.
- Model, K., Prinz, T., Ruiz, T., Radermacher, M., Krimmer, T., Kühlbrandt, W., Pfanner, N., et al. (2002). Protein translocase of the outer mitochondrial membrane: role of import receptors in the structural organization of the TOM complex. *Journal of molecular biology*, 316(3), 657-66.
- Mokranjac, D., & Neupert, W. (2010). The many faces of the mitochondrial TIM23 complex. *Biochimica et biophysica acta*, 1797(6-7), 1045-54.
- Mokranjac, D., Paschen, S. a, Kozany, C., Prokisch, H., Hoppins, S. C., Nargang, F. E., Neupert, W., et al. (2003). Tim50, a novel component of the TIM23 preprotein translocase of mitochondria. *The EMBO journal*, 22(4), 816-25.

6. References

- Mokranjac, D., Popov-Čeleketić, D., Hell, K., & Neupert, W. (2005). Role of Tim21 in mitochondrial translocation contact sites. *The Journal of biological chemistry*, 280(25), 23437-40.
- Mokranjac, D., & Sichtung, M. (2009). Role of Tim50 in the Transfer of Precursor Proteins from the Outer to the Inner Membrane of Mitochondria. *Molecular biology of the cell*, 20(5), 1400-1407.
- Muench, S. P., Trinick, J., & Harrison, M. a. (2011). *Structural divergence of the rotary ATPases. Quarterly reviews of biophysics* (Vol. 44, pp. 311-56).
- Muñoz-Pinedo, C. (2012). Signaling pathways that regulate life and cell death: evolution of apoptosis in the context of self-defense. *Advances in Experimental Medicine and Biology*, 738, 124-143.
- Neuhoff, V., Arold, N., & Taube, D. (1988). Improved staining of proteins in polyacrylamide gels including isoelectric focusing gels with clear background at nanogram sensitivity using Coomassie Brilliant Blue. *Electrophoresis*, 9(6), 255-262.
- Newsholme, P., Gaudel, C., & Krause, M. (2012). Mitochondria and diabetes. An intriguing pathogenetic role. *Advances in Experimental Medicine and Biology*, 942, 235-247.
- Nilsson, B., Moks, T., Jansson, B., Abrahmsén, L., Elmblad, a, Holmgren, E., Henrichson, C., et al. (1987). A synthetic IgG-binding domain based on staphylococcal protein A. *Protein engineering*, 1(2), 107-13.
- Nunnari, J., & Suomalainen, A. (2012). Mitochondria: In Sickness and in Health. *Cell*, 148(6), 1145-1159.
- Oyedotun, K. S., & Lemire, B. D. (2004). The quaternary structure of the *Saccharomyces cerevisiae* succinate dehydrogenase. Homology modeling, cofactor docking, and molecular dynamics simulation studies. *The Journal of biological chemistry*, 279(10), 9424-31.
- Park, K.-H., Berrier, C., Lebaupain, F., Pucci, B., Popot, J.-L., Ghazi, A., & Zito, F. (2007). Fluorinated and hemifluorinated surfactants as alternatives to detergents for membrane protein cell-free synthesis. *The Biochemical journal*, 403(1), 183-7.
- Pettersen, E. F., Goddard, T. D., Huang, C. C., Couch, G. S., Greenblatt, D. M., Meng, E. C., & Ferrin, T. E. (2004). UCSF Chimera-a visualization system for exploratory research and analysis. *Journal of Computational Chemistry*, 25(13), 1605-12.
- Popot, J.-L. (2010). Amphipols, nanodiscs, and fluorinated surfactants: three nonconventional approaches to studying membrane proteins in aqueous solutions. *Annual review of biochemistry*, 79, 737-75.
- Popov-Čeleketić, D., Mapa, K., Neupert, W., & Mokranjac, D. (2008). Active remodelling of the TIM23 complex during translocation of preproteins into mitochondria. *The EMBO journal*, 27(10), 1469-80.
- Popov-Čeleketić, D., Waagemann, K., Mapa, K., Neupert, W., & Mokranjac, D. (2011). Role of the import motor in insertion of transmembrane segments by the mitochondrial TIM23 complex. *EMBO reports*, 12(6), 542-8.
- Prokisch, H., Scharfe, C., Camp, D. G., Xiao, W., David, L., Andreoli, C., Monroe, M. E., et al. (2004). Integrative analysis of the mitochondrial proteome in yeast. *PLoS biology*, 2(6), e160.
- Qian, X., Gebert, M., Höpker, J., Yan, M., Li, J., Wiedemann, N., van der Laan, M., Pfanner, N., & Sha, B. (2011). Structural Basis for the Function of Tim50 in the Mitochondrial Presequence Translocase. *Journal of molecular biology*, 411(3), 513-519.
- Radermacher, M. (1988). Three-dimensional reconstruction of single particles from random and nonrandom tilt series. *Journal of Electron Microscopy Technique*, 9(4), 359-394.

6. References

- Rassow, J., Guiard, B., Wienhues, U., Herzog, V., Hartl, F. U., & Neupert, W. (1989). Translocation arrest by reversible folding of a precursor protein imported into mitochondria. A means to quantitate translocation contact sites. *The Journal of cell biology*, 109(4 Pt 1), 1421-8.
- Rehling, P., Model, K., Brandner, K., Kovermann, P., Sickmann, A., Meyer, H. E., Kühlbrandt, W., et al. (2003). Protein insertion into the mitochondrial inner membrane by a twin-pore translocase. *Science*, 299(5613), 1747-51.
- Reinders, J., Zahedi, R., & Pfanner, N. (2006). Toward the Complete Yeast Mitochondrial Proteome: Multidimensional Separation Techniques for Mitochondrial Proteomics. *Journal of proteome research*, 5(7), 1543-1554.
- Richter, F. M., Sander, B., Golas, M. M., Stark, H., & Urlaub, H. (2010). Merging molecular electron microscopy and mass spectrometry by carbon film-assisted endoprotease digestion. *Molecular & cellular proteomics*, 9(8), 1729-41.
- Rubinstein, J. L. (2007). Structural analysis of membrane protein complexes by single particle electron microscopy. *Methods*, 41(4), 409-16.
- Rubinstein, J. L., Dickson, V. K., Runswick, M. J., & Walker, J. E. (2005). ATP synthase from *Saccharomyces cerevisiae*: location of subunit h in the peripheral stalk region. *Journal of molecular biology*, 345(3), 513-20.
- Rubinstein, J. L., Walker, J. E., & Henderson, R. (2003). Structure of the mitochondrial ATP synthase by electron cryomicroscopy. *The EMBO journal*, 22(23), 6182-92.
- Ryan, M., Voos, W., & Pfanner, N. (2001). Assaying protein import into mitochondria. *Methods in Cell Biology*, 65, 189-215.
- Sambrook, J., & Russell, D. (2000). *Molecular cloning: A laboratory manual*. Cold Spring Harbor Laboratory Press.
- Schafmeister, C. E., Miercke, L. J., & Stroud, R. M. (1993). Structure at 2.5 Å of a designed peptide that maintains solubility of membrane proteins. *Science*, 262(5134), 734-8.
- Schiller, D. (2009). Pam17 and Tim44 act sequentially in protein import into the mitochondrial matrix. *The international journal of biochemistry & cell biology*, 41(11), 2343-9.
- Schmidt, O., Pfanner, N., & Meisinger, C. (2010). Mitochondrial protein import: from proteomics to functional mechanisms. *Nature reviews. Molecular cell biology*, 11(9), 655-67.
- Schmidt-Krey, I., & Rubinstein, J. L. (2011). Electron cryomicroscopy of membrane proteins: specimen preparation for two-dimensional crystals and single particles. *Micron*, 42(2), 107-16. Elsevier Ltd.
- Schulz, C., Lytovchenko, O., Melin, J., Chacinska, A., Guiard, B., Neumann, P., Ficner, R., et al. (2011). Tim50's presequence receptor domain is essential for signal driven transport across the TIM23 complex. *The Journal of cell biology*, 195(4), 643-56.
- Schägger, H., & von Jagow, G. (1991). Blue native electrophoresis for isolation of membrane protein complexes in enzymatically active form. *Analytical Biochemistry*, 199(2), 223-231.
- Shiflett, A. M., & Johnson, P. J. (2010). Mitochondrion-related organelles in eukaryotic protists. *Annual review of microbiology*, 64, 409-29.
- Shiota, T., Mabuchi, H., Tanaka-Yamano, S., Yamano, K., & Endo, T. (2011). In vivo protein-interaction mapping of a mitochondrial translocator protein Tom22 at work. *Proceedings of the National Academy of Sciences of the United States of America*, 108(37), 15179-15183.

6. References

- Sickmann, A., Reinders, J., Wagner, Y., Joppich, C., Zahedi, R., Meyer, H. E., Schönfisch, B., et al. (2003). The proteome of *Saccharomyces cerevisiae* mitochondria. *Proceedings of the National Academy of Sciences of the United States of America*, 100(23), 13207-12.
- Signorell, G. a, Kaufmann, T. C., Kukulski, W., Engel, A., & Rémigy, H.-W. (2007). Controlled 2D crystallization of membrane proteins using methyl-beta-cyclodextrin. *Journal of structural biology*, 157(2), 321-8.
- Sikorski, R. S., & Hieter, P. (1989). A system of shuttle vectors and yeast host strains designed for efficient manipulation of DNA in *Saccharomyces cerevisiae*. *Genetics*, 122(1), 19-27.
- Smith, E., & Pickels, E. (1940). Micelle Formation in Aqueous Solutions of Digitonin. *Proceedings of the National Academy of Sciences of the United States of America*, 26(4), 272-277.
- Stark, H. (2010). GraFix: stabilization of fragile macromolecular complexes for single particle cryo-EM. *Methods in Enzymology*, 481, 109-126.
- Tamura, Y., Harada, Y., Shiota, T., Yamano, K., Watanabe, K., Yokota, M., Yamamoto, H., et al. (2009). Tim23-Tim50 pair coordinates functions of translocators and motor proteins in mitochondrial protein import. *The Journal of cell biology*, 184(1), 129-41.
- Tribet, C., Audebert, R., & Popot, J. L. (1996). Amphipols: polymers that keep membrane proteins soluble in aqueous solutions. *Proceedings of the National Academy of Sciences of the United States of America*, 93(26), 15047-50.
- Truscott, K. N., Kovermann, P., Geissler, A., Merlin, A., Meijer, M., Driessen, A. J. M., Rassow, J., et al. (2001). A presequence- and voltage-sensitive channel of the mitochondrial preprotein translocase formed by Tim23. *Nature Structural & Molecular Biology*, 8(12), 1074-1082.
- Van Heel, M. (1987). Angular reconstitution: a posteriori assignment of projection directions for 3D reconstruction. *Ultramicroscopy*, 21(2), 111-123.
- Vukotic, M., Oeljeklaus, S., Wiese, S., Vögtle, F., Meisinger, C., Meyer, H. E., Zieseniss, A., et al. (2012). Rcf1 mediates cytochrome oxidase assembly and respirasome formation, revealing heterogeneity of the enzyme complex. *Cell Metabolism*, 15(3), 336-347.
- Vögtle, F.-N., Wortelkamp, S., Zahedi, R. P., Becker, D., Leidhold, C., Gevaert, K., Kellermann, J., et al. (2009). Global analysis of the mitochondrial N-proteome identifies a processing peptidase critical for protein stability. *Cell*, 139(2), 428-39.
- Wagner, K., Rehling, P., Sanjuán Szklarz, L. K., Taylor, R. D., Pfanner, N., & van der Laan, M. (2009). Mitochondrial F1Fo-ATP synthase: the small subunits e and g associate with monomeric complexes to trigger dimerization. *Journal of molecular biology*, 392(4), 855-61. Elsevier Ltd.
- Wiedemann, N, Pfanner, N., & Rehling, P. (2006). Import of precursor proteins into isolated yeast mitochondria. *Methods in molecular biology*, 313, 373-383.
- Wiedemann, Nils, van der Laan, M., Hutu, D. P., Rehling, P., & Pfanner, N. (2007). Sorting switch of mitochondrial presequence translocase involves coupling of motor module to respiratory chain. *The Journal of cell biology*, 179(6), 1115-22.
- Yamamoto, H., Esaki, M., Kanamori, T., Tamura, Y., Nishikawa, S. I., & Endo, T. (2002). Tim50 is a subunit of the TIM23 complex that links protein translocation across the outer and inner mitochondrial membranes. *Cell*, 111(4), 519-28.

6. References

- Zhang, Y., Deng, H., Zhao, Q., & Li, S. J. (2012). Interaction of presequence with human translocase of the inner membrane of mitochondria Tim50. *The journal of physical chemistry*, 116(9), 2990-8.
- de la Cruz, L., Bajaj, R., Becker, S., & Zweckstetter, M. (2010). The intermembrane space domain of Tim23 is intrinsically disordered with a distinct binding region for presequences. *Protein science : a publication of the Protein Society*, 19(11), 2045-54.
- van Heel, M., Harauz, G., Orlova, E. V., Schmidt, R., & Schatz, M. (1996). A new generation of the IMAGIC image processing system. *Journal of structural biology*, 116(1), 17-24.
- van der Giezen, M., & Tovar, J. (2005). Degenerate mitochondria. *EMBO reports*, 6(6), 525-30.
- van der Laan, M., Meinecke, M., Dudek, J., Hutu, D. P., Lind, M., Perschil, I., Guiard, B., et al. (2007). Motor-free mitochondrial presequence translocase drives membrane integration of preproteins. *Nature Cell Biology*, 9(10), 1152-1159.
- van der Laan, M., Rissler, M., & Rehling, P. (2006). Mitochondrial preprotein translocases as dynamic molecular machines. *FEMS Yeast Research*, 6(6), 849-61.
- van der Laan, M., Wiedemann, N., Mick, D. U., Guiard, B., Rehling, P., & Pfanner, N. (2006). A role for Tim21 in membrane-potential-dependent preprotein sorting in mitochondria. *Current biology*, 16(22), 2271-2276.

Curriculum Vitae

Personal information

Name	Oleksandr Lytovchenko
Date of birth	13. 12. 1985
Place of birth	Kharkiv, Ukraine

Education

Since 01/2009	Georg August University, Göttingen, Germany Department of Biochemistry II PhD project: Structural and functional analysis of the TIM23 presequence translocase Supervisors: Prof. Dr. P. Rehling, Prof. Dr. H. Stark, Prof. Dr. D. Fasshauer
10/2006–12/2008	International Max Planck Research School MSc/PhD Molecular Biology Program, Göttingen MSc degree in molecular biology (2008) Thesis: Expression of DOR during adipogenesis and in adipose tissue Supervisors: Dr. B. Baumgartner, Prof. Dr. A. Mansouri, Prof. Dr. H. Hahn
09/2002-09/2006	V.N. Karazin Kharkiv National University, Kharkiv, Ukraine School of Biology BSc degree in biochemistry (2006) Thesis: Molecular cloning and expression of <i>Chlamydia trachomatis omp1</i> gene in <i>E. coli</i> Supervisors: Dr. Sc. A. Bilozorov, Dr. S. Ochrymenko
09/1995-06/2002	Physical and Mathematical Lyceum No 27, Kharkiv, Ukraine.